STUDIES ON OPTICAL ATTENUATION IN SEA WATER USING DYE LASER AND LASER PROPAGATION IN A TURBULENT MEDIUM

A. T. REGHUNATH

THESIS SUBMITTED TO
THE COCHIN UNIVERSITY OF SCIENCE & TECHNOLOGY
FOR THE AWARD OF THE DEGREE OF
DOCTOR OF PHILOSOPHY

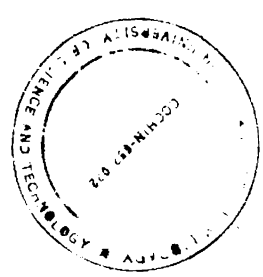

LASER DIVISION
DEPARTMENT OF PHYSICS
COCHIN UNIVERSITY OF SCIENCE AND TECHNOLOGY
COCHIN - 682 022

1987

DECLARATION

I hereby declare that the work described in this thesis is original and is carried out by me under the supervision of Dr.V.P.N.Nampoori, Reader, Department of Physics, Cochin University of Science and Technology and has not been included in any other thesis submitted previously for the award of any degree.

Cochin - 682022
November 19, 1987

A.T.Reghunath.

CERTIFICATE

Certified that the work presented in this thesis is based on the bona fide work done by Mr.A.T.Reghunath under my guidance in the Department of Physics, Cochin University of Science and Technology, and has not been included in any other thesis submitted previously for the award of any degree.

Cochin - 682022
November 19, 1987

Dr.V.P.N.Nampoori
(Supervising Teacher).

ACKNOWLEDGEMENTS

The investigations presented in this thesis have been carried out under the guidance of Dr.V.P.N. Nampoori, Reader, Department of Physics, Cochin University of Science and Technology. It is with great pleasure I express my sincere gratitude for his able guidance and competent advice throughout the progress of this work.

I am very much indebted to Prof.K.Sathianandan, Department of Physics, Cochin University, for introducing me to this subject and for the keen interest and encouragement he has shown throughout the course of this work.

I am grateful to Prof.M.G.Krishna Pillai, Head of the Department of Physics, for providing all the necessary facilities for carrying out this work.

I owe much to Mr.M.Ravisankar, who was with me throughout the course of this work, for providing all helps, encouragements and suggestions.

I am thankful to all the faculty members of the Department of Physics, for their whole-hearted encouragement. Thanks are also due to the technical, administrative and library staff of the Department of Physics and staff of the University Science and Instrumentation Centre for their help and co-operation.

I express my sincere thanks to all the research scholars of the Department of Physics for their co-operation with special regard to Dr.Sudha Vijayakumar, Mr.T.M.Abdul Rasheed, Mr.T.Ramachandran, Mr.K.P.B.Moosad, Mr.A.V.Ravikumar

and Mr.M.K.Satheeshkumar. The timely helps from the research students of the Thin Film Division is gratefully acknowledged.

I am thankful to the Department of Electronics, Cochin University for providing the computer facilities. My thanks are due to the research students of the Departments of Electronics and Mathematics & Statistics for their helps.

I thank the Defence Research and Development Organisation, New Delhi, and the Department of Atomic Energy (India) for the financial assistances.

Finally, I thank Mr.K.P.Sasidharan for the neat typing of this manuscript and Mr.V.M.Peter for the binding.

A.T.Reghunath.

PREFACE

A great deal of scientific effort is concentrated to make use of the marine resources and energies. These activities require an effective underwater wide band information transmission system. In the field of defence, the communication with submarines is a subject of vital importance. It is difficult to utilise VLF radio wave or acoustic wave for that purpose because of the increase of attenuation with frequency. In water, another window for the electromagnetic waves is in the visible region, which satisfies the above requirements.

Because of these reasons, with the advent of lasers there has been a revived interest in the field of underwater optical systems. Serious efforts are going on to develop laser based underwater optical systems. In order to develop any optical system the region of minimum attenuation of light in water must be identified. This demands an extensive study of the transmission characteristics of sea water for different wavelengths in the visible region. The dependence of optical attenuation on the concentration of these constituents is an essential scientific information to be gathered. The sea water being in random turbulent motion, the laser propagation in a turbulent medium is also a related area of importance. The variations in the temperature and salinity of sea water

will give rise to refractive index variations in the medium. Eventhough the refractive index variation from the mean value is small the cumulative effect can be very significant. The central theme of the work presented in this thesis is a careful investigation of the factors influencing the attenuation of laser beam through sea water.

The thesis presents a detailed report of the work done by the author on the attenuation studies in sea water and on laser propagation through a turbulent medium. The thesis contains six chapters which are more or less self-contained with separate abstracts and references. The first chapter is divided into two parts. The first part introduces the subject of laser propagation through sea water. It includes a brief description of optical properties of sea water followed by a review of the earlier works on attenuation studies in water. The second part gives the theoretical background of the problem of laser propagation through a turbulent medium.

Chapter 2 gives the fabrication details of a nitrogen laser pumped dye laser used for the attenuation studies in sea water. A description of the energy levels of the dye laser and the working principle is given. The different parts of the dye laser system is explained. The parametric studies of the dye laser which form an important part of the required instrumentation are also described in this chapter.

The experimental setup for the optical attenuation measurements in sea water is given in chapter 3. The split-pulse laser method is adopted using the fabricated nitrogen laser pumped dye laser as the source. The different parts of this experimental arrangement are described. The advantage of this technique over other high sensitive absorption measurement methods are also given in this chapter.

In chapter 4, the results of the attenuation studies in distilled water, 'artificial' sea water and natural sea water are given. Several authors have reported the attenuation coefficient of distilled water. But these values are found to differ by a factor of 2 owing to the low value of attenuation coefficient coupled with several experimental corrections required to arrive at the final experimental result. Hence, the optical attenuation of distilled water is re-investigated using the present setup. The results are compared with the other reported results.

To determine the effect of dissolved constituents of sea water on attenuation, measurements were conducted in 'artificial' sea water prepared by dissolving the respective chemicals in the right proportion in doubly distilled water. Two such samples are studied to separate out the influence of major and minor constituents of sea water. The details of the sample preparation, experimental procedure and results are described.

In addition, the experiments on natural sea water is also included in this chapter. The results of these experiments are compared with that of artificial sea water to study the influence of suspended particles.

Chapter 5 describes the experiment on laser propagation through a turbulent medium. The variance, power spectrum and probability distribution of the intensity fluctuations of the propagated beam is studied. It is shown that the behaviour of the laboratory simulated turbulence is similar to that of atmospheric turbulence.

These studies are then extended to understand the dynamics of the turbulence. A system behaves chaotic, when there exists strange attractors in phase space. The dimension of the attractor of turbulent system is determined. The Kolmogorov entropy which is another parameter which characterises the system is also determined and the results are presented in this chapter.

The present studies have brought out a new method of qualitatively characterising the turbulence which is also included in this chapter.

Chapter 6 gives the general conclusions drawn from the results reported in the earlier chapters.

Part of the investigations presented in the thesis has been published in the form of following papers:

1. A Study of Hydrodynamic Turbulence Using Laser Transmission
   A.T.Reghunath and V.P.N.Nampoori
   Pramana, Vol.29, No.5 (November 1987).

2. Attenuation Studies in Distilled Water Using Split-pulse Laser Techniques
   A.T.Reghunath, M.Ravisankar, K.Sathianandan and V.P.N.Nampoori
   Presented at the International Conference on Laser Applications in Spectroscopy and Optics, Jan.5-10, 1987, IIT, Madras.

3. Characterisation of Hydrodynamic Turbulence Using Laser Propagation
   A.T.Reghunath and V.P.N.Nampoori
   Presented at the International Conference on Laser Applications in Spectroscopy and Optics, Jan.5-10, 1987, IIT, Madras.

4. Laser Propagation Through a Turbulent Media--A Laboratory Simulation
   A.T.Reghunath and V.P.N.Nampoori
   Proceedings of the IV Quantum Electronics Symposium (Cochin), DAE, p.140 (1986).

5. Effect of Major Dissolved Constituents of Sea Water on Optical Attenuation
   M.Ravisankar, A.T.Reghunath, K.Sathianandan and V.P.N.Nampoori
   Proceedings of the IV Quantum Electronics Symposium (Cochin), DAE, p.142 (1986).

C O N T E N T S

Chapter 1

INTRODUCTION

Abstract

The first part of the chapter deals with the subject of laser propagation in sea water. After a brief description of the properties of sea water, the topic is introduced with a description of absorption and scattering processes in water and other relevant optical properties of sea water. A review of earlier studies in this area is also given. The second part introduces the subject of laser propagation in a turbulent medium. The Rytov theory of optical propagation and the behaviour of the variance, power spectrum and probability distribution function of the intensity fluctuations are described.

PART I - LASER PROPAGATION IN SEA WATER

1.1 INTRODUCTION

With the advent of lasers, there have been a revived interest in the field of underwater optical systems. Lasers, because of their high power, narrow bandwidth and low divergence are ideal sources for underwater optical communication, ranging and photography. In order to develop any underwater optical system, the region of minimum attenuation of light in water must be identified. The search for an optical window demands an extensive study of the transmission characteristics of sea water for different wavelengths in the visible region. The sea water being a complex mixture of several dissolved and suspended particles, the dependence of optical attenuation on the concentration of these constituents is an essential scientific information to be gathered.

As light propagates through the water medium, it gets absorbed as well as gets scattered. The absorption can be due to the water molecules, the dissolved substances in the sea water or the undissolved substances drifting in water, like the planktons. The total loss of light due to both absorption and scattering is termed as attenuation.

The received intensity is also affected by the random turbulent motion of the sea. The refractive index of the sea water is a function of both temperature and salinity. The turbulent motion of the sea introduces fluctuations in the temperature and salinity along the propagation path, which results in localised fluctuations in the refractive index of the medium. These random fluctuations in the refractive index will affect the intensity of the propagated laser beam.

The propagation of laser through sea water is thus a complex problem. In this chapter, the properties of sea water, the absorption and scattering processes, the optical properties of sea water derived using the radiative transfer theory and a review of earlier work on the related topics are presented in the first part. The second part deals with the laser propagation in a turbulent medium.

1.2 PROPERTIES OF SEA WATER

The sea water contains a varied collection of chemical substances in solution namely, minerals, organic substances and gases. The dissolved salts which are in measurable proportions are sodium chloride, magnesium chloride, magnesium sulphate, calcium sulphate and magnesium bromide. Many other substances also exist in the sea, and it seems likely that it contains a certain amount of every known terrestial element as well as

possibly some less familiar air-borne materials blown in from interplanetary space. However most of these exist in such minute proportions that they can be measured with extreme difficulty and mainly come to light when concentrated in the bodies of marine animals. For example, vanadium has been found in the blood of ascidians and holothurians, nickel in molluscs and cobalt in lobsters and mussels.[1] As these substances can only have been acquired from the creatures' environment, we must conclude that they exist dissolved in the sea, eventhough they are not easily detected in the sea water. The living cells are therefore better at extracting and concentrating these substances than the chemists.

The properties of sea water which are of relevance to optical propagation are given below.

1.2.1 Dissolved Constituents

The sea water, excluding the suspended particles, is a solution of large number of constituents which can be divided into four groups: water, major solids, minor solids (and liquids) and gases. The major solids are those which have appreciable influence on density. The minor solids compose only of about 0.025% of the total solids in typical sea water. The major solids are composed of salts that are almost completely ionized, the proportion by mass being as given[2] in Table (1.1).

Table (1.1). Proportion by mass of the major constituents of sea water and their mass in 1 kg of sea water of salinity 19 ‰.

Constituent	Proportion to sum %	g/kg of sea water of chlorinity 19‰
Chloride (Cl^-)	55.044	18.980
Sulphate (SO_4^{2-})	7.682	2.649
Bicarbonate (HCO_3^-)	0.406	0.140
Bromide (Br^-)	0.189	0.065
Flouride (Fl^-)	0.003	0.001
Boric Acid (H_3BO_3)	0.075	0.026
Sodium (Na^+)	30.613	10.556
Magnesium (Mg^{2+})	3.689	1.272
Calcium (Ca^{2+})	1.160	0.400
Potassium (K^+)	1.102	0.380
Strontium (Sr^{2+})	0.038	0.013
	100.000	34.482
Water		965.518
		1000.000

Apparently, sodium and chlorine constitute 85% of all the dissolved solid substances of the sea. The gas content of the sea water is subject to considerable variation from place to place and time to time, and hence is not included in the table. The proportions given are fairly constant; which only means that the relative proportion of the dissolved salts would be the same eventhough total quantity per litre of sea water may vary from place to place.

As indicated earlier, the list of components given in the table, is far from complete. While it is true that these account virtually for the whole weight of dissolved matter in the water, there are also elements of which minute traces have been identified in sea water and are a necessity of life to certain organisms. Radio-active matter also occurs naturally in the sea, for example, uranium is found in concentrations of 1-3 mg/cubic metre.

1.2.2 Salinity and Chlorinity

For many purposes, it is not necessary to know the concentration of the individual elements in sea water, it is enough to know the total salt content or the 'salinity'. Salinity is the total amount of salt materials in grams contained in one kilogram of sea water, when all the carbonate has been converted to oxide, the bromine and iodine, replaced by chlorine and all organic matter is completely oxidised.

The direct determination of salinity by evaporating sea water to dryness is too difficult to carry out. One of the methods used, is to determine the chlorinity (which is approximately the ratio by mass of halides to total sample of sea water) by titration. The salinity is thus determined by the proportion given in Table (1.1). It has been found that salinity is 1.80688 times chlorinity.

The chlorinity and salinity of sea water is usually expressed in parts per thousand, parts per mille or by the symbol "‰".

In Table (1.1), the second column gives the quantity by weight of the substance in sea water of chlorinity 19‰. The figures stand for the number of grams of each component per kilogram and not per litre of sea water.

Nowadays most of the salinity measurements are made by determining the electrical conductivity of the sea water. The conductivity however depends very much on temperature of sea water. Advanced techniques have been developed for determining salinity by conductivity measurements with compensation for temperature with an accuracy of 0.003‰in salinity.

In vast majority of places in the oceans, the salinity lies between 34 and 37‰. In places receiving a great deal of

the fresh water, the salinity may be less than 34‰. The salinity of the oceans is high wherever strong evaporation is continually extracting water from the sea.

1.2.3 Temperature

The temperature of ocean water depends on the latitude and climate. In tropical regions, the surface temperature may be as much as 30°C, while in polar sea, it will be of the order of 2°C. As depth increases, the temperature decreases. In the sea, there is a layer at which, greatest drop in temperature occurs. This layer known as the thermocline, is usually found at depths of about 150 metres.

1.2.4 Suspended Particles

Other than the dissolved salts, gases and organic substances, the sea water consists of small amount of undissolved material. They include, organic matter and dust. The dust particles are predominant in the coastal waters. Far into the sea, the concentration of dust is negligible.

Among the living organisms, other than the large size living creatures, such as fish etc., there exists microscopic creatures called planktons. They are the drifting and floating organisms in the sea, largely unable to move independently.

Planktons are of two types; phytoplanktons (vegetable planktons) and zoo planktons (animal planktons). The phytoplanktons as they need light for their existence, are generally confined to the upper sea layer of about 100 metres.

1.2.5 Light in the Sea

The sunlight penetrates into the sea, only upto a depth of 100 metres, beyond which, it is perpetual night. Therefore the subject of light in the sea, mainly refers to the upper few layers, which when compared to the depth of ocean, is quite thin. The light transmitted into the sea is absorbed by 1) the water molecules, 2) the dissolved substances in the sea water and 3) the undissolved particles drifting in water like planktons. Apart from absorption, there is certain amount of scattering of light. To a certain extent, the light entering from above is everywhere scattered in the water in various directions. This scattering is caused both by the water molecules, the undissolved particles and the gas bubbles.

Clarke[3] had observed luminescence of certain living organisms. At certain depths in many localities, this bio-luminescence was found to be often stronger than the light penetrating from the surface.

1.2.6 Refractive Index

The refractive index of sea water is a fluctuating quantity which depends on both temperature and salinity. Since

the temperature and salinity vary with both space and time, the refractive index is also a function of space and time. The refractive index increases as salinity increases and decreases when temperature increases. The topic of optical propagation through a medium of varying refractive index is dealt in more detail in the latter part of this chapter.

1.3 ABSORPTION OF LIGHT IN WATER

For water, the absorption increases strongly for the region below 200 nm in the ultraviolet and above 700 nm in the infrared. The absorption in this 'window region' is 10^4 to 10^6 times weaker than the absorption outside the limits. Absorption spectrum of water outside this 'window' has been studied extensively by various workers.[4,23] Absorption at the high frequency (in the far UV) is due to the electronic transitions. The bands at the near infrared are shown to be due to overtones and combinations.

Tam and Patel[6], based on their measurements of absorption in water by the photoacoustic method, have pointed out that in the visible region the fifth and sixth harmonics of the O-H stretching vibrations are present at the 16550 cm^{-1} and 19460 cm^{-1} respectively. They had also shown that the n^{th} harmonic absorption peak in water is given by the following formula:

$$\nu_n = n\,(3620 - 63\,n)\,cm^{-1} \qquad (1.1)$$

At higher overtone transitions, the fundamental O-H stretching vibration has two modes (symmetric and antisymmetric), the absorption bands of which overlap with each other. The many bands observed in the region from 2.5 μm to 500 nm were assigned to overtones of stretching local mode[5] and another series of bands which are assigned to combination tones ν(O- v) + ν_δ where δ is the deformation or bending (1510 cm^{-1}) mode, by Tsubomura et al.[7] They obtained an anharmonicity parameter of -72 cm^{-1} instead of Tam's value of -63 cm^{-1}. The peak of the sixth harmonic is thus calculated to be at 523 nm against 513 nm obtained by Tam and Patel.

The absorption bands in water can thus be fitted to overtones and combinations.

1.4 SCATTERING

The first interpretation of the phenomenon of light scattering was the theory of scattering dipole developed by Lord Rayliegh. In the case of dust free gases, Rayleigh[8] assumed that the dipoles must be the molecules themselves. This theory was later modified by Rayleigh[9] and Cabannes[10], to take into account the anisotropy of molecules. This form is applicable to gases but is not satisfactory for dense media like liquids. Scattering by liquids, although more intense than that of gases (having equal volume, but not equal mass) was demonstrated a few years later.

Smoluchowski[11] and Einstein[12] formulated a completely different theoretical approach from statistical thermodynamics. This work was primarily meant to explain critical opalescence but was also found to be applicable to density fluctuations of smaller amplitudes such as those present in a fluid in the ordinary state. Though the Rayleigh theory is not applicable to liquids, a number of results obtained from it are valid in the theory of fluctuations. Hence a description of Rayleigh theory is not out of place in the present context.

1.4.1 Rayleigh Theory

A particle of any form placed in an electric field E behaves like a dipole whose induced moment P is given by the formula $P = pE$ where p is the polarisability of the particle. The particle should be small compared to wavelength so that the field E can be considered homogeneous. The scattering is then assumed to result from the oscillation of this dipole at the frequency imposed by the exciting radiation.

If I_o is the intensity of the incident beam (unpolarised), d the distance between detector and scattering particle, θ is the angle between the direction of propagation of incident beam and the direction of observation the scattered intensity $I(\theta)$ is expressed by

$$I(\theta) = \frac{I_o}{2d^2} k^4 p^2 (1 + \cos^2\theta) \qquad (1.2)$$

where $k = 2\pi/\lambda$, λ the wavelength of light. This formula is valid for isotropic particles, ie., the polarisability is scalar. The scattered light is polarised, and the polarisation depends on θ. Let i_1 and i_2 be the dimensionless function of intensity which correspond to the polarised components, respectively perpendicular and parallel to the plane of incidence. Then i_1 and i_2 are related to the total intensity by

$$I(\theta) = \frac{I_o}{2k^2d^2}\left[i_1(\theta) + i_2(\theta)\right] \tag{1.3}$$

and

$$\begin{bmatrix} i_1 \\ i_2 \end{bmatrix} = k^6p^2 \begin{bmatrix} 1 \\ \cos^2\theta \end{bmatrix} \tag{1.4}$$

i_1 is a constant while i_2 is a function of $\cos^2\theta$ At right angles, the scattered light is totally polarised and at 0° and 180° it is totally depolarised.

The Rayleigh ratio R is the volume scattering function at $\theta = 90°$. If there are N particles per unit volume, and if the intensities scattered by the particles are additive, then

$$R \equiv \beta_{90} = \frac{NI_{90}d^2}{I_o}$$

$$= \frac{1}{2}Nk^4p^2 = \frac{N8\pi^4p^2}{\lambda^4} \tag{1.5}$$

This implies that

$$\beta(\theta) = \beta_{90}(1 + \cos^2\theta) \tag{1.6}$$

If the particles are spherical, the polarisability is given by the Lorentz-Lorenz formula,

$$p = \frac{n^2 - 1}{n^2 + 2} r^3 \tag{1.7}$$

When this is substituted and integrated to get the total scattering coefficient,

$$b = \frac{16\pi}{3} 8 \frac{N\pi^4}{\lambda^4} r^6 \left(\frac{n^2-1}{n^2+2}\right)^2 \tag{1.8}$$

Strutt[13] had shown that even in the case of gases, the polarisation is not total at right angle. Rayleigh[9] explained this depolarisation by the anisotropy of molecules and defined the depolarisation ratio $\delta = i_2(90)/i_1(90)$. Cabannes[10] showed that anisotropy brought an increase of scattering which he expressed as a function of δ. If the Rayleigh ratio obtained by equation (1.5) is expressed as R_{iso}, then the total Rayleigh ratio R_{tot} is,

$$R_{tot} = R_{iso} \frac{6+6\delta}{6-7\delta} \tag{1.9}$$

$(6+6\delta)/(6-7\delta)$ is called the Cabennes factor. Then the equations

for $\beta(\theta)$ and b are modified as

$$\beta(\theta) = \beta(90)\left(1 + \frac{1-\delta}{1+\delta}\cos^2\theta\right) \qquad (1.10)$$

and

$$b = \frac{8\pi}{3}\beta(90)\frac{2+\delta}{1+\delta} \qquad (1.11)$$

Note that $\beta(90)$ takes the value of R_{tot}

$$\frac{1-\delta}{1+\delta} = \frac{i_1-i_2}{i_1+i_2}$$

is the degree of polarisation.

1.4.2 Fluctuation Theory

Experiments have shown that, a given mass of fluid scatters much more in gaseous state than in liquid state, which is contrary to Rayleigh's molecular theory. The molecular scattering is applicable to independent scattering particles and so cannot be applied to liquids because of strong intermolecular interactions. The fluctuation theory gives a new expression for intensity (for the isotropic part R_{iso}) which can apply to the case of dense media. The wavelength dependence, the symmetry of scattering diagrams and the polarisation results obtained by Rayleigh theory remain valid in the theory of fluctuations.

Here scattering is considered to be caused by the random motion of molecules which in a sufficiently small volume, causes fluctuation of density and hence corresponding variation in dielectric constant. Only fluctuations whose frequencies are in the optical region are considered. The isotropic part of Rayleigh ratio is given by

$$R_{iso} = \frac{\pi^2}{2\lambda_o^4} \Delta V \langle\overline{\Delta\epsilon}\rangle^2 \qquad (1.12)$$

where $\langle\overline{\Delta\epsilon}\rangle^2$ is the mean square fluctuation in the dielectric constant ϵ, in a small volume element ΔV of the medium, and λ_o is the wavelength in vacuum.

The fluctuations of ϵ are assumed to be due to density fluctuations so that

$$\langle\overline{\Delta\epsilon}\rangle^2 = \left(\frac{d\epsilon}{de}\right)^2 \langle\overline{\Delta e}\rangle^2 \qquad (1.13)$$

The density fluctuations are related to the probability of the occurrence of change in the average number of molecules in volume ΔV. This volume ΔV should be small in comparison to wavelength but large enough to obey the laws of statistical thermodynamics.

The Rayleigh constant R is given by the relation (in the isotropic case),

$$R_{iso} = \frac{\pi^2}{2\lambda_o^4} KT\ \beta_T \rho^2 \left(\frac{d\epsilon}{d\rho}\right)^2$$

$$= \frac{2\pi^2}{\lambda_o^4} KT\ \beta_T \left(\rho n \frac{dn}{d\rho}\right)^2 \qquad (1.14)$$

where β_T is the isothermal compressibility and $\epsilon = n^2$.

The density derivative of ϵ is obtained from the direct relation between ϵ and ρ. Amongst the several empirical relations proposed, consider the Lorentz-Lorenz relation,

$$\frac{n^2 - 1}{n^2 + 2} \frac{1}{\rho} = \text{Constant}$$

This gives

$$R_{iso} = \frac{\pi^2}{2\lambda_o^4} KT\ \beta_T \frac{(n^2-1)^2 (n^2+2)^2}{9} \qquad (1.15)$$

Since the relation between n and ρ involves pressure and temperature, the R_{iso} has been modified to

$$R_{iso} = \frac{2\pi^2}{\lambda_o^4} KT\ n^2 \frac{1}{\beta_T} \left(\frac{dn}{dp}\right)_T^2 \qquad (1.16)$$

or

$$R_{iso} = \frac{2\pi^2}{\lambda_o^4} KT\ n^2 \frac{\beta_T}{\alpha_p} \left(\frac{dn}{dt}\right)_p^2 \qquad (1.17)$$

where α_p is the volume expansion coefficient.

With these equations, the isotropic part of Rayleigh ratio can be determined from the experimental values of β_T and $(\frac{dn}{dp})_T$.

Combining with the depolarisation factor, the R_{tot} can be written as

$$R_{tot} = \frac{2\pi^2}{\lambda_o^4} KT\, n^2 \frac{1}{\beta_T} \left(\frac{dn}{dp}\right)_T^2 \frac{6+6\delta}{6-7\delta} \qquad (1.18)$$

1.4.3 Mie Scattering

When the particles are larger than about one tenth of a wavelength, the light scattered from one point may well be out of phase with light scattered from another point. Hence due to interference, the scattered light distribution will no longer be symmetrical as in the Rayleigh case. With increasing particle size, in fact, the scattered light becomes more concentrated in the forward direction. For larger particles the angular dependance of scattering becomes quite complicated showing a number of maxima and minima.

Mie's theory[14] takes into account not only the size of particles but also their refractive index, refractive index of the surrounding medium, the shape and absorptivity of the particles. It is based on formal solution of Maxwell's equations. The amplitudes of these waves decrease rapidly as the particles become smaller. The theory of Mie scattering is more general and it includes Rayleigh scattering as a special case.

If I_o is the intensity of the light incident on the volume, I', the intensity passed through, the intensity scattered out and lost can be defined as

$$i = I_o - I' \tag{1.19}$$

The Mie extinction coefficient μ is given by

$$\mu = Nk\pi r^2 \tag{1.20}$$

where N is the number of particles per unit volume, r is the radius of the particle and k the extinction factor of the particle. The scattered intensity

$$-i = I_o \mu dx \tag{1.21}$$

If the particles are of continuous size distribution with radii ranging from r_1 to r_2 then,

$$\mu = \pi \int_{r_1}^{r_2} N(r)k(r,n)r^2 dr \tag{1.22}$$

Note that there is no wavelength relationship in this expression.

1.5 OPTICAL PROPERTIES OF SEA WATER

The optical properties of sea water described in this section are those derived from radiative transfer theory as shown by Preisendorfer[15] using the commonly used symbols.

The optical properties of sea water are divided into two exclusive and exhaustive classes. They are the inherent optical properties (IOP) and apparent optical properties (AOP). An optical property is inherent if its operational value at a given point in a given medium is invariant under all changes of radiance distribution at that point. In other words, the IOP directly specify the true scattering and absorbing characteristics of the medium and are dependent upon the dissolved and suspended material in the water and electromagnetic properties of the medium. These properties are of particular practical importance when considering high resolution image transmittance through ocean waters.

An optical property is apparent if its operational value, at a given point in a given medium is not invariant, under all changes of radiance distribution at that point. The apparent optical properties depend in a rather complicated way on the IOP and on the ephimeral light distribution field throughout the medium. The AOP are of importance when considering the penetration of radiant energy to depths in ocean waters.

1.5.1 Inherent Optical Properties

The most basic radiometric quantity is the radiance. It is the amount of radiant flux of a given wavelength crossing unit area within unit solid angle about the normal to the plane of area and is denoted by N. The term $N(\bar{x}, \bar{\xi}, t, \lambda)$ denotes the

radiance of wavelength λ, at the $\bar{x}$, flowing in the direction $\bar{\xi}$, at time t. It is expressed in watts per square meter per unit solid angle.

The equation of transfer for N,

$$\frac{n^2}{V} \frac{D[N/n^2]}{Dt} = -\alpha N + N^* + N\eta \tag{1.23}$$

where $$N^* = \int N\sigma d\Omega \tag{1.24}$$

forms the heart of radiative transfer theory.

To understand the physical significance of various terms in the equation of transfer, we follow in imagination a packet of photons as it traverses through the neighbourhood of a point in a scattering absorbing medium. If n is the refractive index, then the quotient N/n^2 will be invariant along a path through a region which exhibits no scattering absorption or sources of radiant flux. The equation of transfer becomes

$$\frac{1}{v} \frac{D[N/n^2]}{Dt} = 0 \tag{1.25}$$

where v is the velocity of light. If the photons were propagating through a medium in which there was pure absorption devoid of scattering and sources of flux then

$$\frac{1}{v}\frac{D[N/n^2]}{Dt} = -\frac{aN}{n^2} \tag{1.26}$$

where a is the volume absorption function or absorption coefficient. In reality, scattering mechanisms are coexistent with absorbing mechanism. Therefore

$$\frac{1}{v}\frac{D[N/n^2]}{Dt} = -(a+s)N/n^2 \tag{1.27}$$

where s is the total scattering function or the total scattering coefficient. The quantity (a+s) is represented as α the volume attenuation function or the total attenuation coefficient.

The scattering mechanism increases the population of the streaming packet of photons by having photons scattered into the direction of travel. Hence the equation becomes,

$$\frac{1}{v}\frac{D[N/n^2]}{Dt} = -\frac{\alpha N}{n^2} + \frac{N^*}{n^2} \tag{1.28}$$

where $$N^*(\bar{x}, \bar{\xi}, t) = \int_{\Xi} N(\bar{x}, \bar{\xi}', t)\, \sigma(x, \bar{\xi}', \bar{\xi}, t)\, d\Omega(\bar{\xi}') \tag{1.29}$$

defines the path function N* and introduces volume scattering function σ. Ξ is the set of all unity vectors (the unit sphere) in the space.

Light fields in the sea are in the steady state. Furthermore, the values of emission function are all zero. The index of refraction n, can be taken as fairly constant within the body of the sea. Therefore we can write,

$$\frac{dN}{dr} = -\alpha N + N^* \tag{1.30}$$

where $\frac{d}{dr} = \bar{\xi}.\nabla$ and $\bar{\xi} = (\frac{dx}{dr}, \frac{dy}{dr}, \frac{dz}{dr})$

The scattering function

$$s(x) = \int_{\Omega} \sigma(\bar{x}, \bar{\xi}, \bar{\xi}')d\Omega(\bar{\xi}') \tag{1.31}$$

and $\alpha(x) = a(x) + s(x)$.

The volume forward scattering function f(x) and volume backward scattering function b(x) are defined as,

$$f(\bar{x},\bar{n}) = \int_{\bar{\xi}.\bar{n} \geq 0} \sigma(\bar{x}, \bar{\xi}, \bar{\xi}')d\Omega(\bar{\xi}') \tag{1.32}$$

$$b(\bar{x},\bar{n}) = \int_{\bar{\xi}.\bar{n} \leq 0} \sigma(\bar{x}, \bar{\xi}, \bar{\xi}')d\Omega(\bar{\xi}') \tag{1.33}$$

and $s(\bar{x}) = f(\bar{x}) + b(\bar{x})$.

The volume attenuation function

$$\alpha = \frac{N^*}{N} - \frac{1}{N}\frac{dN}{dr} \tag{1.34}$$

If N^* is negligible when compared to $\frac{1}{N}\frac{dN}{dr}$ then,

$$\alpha = -\frac{1}{r}\ln\left(\frac{N_r}{N_o}\right) \tag{1.35}$$

where N_r is the radiance measured at r and N_o is the radiance at $r = 0$.

Similarly an expression can be obtained for σ the volume scattering function. Suppose that the radiance function in the integrand where zero for all directions $\bar{\xi}'$ in Ξ except over a subset Ξ_o of small solid angle $\Delta\Omega_o$ about $\bar{\xi}_o$ a representative direction. Furthermore, suppose that N over Ξ_o is uniform of magnitude $N_o(\bar{x}, \bar{\xi}_o)$. Then the corresponding function value $\Delta N^*(\bar{x},\bar{\xi})$ at $\bar{x}$ in an arbitrary direction $\bar{\xi}$ is related to $\Delta\Omega_o$ and $N_o(\bar{x}, \bar{\xi}_o)$ by the following special case of equation (1.29).

$$\Delta N^*(\bar{x},\bar{\xi}) = N_o(\bar{x}, \bar{\xi}_o)\ \sigma(\bar{x}, \bar{\xi}_o, \bar{\xi})\ \Delta\Omega_o \tag{1.36}$$

Therefore,

$$\sigma(\bar{x}, \bar{\xi}_o, \bar{\xi}) = \frac{\Delta N^*(\bar{x},\bar{\xi})}{N_o(\bar{x}, \bar{\xi}_o)\,\Delta\Omega_o} \tag{1.37}$$

The volume scattering function s(x) can be written in terms of scalar irradiance at $\bar{x}$. The scalar irradiance at $\bar{x}$ is defined as

$$h(\bar{x}) = \int_{\Xi} N(\bar{x},\bar{\xi})\, d\,\Omega(\bar{\xi}) \tag{1.38}$$

Therefore

$$h^*(\bar{x}) = \int_{\Xi} N^*(\bar{x},\bar{\xi})\, d\Omega(\bar{\xi}) \qquad (1.39)$$

$$= h(\bar{x})\, s(\bar{x})$$

or $$s(\bar{x}) = \frac{h^*(\bar{x})}{h(\bar{x})} \qquad (1.40)$$

An expression for the volume absorption function can be obtained using vector irradiance $\bar{H}$, which is defined as

$$\bar{H}(\bar{x}) = \int_{\Xi} \bar{\xi}\, N(\bar{x},\bar{\xi})\, d\Omega(\bar{\xi}) \qquad (1.41)$$

and $$a(\bar{x}) = \frac{-\nabla \cdot H(x)}{h(x)} \qquad (1.42)$$

A detailed treatment of the theory is given by Preisendorfer.[15]

1.5.2 Apparent Optical Properties

The definition of the apparent optical properties are based on the basic irradiance quartet. They are,

$$\begin{matrix} H(z,+) & h(z,+) \\ H(z,-) & h(z,-) \end{matrix} \qquad (1.43)$$

The '+' denotes upwelling and '-' denotes downwelling. The functions h and H are as defined in the preceding section. Further,

$$h(z,+) + h(z,-) = h(z).$$

The apparent optical properties and their expressions are given below.

The reflectance of the sea at depth z, with respect to downwelling flux at that level is

$$R(z,-) = \frac{H(z,+)}{H(z,-)} \tag{1.44}$$

Similarly,

$$R(z,+) = \frac{H(z,-)}{H(z,+)} = \frac{1}{R(z,-)} \tag{1.45}$$

The diffuse attenuation function for radiance is defined as

$$K(z,\bar{\xi}) = \frac{-1}{N} \frac{dN(z,\bar{\xi})}{dz} \tag{1.46}$$

The diffuse attenuation coefficient for upwelling (+) and downwelling (-) irradiance are defined as

$$K(z,\pm) = -\frac{1}{H(z,\pm)} \frac{dH(z,\pm)}{dz} \tag{1.47}$$

The diffuse attenuation coefficients for upwelling (+) and downwelling (-) scalar irradiance are defined as

$$k(z,\pm) = \frac{-1}{h(z,\pm)} \frac{dh(z,\pm)}{dz} \tag{1.48}$$

The distribution function for upwelling (+) and downwelling (-) flux at depth of z are given by

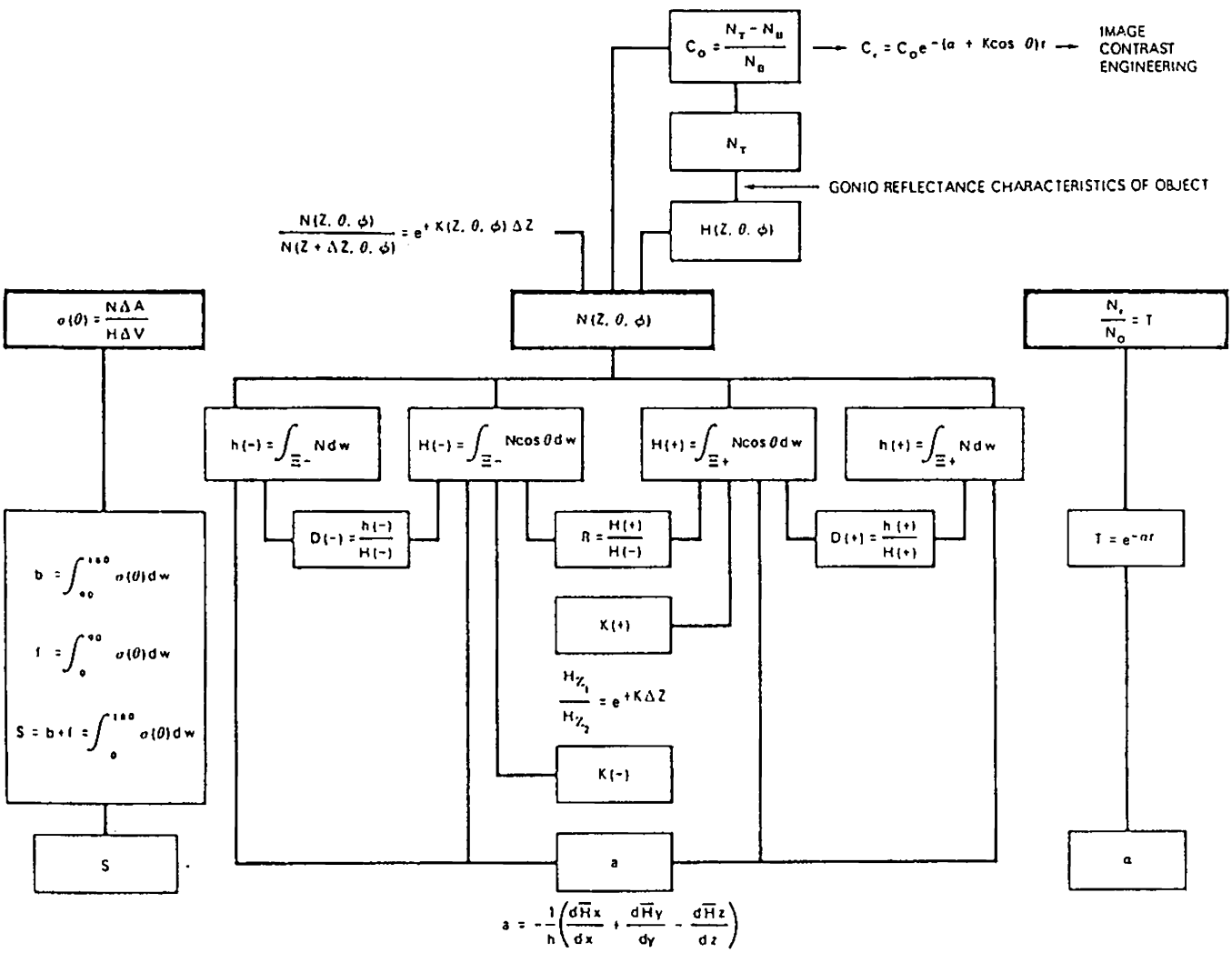

Fig.1.1 Interrelationships between major optical properties of sea water.

$$D(z,\pm) = \frac{h(z,\pm)}{H(z,\pm)} \tag{1.49}$$

This indicates the directional structure of the radiance distribution at z.

The interrelationships between these optical properties are illustrated in Fig.(1.1).

1.6 REVIEW OF EARLIER STUDIES ON OPTICAL ATTENUATION IN WATER

In this section, a brief review of the literature dealing with optical transmission studies in water is given. A review of the in situ studies on optical propagation in sea water is included in chapter 4.

One of the earliest reports in this field is by Hulburt[16] who measured the attenuation of distilled water and natural sea water throughout the visible region from 420 nm to 700 nm. The natural water was collected from Chesapeake Bay and Atlantic ocean. In their experiments a tungsten lamp was used as the source. The sample was taken in a 12 feet long tube of about 4 cm in diameter. The attenuation of water from bay showed very high value. The minimum value of attenuation for water from bay was 32×10^{-4} cm^{-1}, at wavelengths near 550 nm, while for distilled water they obtained a broad minimum in the region 480 nm to 550 nm whose attenuation was near to 5×10^{-4} cm^{-1}.

Curcio and Petty[17] investigated the near infrared absorption spectra of water. They observed five prominent peaks at 0.76, 0.97, 1.19, 1.45 and 1.94 μm in the range 0.7 to 2.5 μm for water at 20°C.

Sullivan[18] conducted a careful investigation of optical attenuation in distilled water, artificial sea water and heavy water using tungsten strip filament lamp as the source. The attenuation coefficient of distilled water and artificial sea water were determined for the region 790 to 580 nm and that of heavy water for the region 790 to 390 nm. He could not detect the absorption bands representing higher harmonics of fundamental frequency in the visible region.

Okoomian[19] studied the transmission characteristics of a frequency doubled Nd:glass laser in water. He measured the point source multipath irradiance function with respect to irradiance produced at extended range by intense pulse of radiation. Drummeter and Knestrich[20] reported the relative variation of attenuation coefficient with wavelength in distilled water and sea water for the region 375 to 685 nm with 0.02 nm resolution. They showed that there are no fine structure in attenuation spectrum of distilled water and sea water. In 1968 Irvine and Pollack[31] published results from a critical review of the existing literature on the optical properties of water for the 0.2 to 200 μm wavelength region. They tabulated

the values of both $k(\lambda)$, the extinction coefficient and $\alpha(\lambda)$, the Lambert absorption coefficient ($\alpha(\lambda) = 4\pi\, k(\lambda)/\lambda$). Zolotarev et al.[22] reported the values for the optical constants of water throughout the spectral region $1\text{-}10^6 \mu$ m. They determined both $k(\lambda)$ and $n(\lambda)$ from their measurements of $\alpha(\lambda)$ and reflectance $R(\lambda)$ for water at 25°C in the 2-50 μm region and measurements of internal reflectance spectra in the 2-10 μm region. From these measurements the values of $k(\lambda)$ were calculated, and $n(\lambda)$ were then obtained from a Kramers-Kronig analysis of $k(\lambda)$ spectrum. In 1973, Hale and Querry[23] published another review of the literature compiling a new set of values for $n(\lambda)$ and $k(\lambda)$.

Austin and Petzold[24] developed the concepts for the determination of α from the measurements of transmittance of radiance in a beam transmissometer. The different factors involved in the design of these instruments, the methods of calibration and the sources of error are discussed. Austin[25] studied the precision considerations in the determination of the volume attenuation coefficient α with transmissometers and found that the optimum measurements path length for such measurements which will minimize the error in α is equal to the length $1/\alpha$.

Laser was used as a source for absorption measurements by Hass and Davisson[26]. They adopted the laser adiabatic calorimetric method in which the rise in temperature due to the quantity

of heat generated because of the absorption is the measured parameter. They used an argon laser as the source and determined the attenuation coefficients at the wavelengths 488 nm and 514.5 nm.

Querry et al.[27] studied the attenuation of de-ionized filtered water using a tunable pulsed dye laser as the source. They introduced the split pulse laser method for measuring the attenuation. This is one of the very sensitive methods to study the attenuation of transparent liquids and is able to provide absolute values of the attenuation coefficient.

Tam and Patel[6] adopted the photoacoustic method to measure the absorption of water. This method has the advantage of being capable of detecting very weak absorption. They identified the fifth and sixth harmonious of O-H stretch in the visible region.

The inherent optical properties of Lake Ontario Coastal waters were studied by Bukata et al.[28] by the measurements of irradiance attenuation coefficient k(0), diffuse reflectance R(0) and total attenuation coefficient C. The inherent optical properties determined were, the forward scattering probability F, the backward scattering probability B, the scattering coefficient b and absorption coefficient a. They showed that F and B are spectrally invariant.

Tsubomura et al.[7] also studied the visible absorption spectrum of water. They searched for the higher overtones of O-H vibrations using specially designed spectrophotometer which they claim to have higher resolution than the photoacoustic method. They observed the fifth overtone at 523 nm. They concluded that the colour of the sea water is mostly because of absorption due to vibrational overtones perceptible to us by day-light reflected mostly from the bottom. Smith and Baker[29] determined the diffuse attenuation coefficient for irradiance, in the clearest natural water for the region 300 to 800 nm.

Wilson[30] reported the studies on the spreading of light beams in ocean water. He measured the irradiance distribution due to a laser beam and the radiance distribution due to a point source. Their results show that the distribution may by scaled as a function of the scattering length rather than attenuation length. Mercier et al.[31] proposed a dual beam method for measuring attenuation coefficient of sea water, in the visible region. They measured the attenuation coefficient of deionized filtered water. This method is similar to Querry's[22] split pulse laser method.

The relation between beam attenuation, chlorophyl and pheophitin pigment concentration and particle size distribution were studied by Kitchen et al.[32] They observed that the slope

of particle size distribution can be obtained if the slope of the beam attenuation spectra is known. They also concluded that chlorophyl and pheophytin pigment content cannot be effectively predicted by means of beam attenuation measurements.

Ramanov et al.[33] compared the refractive indices of distilled water and sea water with salinity 35‰ in the region 200 to 1100 nm and showed that they differ not more than 0.5% and the absorption of light by the precipitation water in this region does not exceed the absorption of light by sea water. The absorption coefficient of distilled water and sea water were determined by optoacoustic spectroscopy by Saizhen et al.[34] for the region 530 to 600 nm.

Serious efforts are being done in the development of underwater laser systems and in the development of lasers suitable for such systems. The use of laser as a carrier for underwater communication was demonstrated in the Adriatic Sea by Stojkovski.[35] A theoretical study on the feasibility of a communication link between earth stations and submarines via satellite was conducted by Shiekh.[36] The satellite was considered as a point source and applied Snell's law and Mie scattering theory to determine the focal plane intensity distribution when using an underwater detector.

Jha et al.[37] have developed an underwater laser communication receiver to be used by a submerged platform upto

a depth of 300 m. Their system is capable of receiving laser signals in the blue-green range transmitted from ground station and reflected via a satellite at 100 km height.

The search for a blue-green laser to suit the requirements of underwater optical systems have contributed two more lasers. The IF laser[38,40,41] which have five transitions in the region 478 to 497 nm can be operated at 70 kW peak power with pulse duration of 30 ns. The $HgBr_2$ dissociation laser[39] another proposed candidate for the applications laser in the wavelengths 502 and 504 nm.

PART II - LASER PROPAGATION IN TURBULENT MEDIUM

1.7 INTRODUCTION

The study of laser propagation through sea water will be complete only when laser propagation through turbulent medium is understood properly. The sea water being in random turbulent motion, there will be fluctuations in the temperature and salinity of sea water, both in space and time. This will introduce random variations in the refractive index of the medium, which affects the propagating optical beam.

Suppose we consider a light beam, traversing a medium with random fluctuations in its index of refraction. Because of the scattering of the light beam by the random fluctuations, there will be a spreading of the beam, beyond that normally caused by diffraction with a corresponding decrease in the beam intensity. In addition, there will be scintillations of the received intensity, a decrease in the spatial and temporal coherence or even in some cases, a distinct wander of the beam from position to position. These and other similar effects can seriously degrade the performance of a laser communication system.

Propagation through a turbulent medium refers to situations where a laser beam is propagating through a clear medium, with small fluctuations in the refractive index. These

small changes in the refractive index are related primarily to the small variations in temperature which are produced by the turbulent motion of the medium (either sea or atmosphere). While the refractive index variation from the mean value is small, in a typical situation of practical interest, a laser beam propagates through a large number of refractive index inhomogeneities and hence the cumulative effect can be very significant. These small inhomogeneities initially produce optical phase effects which in turn lead to angle of arrival fluctuations or beam wander, intensity fluctuations or scintillations and beam broadening.

One of the interesting facts about the history of the work related to laser propagation through turbulent media is that eventhough the first working laser was not announced until 1960, much of the necessary theoretical work and some of the experimental work had been done before that date. The two initial monographs in this field by Chernov[42] and Tatarskii[43] were both published in the Soviet Union before 1960. The reason for this is that, this topic is a sub-topic of a more general problem, ie., propagation of waves in a turbulent medium. This general topic includes a number of other practical applications such as propagation of star light through atmosphere, propagation of sound waves through atmosphere, propagation of radio waves through ionosphere and interplanetary space etc.

In this part of the chapter are included, a description about turbulence, Rytov theory of optical propagation through turbulent media and a discussion on the variance, power spectrum and probability distribution function of the intensity scintillations.

1.8 TURBULENCE

Hydrodynamical turbulence is one of the most enigmatic phenomena of macroscopic physics. It appears as a seemingly chaotic behaviour of flows of fluids when the relevant and only dimensionless parameter, the Reynolds number is sufficiently large, $R_e = v_o L/\nu \gg 1$ where v_o is typical velocity of flow, L is a characteristic length and ν is the molecular velocity. Practically all flows in nature and even in small scale laboratory conditions have very high Reynolds numbers ie., are turbulent. The turbulence is adequately described by the Navier-Stokes equation for the velocity field, $v(r,t)$

$$\frac{\partial \bar{v}}{\partial t} - [\bar{v} \times \bar{\omega}] = -\bar{\nabla}(P/\rho + \tfrac{1}{2}v^2) + \nu \nabla^2 \bar{v} \qquad (1.50)$$

where $\bar{\omega} = \text{curl}\ \bar{v}$ and P is the pressure. Experiments and linear analysis of stability show that upon reaching a certain critical value Re_{cr}, the flow of fluids becomes unstable to perturbations. The value of Re_{cr}, varies from one system to another and depends on many factors, such as geometry, nature of perturbations etc.,

when $Re \gg Re_{cr}$, the velocity and pressure fields at all points start to exhibit an obviously vortical nonstationary chaotic pattern. This phenomenon is referred to as turbulence.

It was considered as a mystery how the appearance of turbulence can be described by purely deterministic Navier-Stokes equation. The research of some of the earlier workers[44,45] show that transition to chaos is a most typical phenomenon in practically all nonlinear dissipative systems and is basically connected with rapid nonlinear accumulation of uncertainty introduced by inevitable interaction with outside factors. Thus the generation of chaos in systems with large number of degrees of freedom such as flows of fluids at large Reynolds numbers would hardly be seen as a miracle.

For a long time, turbulence had been seen as a purely chaotic phenomenon. Gradually, with the works of Taylor, it has been realized that turbulence is a very complicated and dual phenomenon. It contain vast areas of relatively quienscent vortical flow and smaller spots of violent, obstensibly chaotic behaviour embedded among quiescent areas. Moreover it turns out, that practically all turbulent flows contain so called large coherent structures, ie., large areas of seemingly correlated motion with a lifetime apparently exceeding their turnover time (ie., the time in which they have to pass their own length moving with their average internal velocity).

Some of the relevant problems in turbulence are discussed in detail by Levich[46].

1.9 OPTICAL PROPAGATION THROUGH TURBULENT MEDIUM

Most of the studies on the subject of optical propagation through a turbulent medium are conducted in the atmospheric case. The results of such studies are briefly described below.

We shall consider the effect on an optical wave of refractive index fluctuations caused by turbulent effects in the atmosphere. The refractive index fluctuations are primarily the result of small temperature fluctuations transported by the turbulent motion of the medium. The changes in refractive index caused by temperature fluctuations are usually smooth random functions of both space and time. A region of high or low refractive index can be thought of as an eddy which may behave very much as a lens. Thus the whole medium can be thought of as large number of random lenses having different shapes and scale sizes that move randomly through space. It is to be noted that the refractive index is varying within an eddy and no discontinuities in the refractive index are present.

The interaction of an electromagnetic wave with a single refractive index eddy is extremely weak. To first order there is no amplitude change at the position of eddy but merely

a phase change caused by the change in velocity of the small segment of the wave that traverses the eddy. Because the induced phase fluctuations are not same at different points perpendicular to the direction of propagation, they may cause focusing or defocusing effects, local deviations in the direction of wave propagation and through interference, irradiance fluctuation at the receiver. Since these eddies do not have sharp edges the reflections can be ignored. Though the effect of an individual eddy is quite weak, the cumulative effect of many eddies can be extremely strong.

The refractive index fluctuations that we are considering are those that result from naturally occurring random fluctuations due to the turbulent motion of the medium. Turbulence being a random process, it must be described in terms of statistical quantities. Kolmogorov[47] when considering the time variation of the difference of two velocities at two points in space separated by a displacement vector $\bar{r}$ found that the mean square velocity difference could be described by a universal form over a broad range of spatial scale sizes of motion. He defined a structure tensor,

$$D_{ij}(\bar{r}) = \left\langle [v_i(\bar{r}_1+\bar{r}) - v_i(\bar{r}_1)]\,[v_j(\bar{r}_1+\bar{r}) - v_j(\bar{r}_1)] \right\rangle \qquad (1.51)$$

v_i and v_j refer to different components of the velocity and the angle brackets indicate an ensemble average. Two further

assumptions greatly simplify equation (1.51): 1) Assumption of local homogeneity which implies that the velocity difference statistics depends only on the displacement vector $\bar{r}$. 2) The assumption of local isotropy which implies that only the magnitude of $\bar{r}$ is important.

Kolmogorov[47] found that as long as the separation $\bar{r}$ lay in the inertial subrange of turbulence the structure function D_{rr} of the velocity component parallel to the displacement $\bar{r}$ can be written as

$$D_{rr} = C_v^2 r^{2/3} \tag{1.52}$$

where C_v^2 is the structure constant, a measure of the total amount of energy in the turbulence. This relation is valid for values of r between the microscale of turbulence l_o and the outer scale of turbulence L_o. The microscale corresponds to the eddy size below which the dissipation of energy in the eddy through viscous effects becomes important. The outer scale corresponds to the largest scale size for which the eddies may be considered isotropic.

It can be shown[48] that the two-thirds law is valid for the refractive index structure function also.

$$D_n(r) = C_n^2 r^{2/3} \tag{1.53}$$

where $D_n(r) = \langle (n(\bar{r}_1+\bar{r}) - n(\bar{r}_1))^2 \rangle$ (1.54)

and C_n^2 is the refractive index structure constant.

It should be noted that the structure constant is not really a constant but a function of both time and space. It is a coefficient which describes the strength of refractive index turbulence.

1.10 POWER SPECTRAL DENSITY OF REFRACTIVE INDEX FLUCTUATION

We can write the refractive index as the sum of a mean plus a fluctuating part

$$n(\bar{r}) = \langle n(\bar{r}) \rangle + n_1(\bar{r}) \tag{1.55}$$

where $\langle n_1(\bar{r}) \rangle = 0.$

The variable $n_1(r)$ can be decomposed in terms of a three dimensional Fourier-Stieltjes integral

$$n_1(\bar{r}) = \int dN(\bar{K}) e^{i\bar{K}.\bar{r}} \tag{1.56}$$

where $\bar{K} = (K_x, K_y, K_z)$ is the three dimensional spatial wave number and dN is the random spectral amplitude. Now we consider the covariance function of the refractive index field at two positions separated by $\bar{r}$.

$$B_n(\bar{r}_1 + \bar{r}, \bar{r}_1) = \langle n_1(\bar{r} + \bar{r}_1) n(\bar{r}_1) \rangle \tag{1.57}$$

Using equation (1.56), the covariance function can be rewritten as

$$B_n(\bar{r}_1 + \bar{r}, \bar{r}_1) = \iint e^{i\bar{K}.(\bar{r} + \bar{r}) - i\bar{K}'\bar{r}'} \langle dN(K) dN^*(K') \rangle \tag{1.58}$$

Since a statistically homogeneous random field cannot have its average properties depend upon the location in the field at which the average is computed, the same results should be obtained if we translate our sensors to any other position in the field and perform the same operation. ie., $B_n(\bar{r}_1 + \bar{r}, \bar{r}_1) = B_n(\bar{r})$. The double integral in (1.58) will depend only upon $\bar{r}$ and the quantity in the angular brackets must satisfy the relation

$$\langle dN(K) dN^*(K') \rangle = \delta(\bar{K} - \bar{K}') \Phi_n d^3\bar{K} d^3\bar{K}' \tag{1.59}$$

where δ is the three dimensional Dirac delta function and $\Phi_n(K)$ is the three dimensional spectral density of the refractive index fluctuations. Substituting and performing the $\bar{K}'$ integration, we obtain the Fourier transform relation between spectral density and covariance function.

$$B_n(\bar{r}) = \int d^3\bar{K}\, e^{i\bar{K}.\bar{r}}\, \Phi_n(\bar{K}) \tag{1.60}$$

and

$$\Phi_n(\bar{K}) = \frac{1}{(2\pi)^3} \int d^3\bar{r}\, B_n(\bar{r}) e^{-i\bar{K}.\bar{r}} \tag{1.61}$$

Using the assumption of homogeneous isotropic turbulence the spectral density Φ_n in terms of Kolmogorov's inertial subrange model can be written as

$$\Phi_n(K) = \frac{5}{18\pi} C_n^2 K^{-3} \int_{l_o}^{L_o} dr \sin(Kr) r^{-1/3} \tag{1.62}$$

If we let the limits go to 0 to ∞ then it becomes

$$\Phi_n(K) = 0.033 C_n^2 K^{-11/3} \tag{1.63}$$

which is valid for $2\pi L_o^{-1} \ll K \ll 2\pi l_o^{-1}$. For eddy sizes less than the microscale of turbulence l_o, the energy of the turbulence is dissipated due to viscosity effects. In this region, the spectrum falls off more rapidly than $K^{-11/3}$. A different model that accomplishes this, was described by Tatarskii[49], that is

$$\Phi_n(K) = 0.033 C_n^2 K^{-11/3} \exp(-K^2/K_m^2) \tag{1.64}$$

where $K_m = 5.92/l_o$.

The spatial spectrum of the refractive index fluctuations in turbulent fluids, were studied in detail by Hill. He has considered the fluctuations not only due to temperature fluctuations in air and liquids but also those arising from humidity fluctuations in air and salinity fluctuations in water.[50-52]

1.11 RYTOV THEORY OF OPTICAL PROPAGATION IN TURBULENT MEDIUM

The theory of line of sight propagation through the atmosphere and other random media were extensively studied by various workers. The early works of Chernov[42] and Tatarskii[40] solved the wave equation directly using perturbation techniques. There were other approaches also to the problem put forward by Lee and Harp[53] and Fante[54]. Here we adopt Tatarskii's approach and assume that a plane wave is incident upon the random medium and consider the resultant fluctuations of amplitude and phase only. This is based on Rytov approximation which had a much greater range of validity than the earlier used geometric optics method.

The electric field $\bar{E}$ of a narrow band beam propagating in a random medium is governed by the Maxwell wave equation

$$\nabla^2\bar{E} + k^2(1+n_1)^2\bar{E} - \nabla(\nabla.\bar{E}) = 0 \qquad (1.65)$$

It can be shown that[55,56] the last term of the equation which represents depolarization effects is negligible. Consequently, it can be written as

$$\nabla^2\bar{E} + k^2(1 + n_1)^2\bar{E} = 0 \qquad (1.66)$$

We next write

$$\bar{E} = \exp(\psi) = \exp(\chi + iS) \qquad (1.67)$$

Substituting we get

$$\nabla^2\psi - (\nabla\psi)^2 + k^2(1 + n_1)^2 = 0 \qquad (1.68)$$

In the Rytov method ψ is next written as $\psi = \psi_0 + \psi_1$, (ψ_0 is the non-fluctuating part of ψ and ψ_1 is the random component) where ψ_0 satisfies

$$\nabla^2\psi_0 + (\nabla\psi_0)^2 + k^2 = 0 \qquad (1.69)$$

If we substitute $\psi = \psi_0 + \psi_1$ in (1.68), use (1.69), and then neglect $|\nabla\psi_1|$ in comparison with $|\nabla\psi_0|$ and n_1^2 in comparison to $2n_1$ it is found that ψ_1 satisfies

$$\nabla^2\psi_1 + 2\nabla\psi_0\cdot\nabla\psi_1 + 2k^2 n_1 = 0 \qquad (1.70)$$

which has a solution $\psi_1 = \chi_1 + iS_1$ given by

$$\psi_1(\bar{r}) = \frac{k^2}{2\pi E_0(r)} \int_V d^3\bar{r}'\, n(\bar{r}')E_0 \frac{\exp(ik|\bar{r}-\bar{r}'|)}{|r-r'|} \qquad (1.71)$$

where $E_0 = \exp(\psi_0)$

This equation states that the scattered field observed at $\bar{r}$ is that due to a spherical wave emitted at $\bar{r}'$, ie., $|\bar{r}-\bar{r}'|^{-1} \exp[ik(\bar{r}-\bar{r}')]$, whose amplitude is proportional to the product of the local refractive index fluctuation $n_1(\bar{r}')$, and the

strength of the incident radiation and whose phase is determined by the total number of wavelengths along the path from source to scatter to receiver. We then integrate these contributions from all points $\bar{r}'$ over the entire scattering volume v.

The assumption that $|\nabla\Psi_1| << |\nabla\Psi_0|$ leads to an important restriction on the range of validity of Rytov method. When this method was first developed it appeared to give quite good agreement with all the available experimental data, which had been taken over propagation paths of less than 1 km in the atmosphere. Experiments performed using horizontal paths much greater than 1 km showed that the experimental data deviated significantly from the predictions made using the Rytov method. In particular, it was found that if the propagation path L is such that the parameter $\sigma_R^2 = 1.23\, k^{7/6} C_n^2 L^{11/6}$ is greater than 0.3, then the Rytov approximation is invalid. It was soon recognized that because the Rytov approximation is equivalent to the scatter of the incident wave by a series of random phase screens[53], it did not adequately account for multiple scatter of the electromagnetic wave by the turbulent eddies. This spurred attempts to develop new theories which properly included multiple scatter and led to various other approaches[57].

1.12 INTENSITY SCINTILLATIONS

If we measured the intensity of a laser beam in the plane L, in a turbulent medium, we would find that the measured

value of I would fluctuate with time, about its average value $\langle I \rangle$. It is desirable to be able to predict the magnitude of the intensity scintillations, since this is an important consideration in the design of any receiver system. The various experimental data[58] available on the intensity scintillation show that the theory is complete only for very low strengths of turbulence. The expression for the variance of log-intensity (which is usually the measured quantity) for a plane wave as given by Lawrence and Strohbehn[59] calculated by Rytov method is

$$\sigma_R^2 = 1.23\, C_n^2\, k^{7/6} L^{11/6} \qquad (1.72)$$

Experiments showed that the relation is valid only for the region $\sigma_R^2 << 1$ which is known as the weak turbulence region. As the C_n^2 or the path length L is increased, it was found that the variance $\sigma_{\ln I}^2$ (measured) saturates at about 1, and certain authors even noted a decrease in the variance beyond 1. This region is called saturation region or strong turbulence region.

Physically, the reason for the failure of Rytov method is that it does not properly account for the fact that the incident wave becomes more and more incoherent as it propagates into the medium. Thus the turbulent eddies are not scattering a coherent wave, but a partially coherent wave.

1.13 TEMPORAL POWER SPECTRUM OF SCINTILLATIONS

In some applications, it is desirable to know the frequency spectrum of intensity fluctuations of a light beam propagated through a turbulent medium. The frequency spectrum of the intensity fluctuations, are caused by the motion of the medium. This motion is because of 1) the mean motion of the eddies, 2) the changes in the direction of motion and 3) the internal mixing motion due to the evolution of turbulence. Tatarskii[43,49] had studied these effects theoretically in detail for the atmospheric turbulence. Under Taylor's hypothesis of frozen 'turbulence' the temporal variations of some quantity measured at a point are caused by the motion of the atmosphere past the point and that the internal motions of the medium may be neglected. For propagation problems it is assumed that the only motion of interest is perpendicular to the path.

Under Taylor's hypothesis,

$$\chi(\bar{r}, t+\tau) = \chi(\bar{r}-\bar{v}_{\perp}\tau, t) \tag{1.73}$$

where $v_{\perp}$ is the average velocity component perpendicular to the path. The autocorrelation function is

$$R_{\chi}(\tau) = \langle \chi(\bar{r}, t+\tau)\ \chi(\bar{r}, t) \rangle \tag{1.74}$$

$$= B_{\chi}(v_{\perp}, \tau)$$

The definition of the frequency spectrum,

$$W_\chi(f) = 4\int_0^\infty \cos(2\pi f\tau) R_\chi(\tau)\, d\tau \qquad (1.75)$$

$$= 4\int_0^\infty \cos(2\pi f\tau) B_\chi(v_\perp \tau)\, d\tau$$

gives the general relation between the spatial covariance function $B_\chi(\rho)$ and frequency spectrum $W_\chi(f)$ under the assumption of frozen turbulence.

Tatarskii evaluated the frequency spectrum for a plane wave propagating through a medium with a refractive index spectrum given by equation (1.64). His results show that

$$W_\chi(f) = 0.15\langle\chi^2\rangle \frac{1}{f_o}(1 + 0.48\,\Omega^{4/3} + \ldots) \text{ for } \Omega \ll 1 \qquad (1.76)$$

and

$$W_\chi(f) = 1.14\langle\chi^2\rangle \frac{\Omega^{-8/3}}{f_o} \quad \text{for } \Omega \gg 1 \qquad (1.77)$$

where $f_o = v_\perp/(2\pi\lambda L)^{1/2}$ and $\Omega = f/f_o$

In summary Tatarskii concluded that for the case where the standard deviation for the wind speed $\sigma \ll v_\perp$ these relations hold and the spectral peak is at $f = f_o$. For $\sigma \sim v_\perp$ the maximum of the spectrum begins to move towards zero and for $\sigma \gg v_\perp$ the maximum begins to grow.

1.14 PROBABILITY DISTRIBUTION FUNCTION

The form of the probability distribution of the irradiance fluctuations of an optical wave propagating in a turbulent medium is a matter of controversy especially in the saturation region. In the region of weak fluctuations, both theoretical work and experimental results seem to support the log-normal probability distribution while in the saturation region, the results are confusing. A review of the state of art of the subject is given by Strohbehn et al.[60]

Let us assume that the wave propagates in the x direction and hence $E = U \exp(ikx)$. When the wave passes through a random medium part of the incident energy is scattered by the irregularities of the random medium. There are two different geometrical situations which lead to different predictions for the probability distribution.

1.14.1 Rice-Nakagami or Rayleigh Distribution

Consider the case where the wave is incident on a thin slab and the receiver is far from the slab. Then we can write

$$u_r = v_d + v_r + iv_i$$

where v_i is the average field and v_r and v_i are random variables. Assume that the field at the receiver is the sum of a large number

of waves scattered from different regions in the slab and that the dielectric constants in the physically different regions are uncorrelated. If we define A as the amplitude of the wave, ie.,

$$A = |E| = (v_d^2 + 2v_d v_r + v_r^2 + v_i^2)^{\frac{1}{2}} \tag{1.78}$$

Thus if v_r and v_i are Guassian random variables, it can be shown that[61,62], A follows Rice-Nakagami distribution.

$$p(A) = (2A/\sigma^2)\exp[-(A^2 + v_d^2)/\sigma^2] \; I_o \; (2Av_d/\sigma^2) \tag{1.79}$$

where $\sigma^2 = \langle v_r^2 \rangle + \langle v_r^2 \rangle = 2\langle v_r^2 \rangle = 2\langle v_i^2 \rangle$ and I_o is the modified Bessel function.

Note that $\langle I \rangle = \langle A^2 \rangle = v_d^2 + \sigma^2$ If $v_d^2 = 0$, then equation (1.79) reduces to Rayleigh distribution,

$$p(A) = (2A/\sigma^2)\exp(-A^2/\sigma^2) \tag{1.80}$$

Normally we work with intensity $I = A^2$ and the distribution becomes,

$$p(I) = (1/\sigma^2)\exp[-(I + v_d^2)/\sigma^2] \quad I_o[2v_d(I)^{\frac{1}{2}}/\sigma^2] \tag{1.81}$$

and Rayleigh distribution in amplitude reduces to exponential distribution in intensity

$$p(I) = (1/\sigma^2)\exp(-I/\sigma^2) \tag{1.82}$$

These are the distributions we expect for a thin scattering layer and the receiver at some distance from it.

1.14.2 Log-normal Distribution

When the receiver is located in the turbulent medium, the received field is the result of multiplicative effects instead of additive effects. To understand this situation, consider the turbulent medium as composed of a large number of independent slabs, (ie., the thickness of each slab is large compared to outer scale length of turbulent medium) oriented perpendicular to the direction of propagation. Since the received field is the product of the incident field times a number of independent multiplication terms, the application of the central limit theorem to the logarithm of the field leads to a prediction of log-normal probability distribution.

$$p(I) = \left[1/I(2\pi)^{\frac{1}{2}}\,\sigma_{\ln I}\right] \exp\left[-(\ln I - \overline{\ln I})^2/2\,\sigma^2_{\ln I}\right] \tag{1.83}$$

The condition for log-normal distribution to be valid is that the multiple scattering should be considered in such a way that large angle scattering is ignored. This condition is met in Rytov method.

Several other distributions were put forwarded by different authors. Wang and Strohbehn[63] proposed a distribution

for the saturation region, where neither log-normal nor Rice-Nakagami distribution can be strictly true theoretically. For long path or for strong turbulence the large angle multiple scattering cannot be neglected. Hence both multiplicative and additive effects are important. The perturbed log-normal distribution which they proposed is a combination of both log-normal and Rice-Nakagami. Clifford and Hill[64] suggested the k distribution for scintillation in the region of maximum variance.

The propagation characteristics of optical beam will also help us in understanding the phenomena of turbulence and its characterisation.

The details of the experiments on laser propagation through laboratory simulated turbulent medium and its results are described in chapter 5.

REFERENCES

1. R.Carrington, 'A Biography of the Sea', (Chatto & Windus, London, 1960), p.29.

2. P.Groen, 'The Waters of the Sea', (Van Nostrand Reinhold Company, London, 1969), p.40.

3. G.L.Clarke in 'Oceanography', Ed. R.Gordon Prie, (Oxford University Press, 1973), p.218.

4. L.R.Painter, R.D.Birkhoff and E.T.Arakawa, J.Chem.Phys., 51, 243 (1969).

5. B.R.Henry in 'Vibrational Spectra and Structure', (Elsevier, NY, 1981), Vol.10, p.269.

6. A.C Tam and C.K.N.Patel, Appl.Opt., 18, 3348 (1979).

7. H.Tsubomura, N.Yamamoto, N.Matsuo and Y.Okada, Proc.Japan Acad., 56, Ser B, 403 (1980).

8. Lord Rayleigh, Phil.Mag., 47, 375 (1899).

9. Lord Rayleigh, Proc.Roy.Soc., 97, 435 (1920).

10. J.Cabannes, J.Phys., 6, 129 (1920).

11. M.Smoluchowski, Ann.Physik., 25, 205 (1908).

12. A.Einstein, Ann.Physik., 33, 1275 (1910).

13. R.J.Strutt, Proc.Roy.Soc., 95, 155, (1918).

14. G.Mie, Ann.Physik., (4), 25, 377 (1908).

15. R.W.Preisendorfer in 'Light in the Sea', Ed.J.E.Tyler, (Dowden, Hutchinson & Ross Inc., Stroudsburg, 1977), p.46.

16. E.O.Hulburt, J.Opt.Soc.Am., 35, 698 (1945).

17. J.A.Curcio and C.C.Petty, J.Opt.Soc.Am., 41, 302 (1951).

18. S.A.Sullivan, J.Opt.Soc.Am., 53, 962 (1963).

19. H.J.Okoomian, Appl.Opt., 5, 1441 (1966).

20. L.F.Drummeter Jr.and G.L.Knestrick, Appl.Opt., 6, 2101 (1967).

21. W.M.Irvine and J.B.Pollack, Icarus, 8, 324 (1968).

22. V.M.Zolotarev, B.A.Mikhailov, L.I.Aperovich and S.I.Popov, Opt.Spektrosk., 27, 790 (1960) (Opt.Spectrosc., 27, 430, (1969)).

23. G.M.Hale and M.R.Querry, Appl.Opt., 12, 555 (1973).

24. R.W.Austin and T.J.Petzold in 'Light in the Sea', Ed. J.E.Tyler (Dowden, Hutchinson & Ross, Inc., Stroudsburg, 1977), p.104.

25. R.W.Austin, ibid., p.121.

26. M.Hass and J.W.Davisson, J.Opt.Soc.Am., 67, 622 (1977).

27. M.R.Querry, P.G.Cary, and R.C.Waring, Appl.Opt., 17, 3587 (1978).

28. R.P.Bukata, J.H.Jerome, J.E.Bruton and S.C.Jain, Appl.Opt., 18, 3926 (1979).

29. R.C.Smith and K.S.Baker, Appl.Opt., 20, 177 (1981).

30. W.H.Wilson, Proc. SPIE (USA), 208, 64 (1979).

31. H.Mercier, F.Gaillard, J.Cariou and J.Lotrian, J.Phys.D., 15, 563 (1982).

32. J.C.Kitchen, J.R.V.Zaneveld and H.Pak, Appl.Opt., 21, 3913 (1982).

33. N.P.Ramanov and V.S.Shuklin, J.Sov.Laser Res. (USA), 5, 75 (1984).

34. Wei Saizhen, Cai Shaufu, Ying Xiaohong and Cheng Gensong, J.Zhejiang Univ. (China), 18, 72 (1984).

35. G.Stojkovski, Proc.SPIE (USA), 164, 77 (1978).

36. M.A.Sheikh, Canadian Communications and Energy Conference, Montreal, Que, Canada, 13-15 Oct. 1982, (New York, USA, IEEE,1982), p.269.

37. B.B.Jha, V.Rajendran, A.Jhunjhunwala and M.Mukunda Rao, J.Opt. (India), 15, 79 (1986).

38. M.L.Dlabal, S.B.Hutchinson, J.G.Eden and J.T.Verdeyen, 33rd Annual Gaseous Electronics Conference; Program and Abstracts Norman OK, USA (7-10 Oct. 1980) (Norma, OK, USA: Univ. Oklahoma, 1980), p.63.

39. R.Burhnham and W.T.Whitney, ibid., p.64.

40. N.G.Basov, V.S.Zuev, L.D.Mikheev and V.I.Yalovoi, Sov.J.Quant. Electron. (USA), 12, 674 (1982).

41. N.G.Basov, V.S.Zuev, L.D.Mikheev, Yu.Yu.Stoilov, Bull.Acad. Sci. USSR.Phys.Ser.(USA), 46, 62 (1982).

42. L.A.Chernov, 'Wave Propagation in a Random Medium', (Mc Graw-Hill, New York, 1960).

43. V.I.Tatarskii,'Wave Propagation in a Turbulent Medium', (Mc Graw-Hill, New York, 1961).

44. E.N.Lorentz, J.Atmos.Sci., 19, 39 (1962).

45. J.P.Eckman and D.Ruelle, Rev.Mod.Phys., 57, 617 (1985).

46. E.Levich, Phys.Reports, 151, 129 (1987).

47. A.Kolmogorov, in 'Turbulence, Classical Papers on Statistical Theory', Ed. S.K.Friedlander and L.Topper (Interscience, New York, 1961), p.151.

48. S.F.Clifford in 'Laser Beam Propagation in the Atmosphere', Ed. J.W.Strohbehn, (Springer Verlag, Berlin, 1978), p.13.

49. V.I.Tatarskii, 'The Effects of Turbulent Atmosphere on Wave Propagation' (National Technical Information Service, Springfield, Va, 1971)-TT-68-50464.

50. R.J.Hill, Radio Sci., 13, 953 (1978).

51. R.J.Hill, J.Opt.Soc.Am., 68, 1067 (1978).

52. R.J.Hill and S.F.Clifford, J.Opt.Soc.Am., 68, 892 (1978).

53. R.W.Lee and J.C.Harp, Proc.IEEE, 57, 375 (1969).

54. R.L.Fante, IEEE Trans., AP-21, 750 (1973).

55. J.W.Strohbehn and S.F.Clifford, IEEE Trans. AP-15, 416 (1967).

56. E.Collet and R.Alferness, J.Opt.Soc.Am., 62, 529 (1972).

57. J.W.Strohbehn, 'Laser Beam Propagation in the Atmosphere' (Springer-Verlag, Berlin, 1978), pp.45-106.

58. M.E.Gracheva, A.S.Gurvich, S.S.Kashkarov and VI.V.Pokasov, ibid., pp.107-127.

59. R.S.Lawrence and J.W.Strohbehn, Proc.IEEE, 58, 1523 (1970).

60. J.W.Strohbehn, T.I.Wang and J.P.Speck., Rad.Sci., 10, 59 (1975).

61. P.Beckman, 'Probability in Communication Engineering', (Harcourt, Brace and Lored, New York, 1967), p.511.

62. K.A.Norton, L.E.Vogler, W.V.Mansfield and P.J.Short, Proc. IRE, 43, 1354 (1955).

63. T.I.Wang and J.W.Strohbehn, J.Opt.Soc.Am., 64, 994 (1974).

64. S.F.Clifford and R.J.Hill, J.Opt.Soc.Am., 71, 112 (1981).

Chapter 2

FABRICATION OF A PULSED DYE LASER

Abstract

The chapter describes the fabrication details of a nitrogen laser pumped dye laser. The working mechanism of a dye laser and the various processes of excitation and de-excitation in a dye molecule is described. A review of development in the design of pulsed dye lasers is given. The various parts of the fabricated dye laser system are explained followed by the details of the parametric studies. A line width of 0.04 nm, and divergence of 0.31 mrad are achieved.

2.1 INTRODUCTION

Dye lasers have become an important tool in many areas of laser research and applications because of its continuous tunability and wide spectral range. The field of dye laser has progressed rapidly since its discovery by Sorokin and Lankard[1] in 1966. Sophisticated dye laser systems with a wide range of specifications are now commercially available.

Dye lasers can be operated both in continuous wave (CW) mode and pulsed mode. CW dye lasers are pumped by CW argon ion or krypton ion lasers. It is tunable over the range 360 to 1000 nm. Pulsed dye lasers are pumped by nitrogen laser (λ= 337.1 nm), Nd:YAG laser (1064 nm) and its harmonics (532 nm, 355 nm, 266 nm) or flash lamps. The wavelength of dye laser ranges from the near UV at 310 nm to the near IR, 1285 nm, which can be extended further into the UV and IR by frequency mixing in nonlinear optical materials.

The choice of the pump source depends on the requirements of the dye laser pulse. Copper vapour lasers are used as the pumping source where high repetition rate pulses (of the order of kilohertz) are required. In low repetition rate cases, Nd:YAG, excimer or nitrogen lasers are chosen as the pump source. Sorokin and Lankard[2] had demonstrated the use of flash lamps as pump sources for dye lasers. Eventhough flash lamps allow simple

design of dye lasers, their short lifetime for operation at high repetition rate made it uneconomical. Because of the simple construction and easiness, the nitrogen laser is very commonly used as a pump source since the first report of nitrogen laser pumped dye laser by Meyer et al.[3] A simple medium power nitrogen laser when used as the pump source, can give dye laser pulses of nanosecond duration and very small line width.

The fluorescence spectrum of a dye is generally very broad ($\backsim$10-50 nm). The peak of the fluorescence band can be changed (coarse tuning) by changing the solvent and concentration of the dye solution. But most of the experiments, in which dye lasers are used, require spectrally narrow and tunable light sources. This is achieved by using a frequency selective component inside the resonator. The spectral narrowing in dye laser was first realised by Soffer and Mc Farland[4] by replacing one of the plane mirrors of the resonator with a diffraction grating. They found that the spectral width narrowed from 6 nm to 0.06 nm, while the output energy was 70% of the initial energy. Since then different techniques for spectral narrowing and tuning have been developed for dye lasers.

The minimum possible linewidth achievable in a pulsed dye laser is limited by the Fourier transform limit imposed by the pulse duration. For a 5 ns pulse (FWHM) duration, this is

about 30 MHz. In CW dye lasers, working in single mode, linewidth of the order of 1 MHz have been obtained. Recently, single mode operation is reported in Nd:YAG laser pumped dye laser by Littmann.[5]

2.2 PROPERTIES OF LASER DYES

Organic compounds can be divided into saturated and unsaturated compounds. The unsaturated compounds are those which contain atleast one double or triple bond. When two double bonds are separated by a single bond, the two double bonds are called conjugated. The term dye is usually used in a wider sense, so as to encompass all substances containing conjugated double bonds. All dyes absorb light at wavelengths above 200 nm. The basic mechanism responsible for light absorption by compounds containing conjugated double bonds is the same.

The energy levels of a typical dye molecule in a solution consist of a manifold of singlet electronic states $S_o, \ldots S_n$ and triplet states $T_1, \ldots T_n$. The five important levels required for the description of the dye laser are shown in Fig.(2.1). The optical absorption and radiative emission processes are denoted by straight arrows. The radiative emission from singlet state is fluorescence and that from triplet state is phosphorescence. The internal conversion (IC) between

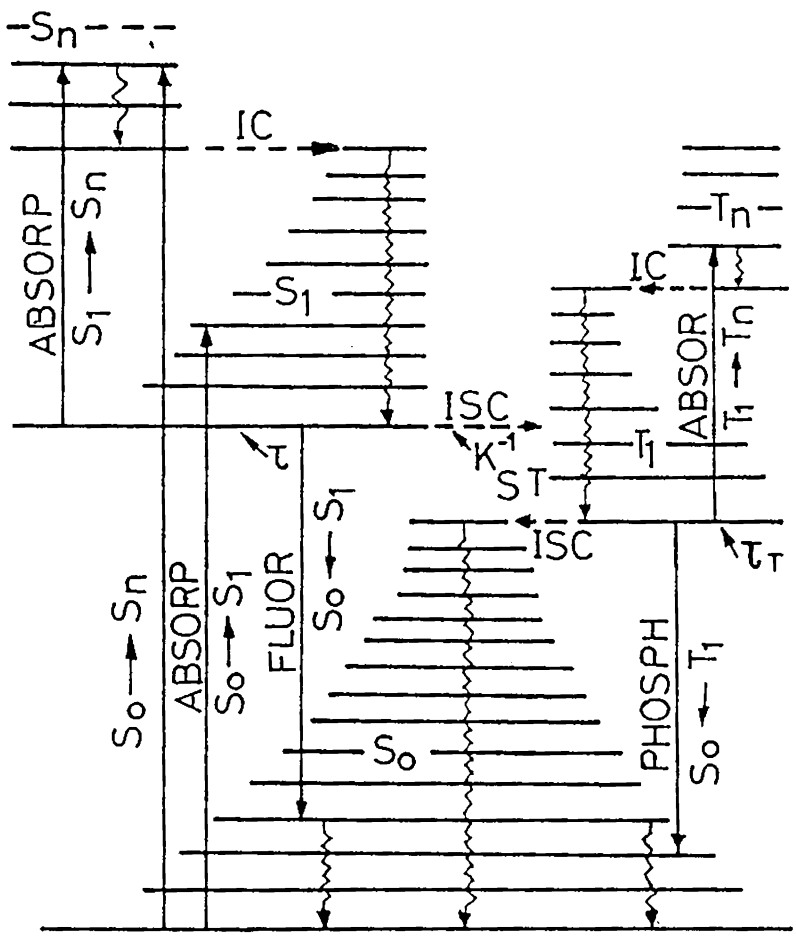

Fig.2.1 Energy levels of a dye molecule.

states of same multiplicity and inter system crossing (ISC) between states of different multiplicity are also indicated in the figure.

Each electronic state has a number of vibrational levels superimposed on it. Each vibrational level is further split into rotational levels. These rotational levels are broadened by frequent collisions with the solvent molecules and form a continuum between the vibrational levels. This gives rise to the broad absorption and emission bands in the electronic spectra of dye molecule in solution. At room temperature, most of the molecules will be in the lowest vibrational level of S_o. In the absorption process, depending on the wavelength of excitation, the molecules may be excited to various vibrational levels of first excited state S_1 or higher excited state S_n $(n > 1)$. In the case of laser dyes pumped by UV sources, the molecules are excited to higher excited state S_n.

The molecular absorption cross section $\sigma^o(\lambda)$ is defined by the relation

$$I(1, \lambda) = I(0, \lambda) \exp[-\sigma^o(\lambda) N l] \qquad (2.1)$$

where $I(0, \lambda)$ is the incident intensity on the sample of length l, N is the molecular concentration and $I(1, \lambda)$ is the transmitted intensity.

De-excitation of the excited dye molecule can occur through fluorescence emission or through non-radiative processes. The probability for the different types of de-excitation processes is determined by the structure of the dye and properties of solvent used.[6] From the higher excited singlet states S_n, there occurs rapid non-radiative transitions (internal conversions) to S_1, in about 10^{-11} to 10^{-12} seconds. Again in the S_1, the vibrational relaxation occurs in times of the order of picoseconds.[7] Since the lifetime of S_1 is of the order of nanoseconds (usually within one nanosecond), most of the molecules excited to higher excited states will relax to lower vibrational levels of S_1.

Fluorescence (and hence the stimulated emission) takes place from the lowest vibronic level of S_1, to various vibrational rotational levels of S_o in accordance with Frank-Condon principle. From here fast vibrational relaxation brings the molecule back to the lowest vibronic level of S_o. Therefore the dye laser can be considered as a true four level system with all the four levels lying in the singlet manifold.

But in practice, this is not the case. There are certain other important processes involved in the mechanism. They are the intersystem crossing from $S_1 \longrightarrow T_1$, and subsequent $T_1 \longrightarrow T_n$ absorption at pump or laser wavelengths. Another process is the excited state absorption from $S_1 \longrightarrow S_n$, which may also occur at pump or laser wavelengths. All these processes influence the performance of the dye laser.

The stimulated emission cross section $\sigma_s(\lambda)$ is defined by the relation[8]

$$\sigma_s(\lambda) = \frac{\lambda^4 E(\lambda)}{8\pi\tau c\eta^2} \tag{2.2}$$

where $E(\lambda)$ is the fluorescence line shape function normalized such that

$$\int_0^\infty E(\lambda)d\lambda = Q_F \tag{2.3}$$

Q_F is the fluorescence quantum efficiency, η is the refractive index of the dye solution at wavelength λ and τ is the fluorescence lifetime (observed lifetime of the S_1 state in the absence of stimulated emission). $E(\lambda)$ is obtained from the fluorescence spectrum of a very dilute solution of the dye.

In the absence of non-radiative processes $\tau = \tau_r$ where τ_r is the radiative lifetime of the S_1 state. This is defined as the reciprocal of the radiative transition probability which is Einstein A coefficient summed over the complete fluorescence spectrum.[7]

If K_{SS} is the rate of internal conversion and K_{ST} the rate of intersystem crossing, then the fluorescence lifetime

$$\tau = \frac{1}{K_{SS} + K_{ST} + 1/\tau_r} \qquad (2.4)$$

and $$Q_F = \tau/\tau_r \qquad (2.5)$$

Thus finite values of K_{SS} and K_{ST} decrease the fluorescence quantum efficiency. Intersystem crossing, in addition, populates the triplet states and results in subsequent $T_1 \longrightarrow T_n$ absorption. This causes severe losses in dye lasers.

The gain coefficient of dye laser medium at wavelength λ (in the absence of external losses) is defined as

$$g(\lambda) = \sigma_s(\lambda)N_1 - \sigma^o(\lambda)N_o - \sigma^1(\lambda)N_1 - \sigma^\tau(\lambda)N_T \qquad (2.6)$$

where N_o, N_1, N_T are the molecular population densities (molecules/cm^3) in the states S_o, S_1 and T_1 respectively. σ_s, σ^o, σ^1 and σ^τ are respectively the stimulated emission cross section, $S_o \longrightarrow S_1/S_n$ absorption cross section, $S_1 \longrightarrow S_n$ absorption cross section and triplet-triplet ($T_1 \longrightarrow T_n$) absorption cross section. The last three terms of the equation (2.6), which led to the decrease in the gain at a given λ are the ground state absorption, excited singlet state absorption and triplet-triplet absorption.

The ground state absorption at the lasing wavelength is because of the partial overlap of the fluorescence and absorption spectrum of the dye. This absorption is due to the molecular population in the higher rotational vibrational levels of S_o. But the probability for the higher levels of S_o to be populated is very small. Since ground state absorption is a process of repumping the dye molecules to S_1 the absorbed photons are not lost in the lasing activity.

The excited state absorption ($S_1 \longrightarrow S_n$) is the process in which the molecules in the excited state S_1, absorbs either pump or dye laser photons and go to higher excited singlet states. The rapid radiationless decay from S_n brings the molecules back to the lowest vibrational level of S_1. The excited state absorption, therefore in general, does not cause an inversion loss. But the $S_n \longrightarrow S_1$ transition being radiationless, the absorbed radiation reappear as heat leading to deterioration in laser performance.

Another problem associated with the dye lasers is the intersystem crossing ($S_1 \longrightarrow T_1$) and subsequent triplet ($T_1 \longrightarrow T_n$) absorption. Since the transition $T_1 \longrightarrow S_o$ is spin forbidden, the triplet state lifetime τ_T is relatively long ($\sim$ milliseconds). Therefore the molecules crossed over to triplet state are trapped there. Moreover in most of the dyes, the $T_1 \longrightarrow T_n$ absorption spectrum overlaps with the $S_1 \longrightarrow S_o$ fluorescence spectrum. The intersystem $S_1 \longrightarrow T_1$ crossing time K_{ST}^{-1} is usually of the order

of 100 ns. Hence for a pulsed dye laser, if the pump pulse duration is 5 to 30 ns, as in the case of nitrogen laser, then the triplet state effects can be ignored and no appreciable population can build up in the triplet state during the short pulse. In flash lamp pumped and CW dye lasers, the triplet state must be taken into account.

2.3 DYE LASER RATE EQUATIONS

The rate equations have been extensively used to describe various aspects of dye laser theoretically. The first theoretical analysis of dye laser was made by Sorokin et al.[9] In order to describe the dye laser they had followed the rate equations of Statz and Mars[10] for solid state lasers. Since then, several authors had reported different rate equations, to study different parameters of dye laser such as laser gain, the effect of quenching of triplet state, spectral narrowing etc. The rate equations of Ganiel et al.[11] is adopted here as it is found to be more relevant to the nitrogen laser pumped dye lasers.

The dye laser is represented by an ideal four level system. Transverse pump geometry is considered. The resonator is made up of two flat mirrors of reflectivities R_1 and R_2 and and an active medium of length l. The laser light within the resonator is split into two components $I^+(x,t,\lambda)$ propagating in the x direction and $I^-(x,t,\lambda)$ in the opposite direction.

$I^{\pm}(x,t,\lambda)$ is the photon spectral density (i.e., photon flux per unit wavelength photons/s/cm^3) at x, time t and wavelength λ. The total spectral intensity at any point is

$$I(x,t,\lambda) = I^{+}(x,t,\lambda) + I^{-}(x,t,\lambda) \qquad (2.7)$$

In this treatment, all variations in $I^{\pm}(x,t,\lambda)$ and the molecular population normal to the laser axis are assumed to be averaged out. Phenomenon such as hole burning is not considered.

If W(x,t) is the pump rate (s^{-1}), the rate equation for the molecular population density in S_1 can be written using notation in eqn.(2.6) as

$$\frac{\partial N_1(x,t)}{\partial t} = W(x,t)N_o(x,t) - \frac{N_1(x,t)}{\tau} - N_1(x,t)\int \sigma_s(\lambda)\, I(x,t,\lambda)\, d\lambda + N_o(x,t)\int \sigma^{o}(\lambda)\, I(x,t,\lambda)\, d\lambda \qquad (2.8)$$

The four terms in the right hand side represents respectively (1) the pump excitation $S_o \longrightarrow S_1$, (2) spontaneous emission from S_1, (3) stimulated emission from S_1 and (4) the ground state absorption of laser radiation. For a monochromatic pump source, $W(x,t) = \sigma_p I_p(x,t)$ where $I_p(x,t)$ is the pump photon flux. The intersystem crossing rate K_{ST} is included in the fluorescence

lifetime τ. The depopulation of S_1 due to excited state absorption is neglected due to the short duration of $S_n \longrightarrow S_1$ transition.

The equation for the population density T_1 can be written as

$$\frac{\partial N_T(x,t)}{\partial t} = K_{ST} N_1(x,t) - \frac{N_T(x,t)}{\tau_T} \tag{2.9}$$

where τ_T is the lifetime of the triplet state. The triplet absorption $T_1 \longrightarrow T_n$ is not considered since, the decay from the excited triplet states T_n to T_1 is very fast.

The total molecular density N is assumed constant.

$$N = N_o(x,t) + N_1(x,t) + N_T(x,t) \tag{2.10}$$

The rate equation for the photon spectral intensity inside the active medium is given by

$$\frac{\eta}{c} \frac{\partial I^{\pm}(x,t,\lambda)}{\partial t} \pm \frac{\partial I^{\pm}(x,t,\lambda)}{\partial t}$$

$$= I^{\pm}(x,t,\lambda) \left\{ \left(\sigma_s(\lambda) - \sigma^1(\lambda) \right) N_1(x,t) - \sigma^o(\lambda) N_o(x,t) \right.$$

$$\left. - \sigma^T N_T(x,t) \right\} + b^{\pm}(x) \frac{N_1(x,t)}{\tau} E(\lambda) \tag{2.11}$$

$b^{\pm}(x)$ denotes the geometrical factors which takes into account the fraction of spontaneous emission going into the active volume.

These are the set of equations used to describe dye lasers. Without any approximations, these equations can be solved only by numerical methods. Nair[12] has solved these equations numerically and has studied spectral and temporal evolution of a nitrogen laser pumped dye laser.

2.4 TUNING MECHANISM IN DYE LASERS

A coarse selection of the dye laser emission wavelength is possible by the choice of the dye, the solvent and the resonator parameters. Fine tuning and simultaneous attainment of small linewidths can only be achieved by using a wavelength selective resonator. A variety of wavelength selective devices have been used within the resonator.[12] They include devices for spatial wavelength discrimination, devices for rotational dispersion and wavelength selective distributed feedback.

2.5 DESIGN CONSIDERATIONS

A large number of designs have been developed for narrow band, low divergence, high conversion efficiency and tunable nitrogen laser pumped dye laser. The key element in determining the quality of the dye laser in these designs

is the beam expander. The beam expander is necessary because the resolution obtained using a grating is proportional to the number of groves illuminated. Telescopes, single and multiple prisms and grating in grazing incidence are some of the commonly used beam expanding devices.

The dye laser cavity consists of an active medium (dye solution in a cell), a feedback element, a mechanism for beam expansion and a tuning element. The first design of an efficient tunable pulsed dye laser was reported by Hansch in 1971.[13] He used a diffraction grating as the tuning element. A high power telescope was used as a beam expander and a 4% reflecting plane glass plate as the feedback cum output coupling element. The grating was set in Littrow angle.

Some of the drawbacks of the Hansch design are (1) the beam being expanded in two dimensions, the grating alignment is very critical, (2) high quality, high magnification achromatic telescope is extremely difficult to design, particularly if it is to be short and (3) the telescopes cannot be used on-axis, due to reflection from the lens surfaces. In spite of these complexities, the Hansch design is still being used in some of the commercial dye laser systems because of its advantages.

The difficulties of the telescope beam expander was overcome when Stokes et al.[14] used a prism as the beam expander.

The prism was kept at an angle of 80° and the resultant magnification attained was 4. One of the important advantages of this arrangement was that due to the absence of a curved surface in the beam expander, there is no distortion to the beam. Also, the expansion being one-dimensional, the grating tilt is non-critical. But the low magnification and inherent dispersion of the prism affects the versatality of the system.

Stokes' design was modified by Hanna et al.[15] by replacing the partially reflecting output coupler by fully reflecting mirror. The angle of incidence at the prism was increased to 89° to increase the magnification. The reflection from the prism surface was taken as the output. But in this type of arrangement, the superradiant background emission increased considerably. Because of the low magnification for the prism several workers suggested the use of multiple prisms. In order to avoid reflection losses at the prism surfaces, the beam was made incident at the Brewster angle.

The grazing incidence design, put forward independently by Saikan[16] and Littmann and Metcalf[17] came as a major breakthrough in the search for a simplified beam expander. In all the previous designs, the grating was used in Littrow mounting and served as one of the feedback mirrors, in which case the tuning was achieved by rotating the grating. In the grazing incidence grating (GIG) design, the beam is incident

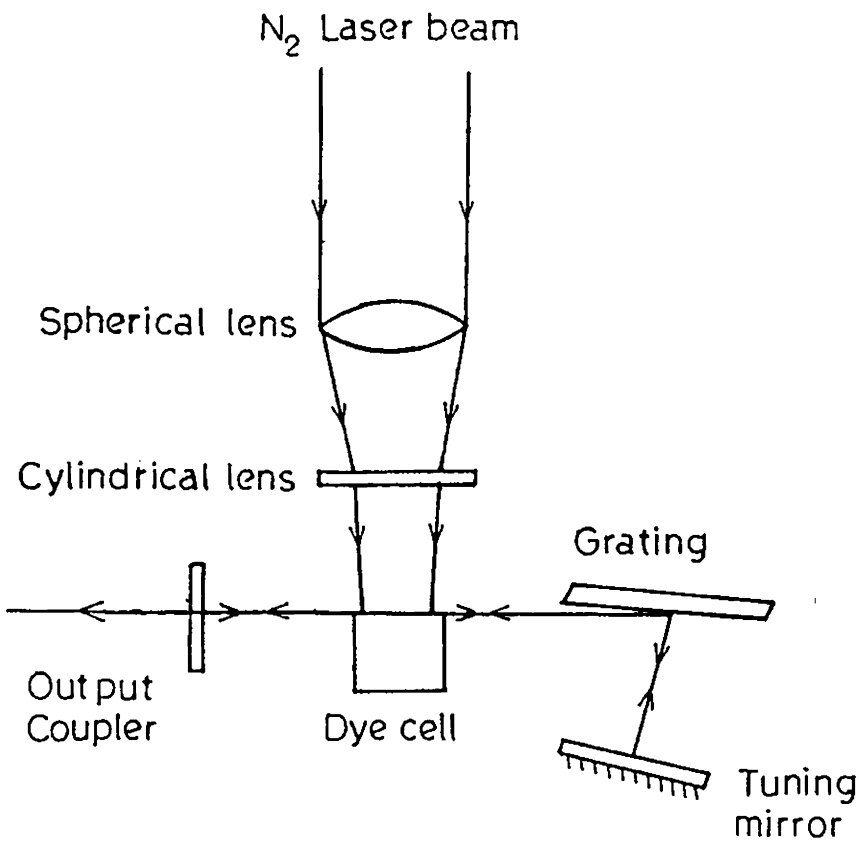

Fig.2.2 The grazing incidence grating arrangement of a dye laser.

on the grating at grazing angle and thus the full length of the grating is utilized (Fig.2.2). The tuning is achieved by rotating the tuning mirror. Very narrow linewidths are being achieved by this technique. The output can be taken either through a partially reflecting output coupler or through the zeroth order of the grating in which case the partially reflecting mirror is replaced by a fully reflecting mirror. In the former case, the output will be[18] narrow band pulses with greatly reduced background while in the latter case, high power pulses will be obtained.

A comparative study of the different types of beam expanders, used in the pulsed dye lasers, by Racz et al[19] showed that as the magnification in the GIG increases above 10, there is sharp decrease in feedback. Therefore in order to increase the feedback, they had suggested to introduce two prism beam expanders prior to the grazing incidence grating, so that at the grating the magnification is $\sim$10, but overall magnification is much more.

In order to reduce the linewidth still further, Shoshan and Oppenheim[20] introduced the double grating design. In this arrangement, the fully reflecting tuning mirror of GIG design was replaced by another grating in littrow mounting. Saikan et al.[21] had proposed a modification to this design using a single grating and a mirror. The tuning mirror of the

GIG design was placed in such a way that for a particular wavelength, the ray reflected from the mirror falls on the grating at the littrow angle. Thus the purpose of two gratings were achieved by a single grating. They had obtained a linewidth of 0.08 cm^{-1}.

The presence of amplified spontaneous emission (ASE) is one of the drawbacks of the GIG design especially for the case, where the output is taken through the zeroth order of the grating. Nair and Das Gupta[22] had suggested a new design to reduce the ASE. They had observed a delay between the ASE and the laser pulse. Therefore in their design, a small fraction of pump power is given first to initiate the oscillation. As the laser oscillation builds up, the rest of the pump power is supplied which is fully utilized for the amplification of the laser.

Littmann[5] reported single mode operation in nitrogen laser pumped dye laser in GIG arrangement. The spectral width was less than 150 MHz. They had reduced the cavity length to such an extent that during the short time in which the population is inverted, there is opportunity for atleast ten round trips in the cavity.

The grazing incidence design thus still continues to be the simplest, yet the most advantageous one existing for the pulsed dye lasers.

2.6 CONSTRUCTIONAL DETAILS

In the present design, the GIG is used. In this set-up as pointed out earlier, the dye is pumped transversely. The emission from the dye which consists of a band of wavelengths is made incident on the grating in grazing incidence. The first order diffracted beam from the grating is incident on a fully reflecting mirror, which will be normal only to a particular wavelength which alone will be retraced. Since in a grating the angles of incidence and diffraction are mutually interchangeable, this beam will be diffracted back to the dye cell where it gets amplified and comes out through the output coupler. About 5% of the output is reflected back as feedback by the output coupler. This method of output coupling is adopted in order to reduce the background radiation.

The different components of the setup (Fig.2.3) are described below.

2.6.1 Dye Cell

A quartz spectrophotometric cell of dimensions 10x10x40 mm with four sides polished, is used as the dye cell. This is fixed on a cell mount which will allow the cell to be rotated about three mutually perpendicular axes. A linear translation of cell in the direction of the pump beam upto 5 mm, is also possible. All these facilities of the cell mount

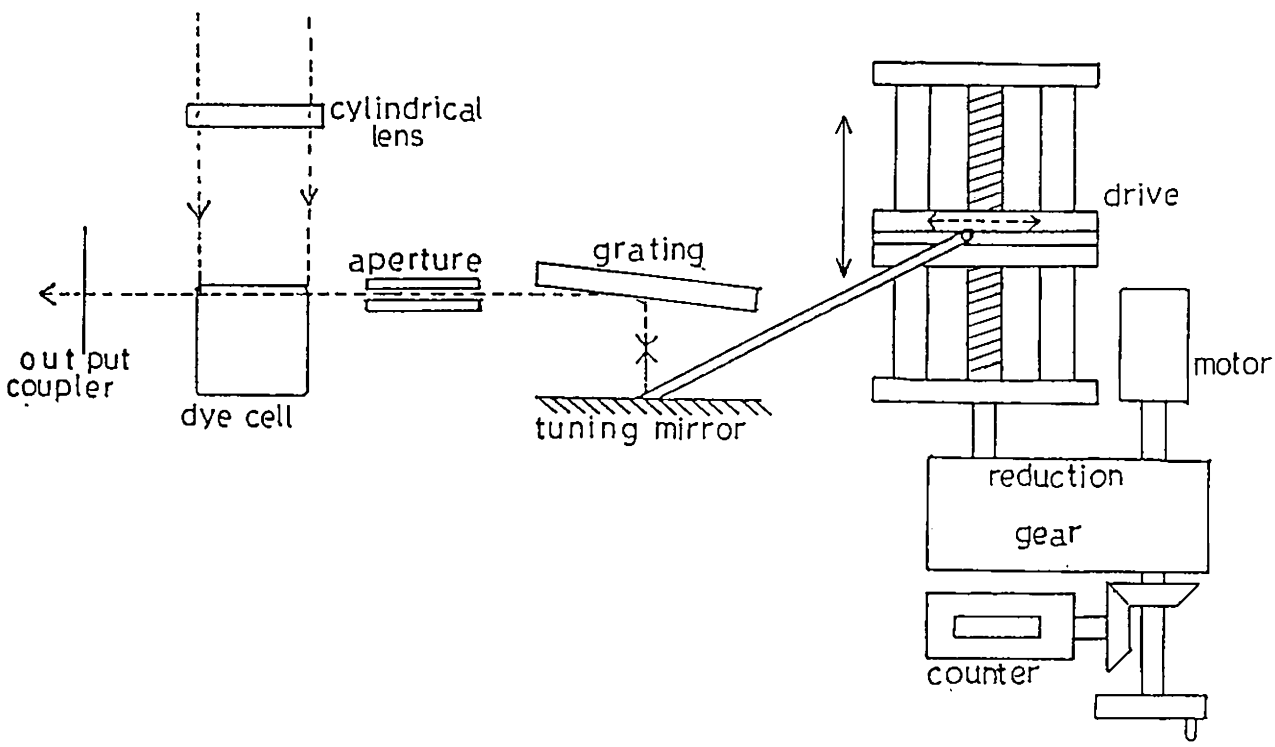

Fig.2.3 The dye laser setup

are found to be essential for initial adjustments, eventhough for further alignments only few of them are necessary.

The cell is so positioned that it makes an angle with the dye laser axis to prevent multiple reflections.

2.6.2 Focusing Lenses

The nitrogen laser beam is focused by a spherical lens and a cylindrical lens on to the dye cell. Quartz lenses of 10 cm focal length are used. The setting of the cylindrical lens is very critical, since that determines the direction of dye laser oscillations. Therefore the mount of the cylindrical lens is in such a way that the lens can be rotated about the direction of pump beam. After the initial adjustments, usually no further alignment is required for the cylindrical lens.

2.6.3 Output Coupler

A polished glass plate of $\lambda/10$ surface accuracy and 25 mm in diameter is used as the output coupler. This has a reflectivity of about 5%. It is fixed on a mount which allows tilts in two perpendicular axes, suitable for aligning the laser.

2.6.4 Grating

The grating used is a holographic one, with 1800 l/mm and 5 cm in length, supplied by PTR optics (model TF-26). This is fixed on a mount which does not have any tilting arrangements. The angle of incidence is kept at 87°.

2.6.5 Tuning Mirror

The tuning mirror is a aluminium coated optical flat of $\lambda/10$ surface accuracy and 60 mm diameter and having a reflectivity of $\sim 95\%$. This is mounted on a mirror mount which allows tilts in two perpendicular directions.

2.6.6 Sine-drive

Since the tuning is achieved by changing the angle of the tuning mirror, whose sine is proportional to wavelength of the laser, a sine-drive is fabricated and attached to the dye laser system (Fig.2.4).

It consists of three metal blocks two of them A and B being fixed. The central block C can move on two rails R_1 and R_2 passing through it. The two rails are fixed to the blocks A and B. A threaded shaft T is passing through the central block, which also is connected to the blocks A and B by ball bearings. When this threaded shaft is rotated the central block C will move forward or backward.

A solid cylinder of diameter 10 mm is put in a slot at the top of the central block which can slide in a direction perpendicular to that of the movement of the central block. To this cylinder is attached a lever L from the axis of the tuning mirror by a ball bearing arrangement. This lever, called the arm of the sine-drive, constitutes the hypotenuse of a right

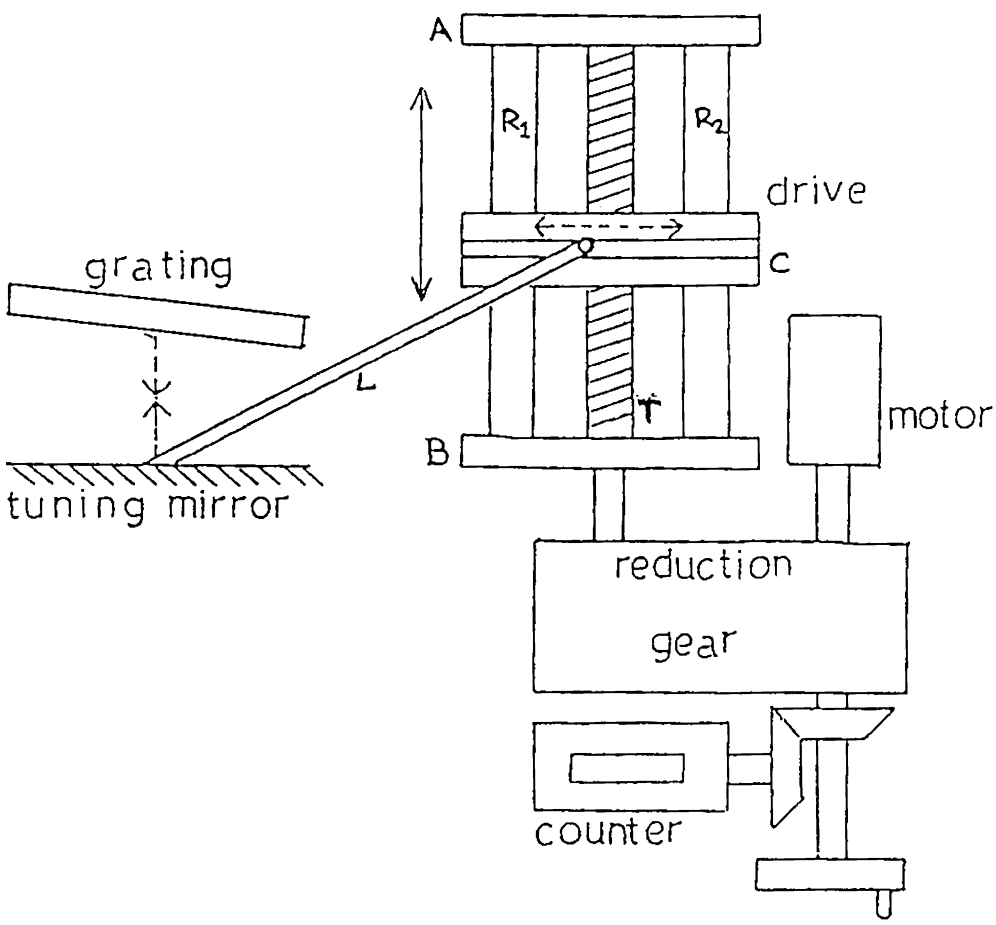

Fig.2.4 The sine-drive and tuning arrangement.

angled triangle. One of the sides of this triangle will be along the direction of motion of the central block.

As the central block moves forward or backward the point where the arm of the sine drive is fixed to the cylinder, will describe an arc whose radius will be the distance of that point to the vertical axis of the tuning mirror. In this arrangement therefore, the tuning mirror will be turned by an angle, the sine of which will be directly related to the displacement of the central block.

The threaded shaft through which the central block moves, is connected to a reduction gear which is coupled to a 12 V dc motor. Thus very small tilts can be given to the mirror and thereby the wavelength of the laser can be very finely tuned. A counter attached to the gear system directly reads wavelength in Angstrom units. For calibration, a 0.5 m Jarrel-Ash scanning monochromator is used. For the experiment using this dye laser, these calibration data are used. The front view of the system is shown in Fig.(2.5).

2.7 PARAMETRIC STUDIES

For the optimisation of the performance of the dye laser, a parametric study of the system is essential. Some of the important parameters of a dye laser are power output, conversion efficiency, pulse duration, divergence, bandwidth and

tunability. These parameters of the dye laser system fabricated for the present investigations, are described in this section.

2.7.1 Pulse Characteristics

The pulse shape and pulse duration are measured using a Boxcar averager. The laser pulse is detected by a Hewlett-Packard pin photodiode (5082-4207) having a risetime of 1 ns and fed to EG&G PARC Boxcar averager fitted with model 163 plug-in-module. The gate of the Boxcar averager was kept at 1 ns. The temporal shape of the pulse obtained by scanning the Boxcar averager is shown in Fig.(2.6). The pulse duration was observed to be 3 ns (FWHM).

2.7.2 Bandwidth

In order to measure the bandwidth, a Jarrel-Ash 0.5 m scanning monochromator with a spectral resolution of 0.015 nm was used along with a EMI 9684 QB photomultiplier tube and chart recorder. A linewidth of 0.04 nm was achieved for an angle of incidence 87° (Fig.2.7). This linewidth was sufficient for the experiments reported in the latter part of this thesis. The use of the monochromator for the linewidth measurements is justifiable since the linewidth of the laser is greater than the resolution of the monochromator.

Still lower linewidths were achievable by increasing the angle of incidence. But the feedback efficiency of the

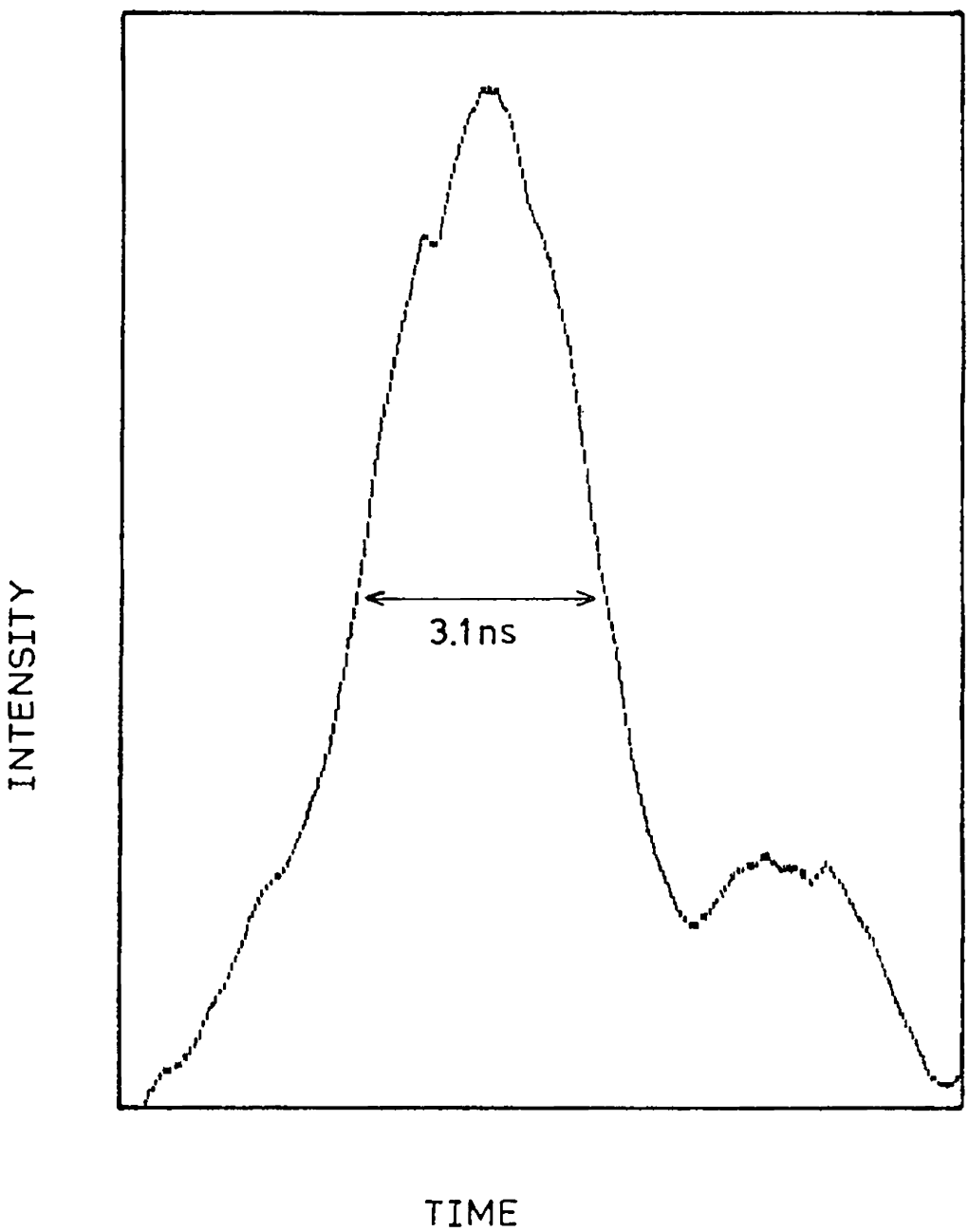

Fig.2.6 Pulse width of the dye laser measured using Boxcar averager (Intensity in arbitrary units).

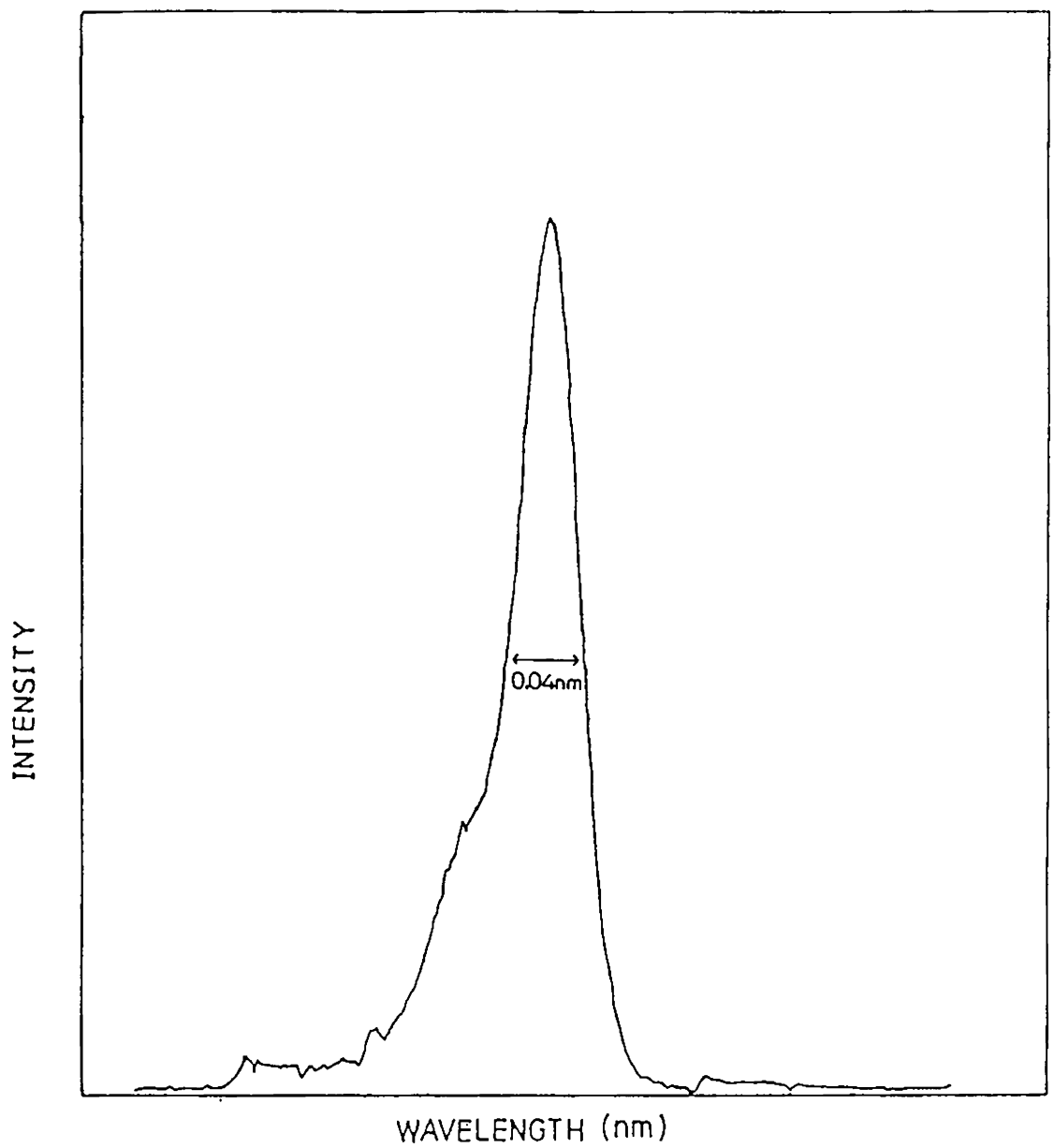

Fig.2.7 Line width of the dye laser. (Intensity in arbitrary units).

grating reduces as the angle of incidence increases. This affects the tunable range and power for a particular dye. For the present experiments, a dye laser which is capable of giving pulses in the entire visible region was necessary. In order to achieve this with less number of dyes, the tunability of each dye had to be kept at a maximum. Therefore, the angle of incidence was kept at 87°.

2.7.3 Power Output and Conversion Efficiency

Power measurements are done using an EG&G Gamma Scientific power meter model 150. The peak power is observed to be 500 W when measured at the wavelength 520 nm. This corresponds to a pulse energy of 1.5 μJ. The pump laser energy is measured to be 300 μJ. Thus the efficiency of the dye laser at that wavelength is found to be 0.5%. Higher efficiency could be achieved by taking the output through zeroth order of the grating.

2.7.4 Divergence

The divergence is determined by measuring the area of cross-section of the beam at two distances 500 cms apart. The divergence is measured to be 0.31 mrad.

The various dyes used and their solvents for different wavelength regions are listed in Table (2.1). In the experiments which are described in the subsequent chapters, the dye laser is operated at the optimum condition.

Table (2.1). List of dyes used to scan the different wavelength regions and their respective solvents.

Wavelength (nm)	Dye	Manufacturer	Solvent
426 - 440	Coumarin 440	Exciton Chemical Co.	Methanol
440 - 457	Coumarin 450	-do-	-do-
459 - 471	Coumarin 450 + Coumarin 470	-do-	-do-
471 - 490	Coumarin 470	-do-	-do-
490 - 510	Coumarin 481	-do-	Dioxane
510 - 535	Coumarin 540A	-do-	-do-
572 - 593	Rhodamin 6G	Loba-Chemie (India)	Methanol
593 - 612	Rhodamin 6G + Rhodamin B	-do- Merck (India)	-do-
612 - 635	Rhodamin B	-do-	-do-

REFERENCES

1. P.P.Sorokin and J.R.Lankard, IBM J.Res.Dev., 10, 162 (1966).

2. P.P.Sorokin and J.R.Lankard, IBM J.Res.Dev., 11, 148 (1967).

3. J.A.Meyer, C.L.Johnson, E.Klerstead, H.D.Sharma and I.Itzkan, Appl.Phys.Lett., 16, 3 (1970).

4. B.H.Soffer and B.B.McFarland, Appl.Phys.Lett., 10, 266 (1967).

5. M.G.Littmann, Appl.Opt., 23, 4465 (1984).

6. F.P.Schafer (Ed.), 'Topics in Applied Physics', Vol.1, Dye Lasers, (Springer, Berlin, 1973).

7. J.B.Birks, 'Photophysics of Aromatic Molecules', (Wiley Interscience, London, 1970).

8. O.G.Peterson, J.P.Wabb, W.C.McColgin and J.H.Eberly, J.Appl.Phys., 42, 1917 (1971).

9. P.P.Sorokin, J.R.Lankard, E.C.Hammond and V.L.Moruzzi, IBM J.Res.Dev., 11, 130 (1967).

10. H.Statz and G.De Mars, in 'Quantum Electronics', Ed. C.H.Townes, (Columbia University Press, New York, 1960).

11. U.Ganiel, A.Hardy, G.Neumann and D.Treves,IEEE J.Quantum Electron., QE-11, 881 (1975).

12. L.G.Nair, Prog.Quant.Electron., 7, 153 (1982).

13. T.W.Hansch, Appl.Opt., 11, 895 (1972).

14. E.D.Stokes, F.B.Danning, R.F.Stebbings, G.K.Walters and R.D.Rundel, Opt.Commun., 5, 267 (1972).

15. D.C.Hanna, P.A.Karkkainen and R.Wyatt, Opt.Quant.Electr., 7, 115 (1975).

16. S.Saikan, Appl.Phys., 17, 41 (1978).

17. M.G.Littman and H.J.Metcalf, Appl.Opt., 17, 2224 (1978).

18. S.Mory, A.Rosenfild, S.Polze and G.Korn, Opt.Commun., 36, 342 (1981).

19. B.Racz, Zs.Bor, S.Szatmari and G.Szabo, Opt.Commun., 36, 399 (1981).

20. I.Shoshan and U.P.Oppenheim, Opt.Commun., 25, 375 (1978).

21. S.Saikan, J.Sei and M.Kiguchi, Jpn.J.Appl.Phys., 20, 1339 (1981).

22. L.G.Nair and K.Dasgupta, Proc. Third Quantum Electronics Symposium, DAE (India), (1985), p.55.

Chapter 3

EXPERIMENTAL SETUP FOR OPTICAL ATTENUATION STUDIES

Abstract

The chapter describes the experimental setup used to study the optical attenuation in sea water. The split-pulse laser method which is the one adopted for the present studies, is explained and its advantages over other conventional techniques are described.

3.1 INTRODUCTION

Experiments to study the attenuation of light in water were started several decades back. Most of the works[1-5] were done using conventional light sources like tungsten filament lamp. One of the common methods adopted by them, was to propagate the light through a cell of finite length containing the liquid. The attenuation coefficient was then determined from the measurements of initial and final intensity of the propagated light.

Major deviation from the conventional experimental techniques sprang up with the advent of lasers. Because of their high power and low divergence, it was possible to measure even very low absorptions. The first report of the absorption measurements in water using laser as a source was by Hass and Davisson.[6] In the laser adiabatic calorimetric technique, which they had developed, the absorption coefficient was determined from the measurements of temperature rise in the sample due to the heat generated by absorption. Using an argon ion laser as the source, they had determined the absorption coefficient of distilled water at the wavelengths 488 nm and 514.5 nm. There are two specific advantages for this method. One is that, the absolute value of the absorption coefficient, which is devoid of the scattering contribution can be obtained. The second advantage lies in the simplicity of the experimental setup, in

which the sample is taken in a comparatively smaller cell, instead of long path cells used by other reported experimenters. However, in a situation of practical interest, the total loss of the beam including the scattering loss is to be measured. In such cases this method cannot be adopted.

Later, Tam and Patel[7] adopted the photoacoustic method to determine the absorption coefficient of distilled water. In this method, the pressure waves generated due to the instantaneous temperature rise by the absorption of the laser pulse is measured using a sensitive piezoelectric transducer. This method is a very sensitive one, which can measure very weak absorption. But like the laser adiabatic calorimetric method, this will give only pure absorption devoid of scattering.

Some of the experimental problems which usually arise in conventional spectroscopic techniques are the following:

1. The reflections at the cell windows need corrections which depend on the window material, liquid in the cell and the wavelength.

2. In order to have sufficient attenuation, the beam is to be passed through considerably long path lengths and the collimation of the radiant flux from an extended source through this length is difficult.

3. In most of the experimental arrangements the initial intensity and final intensity (after propagating through finite length of the liquid medium) were measured at two different times and the temporal intensity variation of the source will affect the final results.

Querry et al.[8] developed the split-pulse laser method to measure the attenuation coefficient of transparent liquids which overcomes all of the above problems. Because of the long path length of about 10 meters, this method is capable of measuring very weak attenuation of transparent liquids. This is one of the accurate methods to obtain the absolute values of the attenuation coefficients. Since the aim of the present studies is to determine the total loss of light energy in water, the split-pulse laser method is adopted as it gives the total attenuation coefficient.

3.2 EXPERIMENTAL SETUP

The experimental setup is as shown in figure (3.1). The source is a wavelength tunable dye laser pumped by a nitrogen laser. The beam from the dye laser encounters a semi-reflecting mirror which acts as a beam splitter. The part of the beam reflected by the beam splitter passes through a reference cell of 15 cms in length containing the liquid. The light pulse is reflected back by the mirror M_1 kept at the end of the reference cell. After traversing the reference cell for the second time,

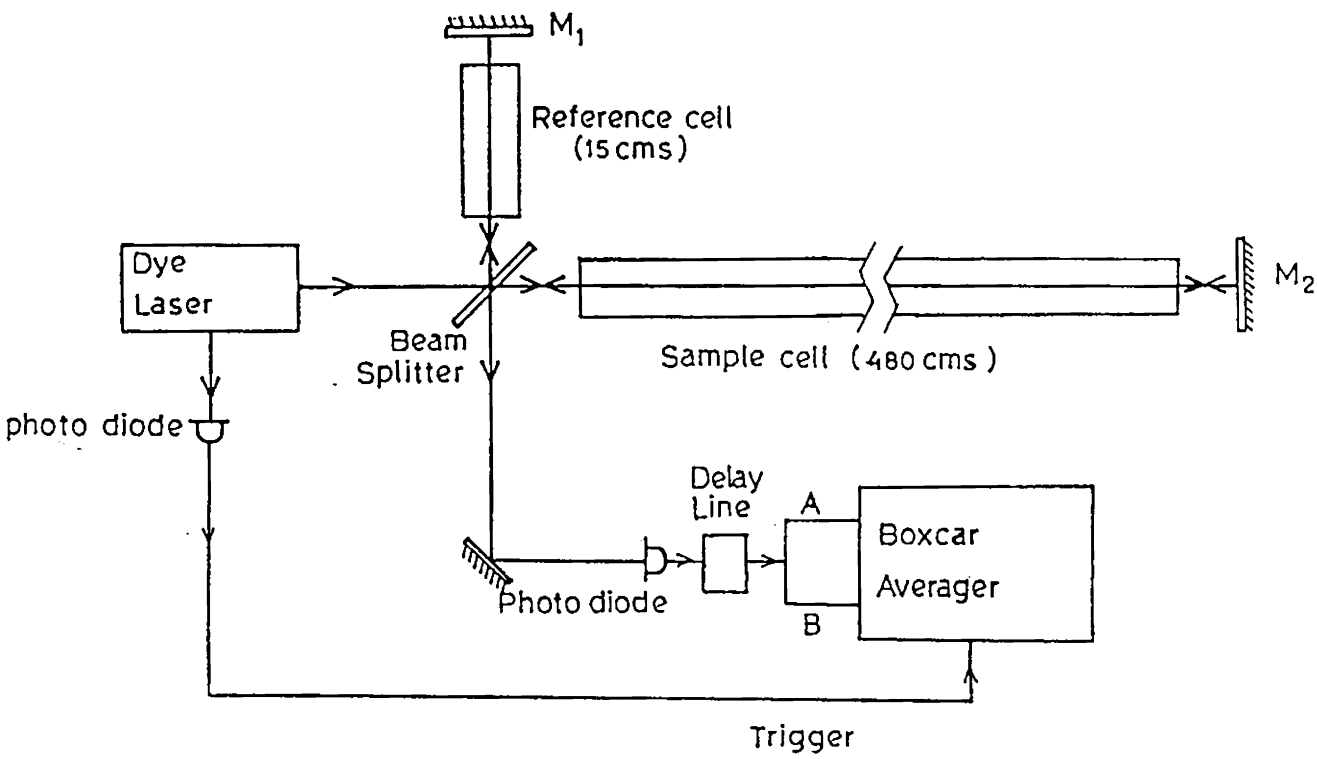

Fig.3.1 Experimental setup for attenuation measurements of sea water.

the pulse encounters the beam splitter once again and the transmitted part of this pulse is detected by a photodiode. The part of the pulse which initially transmitted through the beam splitter passes through the sample cell of 480 cms.in length and is reflected back by the mirror M_2. This pulse after propagating through the sample cell for the second time gets partially reflected by the beam splitter and is detected by the same photodiode. Because of the difference in propagation lengths, the pulse from the sample cell will lag by about 40 ns. The photodiode detects these pulses separately and feeds them to two channels of a Boxcar averager. The gates of the two modules of the Boxcar averager were so adjusted to receive the appropriate pulse. The Boxcar output gives the ratio of the intensity of the two pulses.

The different parts of the experimental setup are described below.

3.2.1 Source

A nitrogen laser pumped dye laser, built specifically for this experiment was used as the source. The dye laser pulses were of 3 ns duration and nearly 500 W peak power with a line width of 0.04 nm. It was operated at a repetition rate of 10 pulses per second. As the nitrogen laser was fitted with a triggered spark gap, the pump pulses were of steady intensity

and repetition rate. The concentration of the dye solutions were also optimised to get stable intensity pulses.

3.2.2 Beam Splitter

The beam splitter was made by coating aluminium on a 3 mm thick optical flat of 50 mm diameter. This was mounted in such a way that the dye laser beam is incident upon this at an angle of 45°.

When a quasi-monochromatic radiation is incident on two boundary surfaces, between three electromagnetically dissimilar media, (eg., air/glass/water) the multiple reflections at the boundaries of the intermediate material can give rise to constructive and destructive interference of the electromagnetic radiation. However, since the coherence time of the laser pulse was less than the time required for the radiation to traverse the two thicknesses of the intermediate material, the possibility of interference can be ruled out.

Aluminium was coated on a single face of beam splitter, and therefore, the reflectivities of the two faces of the beam splitter were different. Also the transmission to reflection ratio of the beam splitter was not exactly 1:1. Because of these reasons, a correction was found necessary to the final measured value of the intensity ratio. This correction factor was determined by measuring the ratio of the intensities of the two pulses

received at the photodiode with the cells removed from the path. This ratio will thus take care of all the errors in the beam splitter.

3.2.3 Cells

Two cells were used to compensate the reflection losses at the cell windows of the sample cell. The sample cell was of length 487 cms and 50 mm internal diameter. Two inlets were provided for the sample cell. The cell was placed on wooden stands which were fixed on two 2.5 meters long heavy tables, made of mild steel angles and sheets, specially fabricated to hold the long sample cell. The reference cell was of length 15 cm and 50 mm internal diameter. This cell was similarly fixed to another table. For both the cells, optically flat windows were fixed using aluminium couplings in such a way that it can be removed as and when desired. The windows of the sample cell and reference cell were cut from the same glass plate, so that they were of same thickness, reflectivity and absorption. The two cells, the beam splitter and the dye laser are shown in Fig.(3.2).

3.2.4 Mirrors

The two mirrors M_1 and M_2 were of same reflectivity made by coating aluminium on the optical flats of $\lambda/10$ surface accuracy and 60 mm diameter. These mirrors were kept on proper mounts fixed on the table at the end of the two cells.

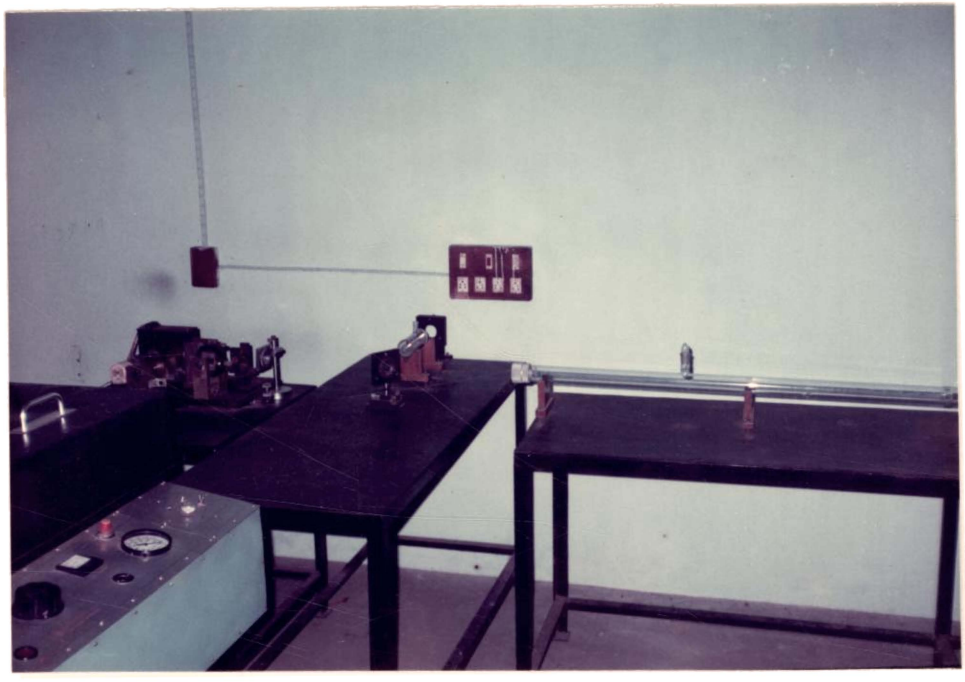

Fig.3.2 Photograph of the two cells and dye laser

3.2.5 Detector

A Hewlett-Packard pin photodiode (5082-4207) was used as the detector. It has a rise time of 1 ns and is fast enough to detect 3 ns pulses. The photodiode was biased at -15 V, and the voltage developed across a resistance of 50 Ω connected in series with the photodiode was taken out and fed to the boxcar averager using RG 58 coaxial cable.

3.2.6 Boxcar Averager

EG&G Boxcar averager, model 162 mainframe fitted with Models 163 and 165 plug-in-modules were used. The gate of model 163 module was adjusted so as to receive the pulse from the reference cell while, Model 165 was adjusted to receive the pulse from the sample cell. For the Boxcar averager the time interval between the trigger pulse and the signal is very critical. This was achieved by triggering the Boxcar using the zeroth order output of the dye laser fed through a photodiode. The signals from the reference cell and sample cells were delayed by about 100 ns using a delay line to suit the requirements of the instrument. From the Boxcar averager, the output, the ratio of the amplitude of the signals, fed to the two channels were determined. This ratio is the ratio of the intensities of the pulses coming from the two cells. The detection part including the Boxcar averager are shown in Fig.(3.3).

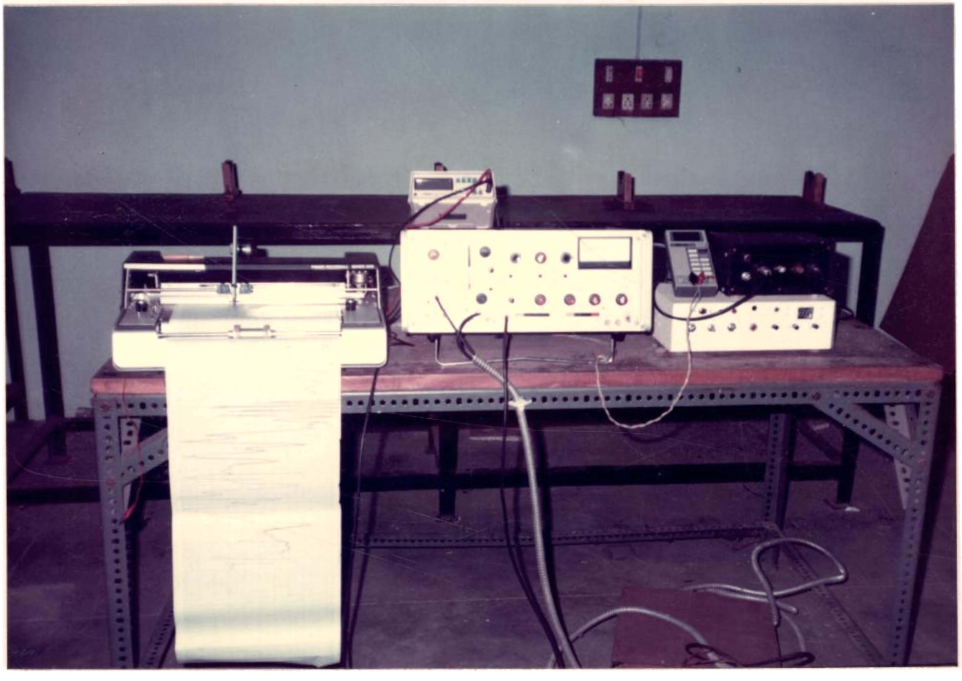

Fig.3.3 Photograph of the detection setup

The windows of the cells being made out of identical glass and both cells being filled with the same liquid, the reflection losses at the cell windows will be the same. Therefore, the additional attenuation suffered by the pulse passing through the sample cell will solely be due to the propagation through the liquid medium for a path length $2(L_s-L_r)$ where L_s and L_r are the lengths of sample cell and reference cell respectively.

The attenuation coefficient α is then given by Lambert-Beer law,

$$\alpha = \frac{1}{2(L_s-L_r)} \ln\left(\frac{I}{I_o}\right) \qquad (3.1)$$

where I is the intensity of the pulse from the sample cell and I_o that from reference cell.

The propagation length of the two pulses being different, the diameters of the beams will be different, when they reach the detector. The sensitive area of the detector was less than 0.2 sq mm. Therefore it was not possible to focus the whole beam to the photodiode. Moreover, if focused, the intensity will be much larger than the saturation limit of the detector. Hence the two signal pulses were, focused to a scatterer and the photodiode was placed at a sufficient distance away ($\sim$7 cm) from the scatterer. It was confirmed that the intensity ratio does not depend upon the distance of detector from the scatterer over a wide distance. Querry et al.[8] have theoretically estimated the distortion of the pulse, as it propagates 10 metres through the liquid.

They have shown that any distortion of the pulse by water is four orders of magnitude less than the attenuation and hence is negligible.

Some of the specific advantages of this method over other methods are given below.

1. Since a laser is used as the source, the beam can be well collimated and can be made to propagate through several meters of path length without any appreciable divergence. The problem of internal reflection from the walls of the cells does not arise in this case.

2. No corrections are necessary to the cell windows since two similar cells were used. The change in intensity between the two pulses will solely be due to the excess propagation length.

3. The temporal variation of the intensity of the source will not affect the results. The laser pulse is split into two and the two pulses pass through two different cells. Since the measured quantity is the ratio of the intensity of the two pulses, the temporal variation of source intensity is taken care of.

4. The setup utilises a path length of ten meters. Therefore very small change in attenuation can be accurately determined.

Using this experimental arrangement, the attenuation coefficient of distilled water, two samples of artificial sea water

and two samples of natural sea water, are determined. The results are described in the following chapter.

The experimental setup to study the beam propagation in turbulent medium is described in chapter 5.

REFERENCES

1. L.H.Dawson and E.O.Hulburt, J.Opt.Soc.Am., 24, 175 (1934).

2. G.L.Clarke and H.R.James, J.Opt.Soc.Am., 29, 43 (1939).

3. E.O.Hulburt, J.Opt.Soc.Am., 35, 698 (1945).

4. S.A.Sullivan, J.Opt.Soc.Am., 53, 962 (1963).

5. L.F.Drummeter Jr. and G.L.Knestrick, Appl.Opt., 6, 2101 (1967).

6. M.Hass and J.W.Davisson, J.Opt.Soc.Am., 67, 622 (1977).

7. A.C.Tam and C.K.N.Patel, Appl.Opt., 18, 3348 (1979).

8. M.R.Querry, P.G.Cary and R.C.Waring, Appl.Opt., 17, 3587 (1978).

Chapter 4

OPTICAL ATTENUATION STUDIES IN SEA WATER

Abstract

The attenuation coefficient of distilled water is reinvestigated and is compared with other existing results. The region of minimum attenuation is found to be around 450 nm. Two samples of artificial sea water were prepared and studied--one constituting only the major constituents and the other constituting both major and minor constituents. The results show that the attenuation is not affected by the presence of the dissolved constituents. The attenuation of two samples of natural sea water show wide variation with that of artificial sea water. It is concluded that the suspended particles contribute much to the attenuation especially in the lower wavelength region.

4.1 INTRODUCTION

A great deal of scientific effort is concentrated to make use of the marine resources and energies. These activities require an effective underwater wide band information transmission system. It is difficult to utilise VLF radio wave or acoustic wave for that purpose because of the increase of attenuation with frequency. In the water, another window for the electromagnetic wave is in the visible region, which satisfies the above requirements.

In the field of defence, the communication with submarines, is a subject of vital importance. The acoustic waves and VLF radio waves are not ideal sources for communication, because of their inherent wide divergence. Apart from the reduction in the amplitude of the signals, the divergence affects the security of the strategic messages. The lasers because of its high power and low divergence, suits the requirements of an ideal source for underwater communications. Advanced techniques have made it possible to obtain lasers of any desired wavelength. The very high frequency of the lasers make it ideal carriers for wide band communications, whose capacity to carry information being limited only by other technical difficulties.

A great deal of experimental and theoretical work about the transmission characteristics of optical radiation in oceanic and limnetic water have been made in the past two

decades. However there are several problems to be solved about the propagation characteristics of laser beam in sea water. One of them is the attenuation of light by the water and its dependance on wavelength. In order to develop an underwater optical communication system, it is essential to identify the wavelength region of minimum attenuation usually referred as the 'optical window'. In this chapter, the studies on the attenuation of sea water for the entire visible region and its dependence on the dissolved constituents and suspended particulate matter are presented. A review of the optical transmission studies in sea water is given first, followed by a detailed report of the present studies on optical attenuation in distilled water, artificial sea water and natural sea water.

4.2 EARLIER STUDIES ON OPTICAL TRANSMISSION IN SEA WATER

The first detailed report of the studies on optical properties of ocean water was by Jerlov[1] based on his data collected during the Swedish Deep Sea Expedition of 1947-48. He classified the ocean water based on spectral transmittance of downward irradiance. He has also made in situ measurements of the volume scattering function at different locations in the eastern North Atlantic Ocean in 1959.[2]

Duntley[3] in 1963, reported his results of investigations spanning two decades, to illustrate the optical nature of ocean water, the distribution of flux diverging from localised

underwater light sources, propagation of highly collimated beams of light and penetration of day-light into sea. Several related topics like underwater photography are also discussed in detail.

The attenuation, absorption and scattering coefficient for sea water at 530 nm were experimentally observed by Morrison[4] at Argus Island Tower in North Atlantic Ocean and in Long Island Sound and Block Island Sound. The three parameters were measured simultaneously. The attenuation coefficient α, the total scattering coefficient s, and absorption coefficient a were determined respectively from the measurements of beam transmittance, volume scattering function and relative irradiance. In their experiments, they used special instruments to include the small angle scattering. Their results showed discrepancies between a+s and α. α was found to be less than a+s in almost all observations. According to Morrison, the possible reason for this was that the measured attenuation coefficients are smaller than the true coefficients, as the transmission meter receives a significant portion of forward scattered light which in theory should be lost permanently from the beam. Correction of the forward scattering of light, reduced the difference from 50% to 15%. Further errors were attributed to the diffraction effects.

Heathershaw and Simpson[5], have studied the light transmittance and its relation to temperature in Irish Sea. Though they could not arrive at a quantitative relation between

transmittance and temperature, they have shown that a significant gradient of transmittance of either sign usually coincide with an appreciable temperature gradient. The relative magnitudes of associated gradients vary widely with frequent examples of substantial transmittance changes corresponding to temperature changes as little as 0.1°C. They observed marked transmittance minima in the regions of highest temperature gradient in the thermocline.

The propagation characteristics of a collimated argon laser beam, in natural sea water were investigated by Miura et al.[6] Their experiments were conducted in the Tago Bay. They have studied the conservation of polarisation and have concluded that polarisation multiplex communication is fairly possible because of the observed 15 dB linear polarisation which existed at 15 attenuation lengths (approximately 200 metres).

Petzold[7] determined the volume scattering function $\sigma(\theta)$ of ocean waters using two different scattering meters, one low angle scattering meter and a general angle scattering meter. From the measured values of $\sigma(\theta)$ the scattering coefficient $s\left(= 2\pi \int_0^{\pi} \sigma(\theta) \sin\theta \, d\theta \right)$, was determined. Their reports are based on the measurements conducted at three locations viz., 1) the 'Tounge of Ocean', Bahama Islands, 2) Offshore Southern California and 3) San Deigo Harbour, California.

A modification to Jerlov's method for optical classification of ocean water by irradiance penetration method, was suggested by Spinrad et al.[8] According to them, irradiance measurements alone, may yield untrue conclusions, about the similarities in particle content or yellow matter (the dissolved organic matter) content of two water masses. In their experiments conducted off the west coast of America, they measured the irradiance and beam transmittance. The transmissivity meter employed an LED (wavelength 650 nm) as the source and had a path length of 0.25 m. The total attenuation coefficient c was obtained from the measured transmissivity data. The fact that the irradiance attenuation coefficient k is measured for a range of wavelengths (from 400 nm to 1000 nm) and c was measured for a single wavelength can be utilised to gain knowledge about the quantity of yellow matter and particulate matter. The existence of yellow matter cannot be detected by the transmissivity measurements alone, as the absorption by the yellow matter is negligible at 650 nm. For lights of shorter wavelengths, both the particulate matter and the yellow substance contribute to the attenuation. The higher value of k/c thus indicates the presence of more yellow matter and less particulate content in the sample.

Bradner and Blackinton[9] have measured the 1/e transmission distance of light in sea water at two different depths at 34 km West of Keahole Point, Hawaii. Measurements were conducted with an uncollimated, 480 nm light. The transmission

distances were, measured as 25.9 m at 1.2 km depth and 24.4 m at 780 m depth. In very clear sea water, the transmission distance β obtained by uncollimated measurements was nearly the reciprocal of α, the attenuation coefficient obtained by collimated measurements.

No systematic study on the possible dependence of dissolved and suspended constituents of sea water on optical attenuation is yet reported. The wavelength of minimum attenuation, and its dependence on various sea conditions such as salinity, temperature, concentration of suspended particulate matter etc., are some of the vital scientific information about which reliable data are not available. In the following sections, the results of the present experiments conducted to study the effect of dissolved constituents of sea water and suspended particulate matter are presented in detail.

The experimental arrangement is described in chapter 3. The measured value α with this setup is the absolute value of the attenuation coefficient. In order to avoid the small angle scattered light reaching the detector, the detector was placed at a distance of 4 metres from the cells. The collecting lens was of diameter 7 cms. Thus among the scattered lights, only those scattered at an angle between 0.5° and -0.5° will reach the detector. The rest of the scattered lights are prevented from reaching the photodiode. These angles are very close

to the limit imposed by the divergence of the laser source used. All experiments reported in this chapter were done at room temperature, 27±1°C.

4.3 ATTENUATION STUDIES IN DISTILLED WATER

4.3.1 Preparation

Distilled water was prepared in high quality glass (Borosil) vessels. Doubly distilled water was used throughout the experiment. The two cells, viz., sample cell and reference cell were cleaned thoroughly and then rinsed with the doubly distilled water before the sample was poured in. The distilled water was carefully transferred to the cells to avoid dust particles and bubbles. First measurement was taken 24 hours after the cells were filled, by which time, the bubbles formed if any, might have moved to the top.

4.3.2 Experiment

Attenuation was measured in steps of 2.5 nm for the spectral region 430 nm to 630 nm. The values for certain regions were not sufficiently accurate due to the lack of suitable dyes. Those values are not presented here. In each scan, the readings taken, were the average of about 1500 pulses. The average of five such scans are given in Table (4.1). The five scans were spread over a period of one month. No significant change in the values of attenuation coefficient was observed which can be

Table (4.1). Attenuation coefficients of distilled water for different wavelengths (in units of $10^{-2}\ m^{-1}$).

Wavelength (nm)	Attn.Coeff.	Wavelength	Attn.Coeff.
434.9	1.8243	530.0	8.7396
437.6	2.2168	532.8	9.1854
440.5	2.5829	535.3	9.4161
442.2	3.1928	537.9	9.5843
446.2	2.0930	540.4	9.3734
449.1	1.8300	542.8	8.8541
451.8	2.2168	546.9	6.8053
454.8	2.4026		
457.0	2.4026	574.4	8.2680
		579.2	9.9630
470.0	2.3660	581.5	10.632
473.0	2.7899	584.0	11.727
479.0	2.9900	586.1	11.871
481.7	2.9900	588.2	12.383
484.2	3.1823	590.4	12.405
486.9	3.6060	592.8	12.746
489.6	3.9987	595.2	23.694
492.2	2.5438	597.5	25.148
494.8	2.7899	599.8	27.818
497.4	2.9877	602.3	30.227
500.0	3.1823	604.6	31.304
502.6	3.6062	606.9	31.921
505.1	3.9986	609.3	31.176
507.8	4.7057	611.5	30.262
510.4	4.8915	613.9	30.270
512.9	4.7293	616.2	31.068
515.5	4.1844	618.5	31.988
517.6	5.8697	620.8	33.148
520.1	7.4601	623.2	33.341
522.7	7.8373	625.5	32.213
525.2	8.1831	627.8	32.147
527.8	8.3434		

related to time. This observation is in variance with that of Sullivan.[10] He had observed that in 24 hours, the fractional transmittance of freshly distilled water decreased from 88.5% to 80% at a wavelength of 470 nm. He had attributed this to the deterioration of the optical purity of distilled water.

4.3.3 Results and Discussion

The values of the attenuation coefficient of distilled water for different wavelengths are presented in Table (4.1). These values are plotted in Fig.(4.1) along with some of the earlier reported results.[10-13] One of the important observations is that the present values of $\alpha(\lambda)$ for all wavelengths below 540 nm are higher than those reported by Tam and Patel. This is due to the fact that the values of attenuation coefficients depend both on absorption and scattering. The values reported by Tam and Patel contain only the absorption coefficient while the present values include molecular scattering also. Thus the relatively high values obtained here as compared to the reported values of Tam and Patel are due to the contribution from scattering. Above 580 nm there is a sharp increase in the value of $\alpha(\lambda)$ and all earlier reported values coincide in this region within the experimental limits. This clearly demonstrates that absorption is very high in this region compared to the scattering. In our studies the lowest values of attenuation was observed in the region 435-450 nm. This value is lower than the value reported

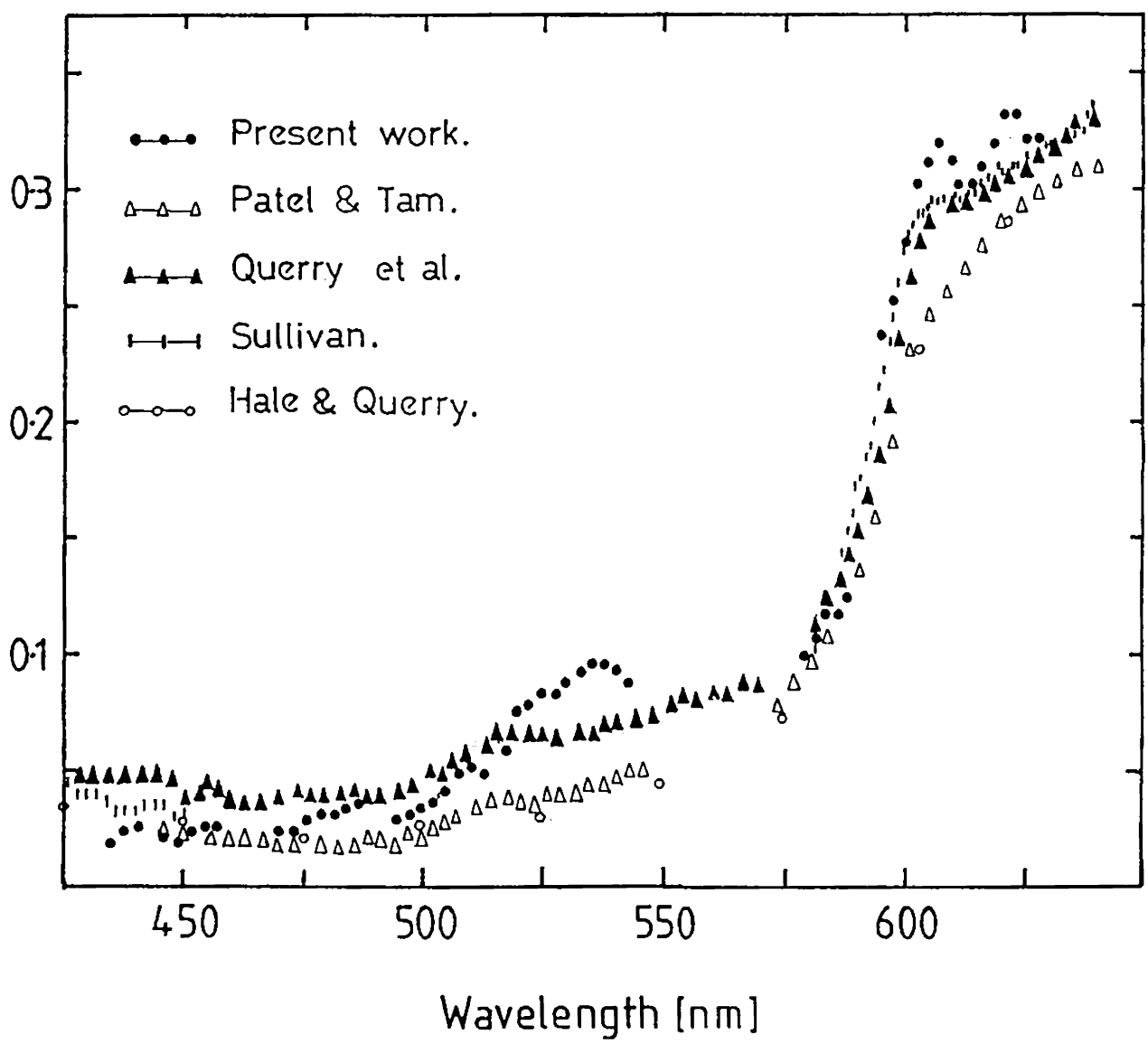

Fig.4.1 A graphical comparison of attenuation coefficients from the present investigation with those obtained by previous investigators.

by earlier workers. To obtain a more reliable information on this minimum, this region was scanned using two dyes Coumarin 440 and Coumarin 450 (Exciton Chemical Company). Because of the very low value of attenuation coefficient in this region the reported values are not as accurate as the values given for other regions. However there is no ambiguity in establishing the lowest attenuation in this region which is the optical window region.

4.4 ATTENUATION STUDIES IN 'ARTIFICIAL' SEA WATER

4.4.1 Preparation

Artificial sea water was prepared by adding the required salts in the right proportion to match the ratios of these salts in natural sea water. Analar grade salts were dissolved in doubly distilled water. Two samples of artificial sea water both of salinity 35 ppt (parts per thousand) were prepared and studied. The proportion by mass of the constituents of the two samples are shown in Table (4.2). The corresponding values for natural sea water are also given for comparison. Of the two samples, sample I was prepared by adding only the major constituents, whereas sample II was prepared by adding major and minor constituents in order to elucidate information on the influence of the minor constituents on optical attenuation. The different salts used to prepare the two samples and their respective mass dissolved in one litre of doubly distilled water are shown in Table (4.3).

TABLE (4.2). The percentage by mass of the constituents of natural sea water and the two samples of artificial sea water.

Constituents	Natural Sea Water	Artificial Sea Water	
		Sample I	Sample II
Sodium (Na^{+})	30.61	32.42	31.618
Magnesium (Mg^{2+})	3.69	3.93	3.809
Calcium (Ca^{2+})	1.16	-	0.036
Potassium (K^{+})	1.10	-	1.139
Strontium (Sr^{2+})	0.04	-	-
Chloride (Cl^{-})	55.04	55.45	54.773
Sulphate (SO_4^{2-})	7.68	8.19	7.935
Bicarbonate (HCO_3^{-})	0.41	-	0.419
Bromide (Br^{-})	0.19	-	0.193
Boric Acid (H_3BO_3)	0.07	-	0.078

TABLE (4.3). Salts used to prepare the two samples of artificial sea water and their respective mass in grams added to one one litre of distilled water.

Salt	Sample I	Sample II
Sodium Chloride (NaCl)	24.534	24.534
Magnesium Chloride ($MgCl_2.6H_2O$)	11.112	11.112
Sodium Sulphate (Na_2SO_4)	4.094	4.094
Potassium Chloride (KCl)	--	0.695
Sodium Bicarbonate ($NaHCO_3$)	--	0.201
Potassium Bromide (KBr)	--	0.101
Boric Acid (H_3BO_3)	--	0.027
Calcium Chloride ($CaCl_2$)	--	0.035

The cells were cleaned thoroughly with distilled water and rinsed with the new solution every time, before the new sample was filled in. The solution was kept in the cells for several days to give sufficient time for the minute salt particles if any to get dissolved.

The experimental procedures were same as that for distilled water.

4.4.2 Results and Discussion

The values of the attenuation coefficients of the two samples for the region 435 to 635 nm are given in Table (4.4) and plotted in Fig.(4.2) along with the values for distilled water. The values for both samples are almost same as that of distilled water. Comparing sample I and distilled water, it can be said that the presence of major dissolved constituents Na^{+}, Mg^{++}, Cl^{-} and SO_4^{--}, within the concentration levels applicable to sea water, do not cause any additional attenuation. The overlapping of the curves for samples I and II shows that the minor constituents (Ca^{++}, K^{+}, HCO_3^{-} and H_3BO_3) do not have any influence on the attenuation of sea water. It can safely be concluded within the present experimental limits that the dissolved constituents of sea water do not play any significant role in the optical attenuation.

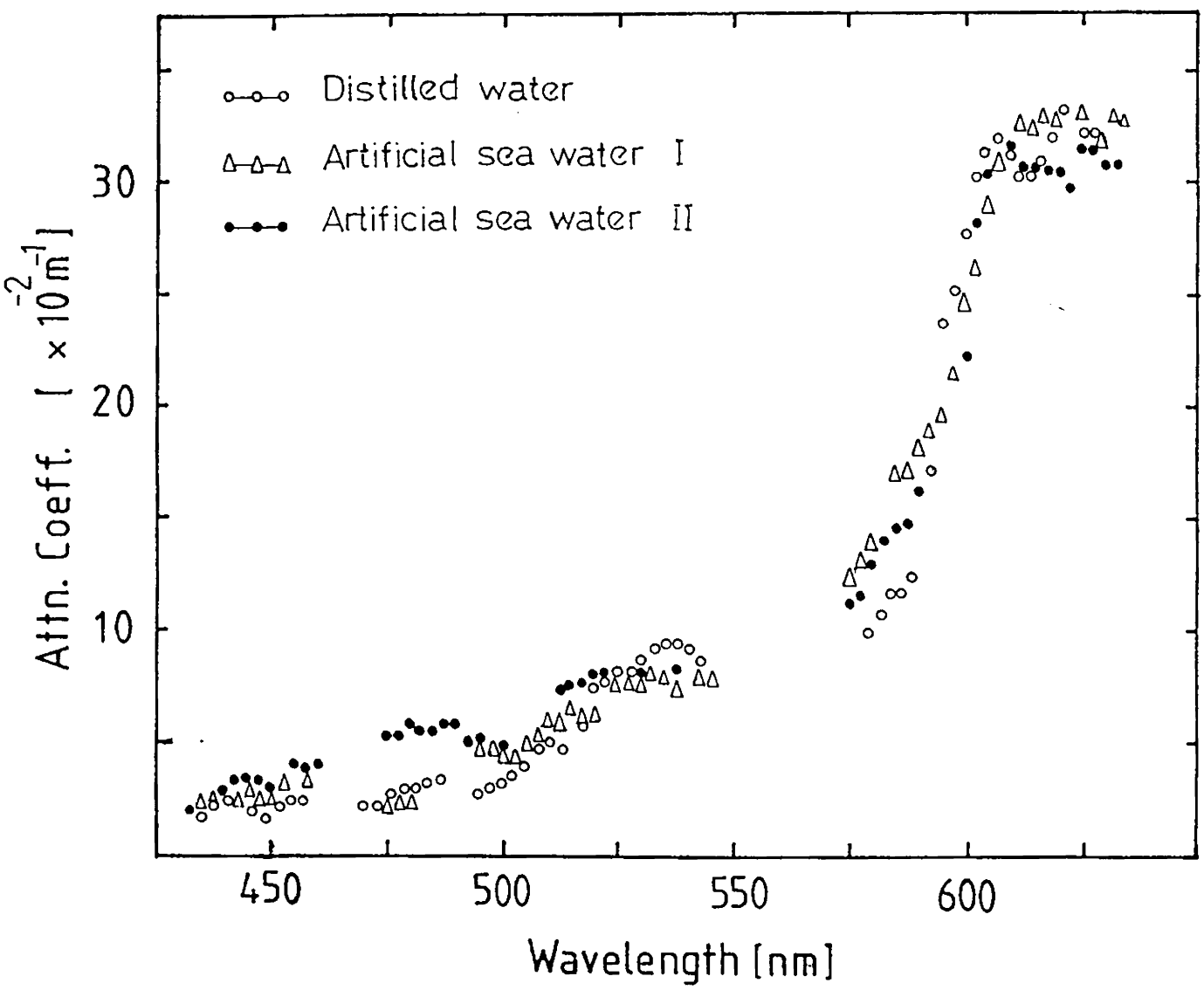

Fig.4.2 Attenuation coefficients of the two samples of artificial sea water compared with those of distilled water.

TABLE (4.4). ATTENUATION COEFFICIENTS OF ATRIFICIAL SEA WATER AND NATURAL SEA WATER (IN UNITS OF 10^{-2} m^{-1}).

Wavelength (nm)	Arti.sea water I	Arti.sea water II	Nat. sea water I	Nat. Sea Water II
426.4			10.434	
429.4	2.366	1.9398	10.504	32.753
432.0	2.2157	1.9957	10.674	33.018
434.9	2.4983	2.5137	10.578	31.595
437.7	2.4556	3.1714	10.456	29.143
440.5	2.6486	3.1746	10.641	29.539
443.2	2.3104	3.1340	10.469	26.248
446.2	2.3660	2.7731	10.271	25.127
449.2	3.1823	3.5772	10.660	23.270
451.8	3.9918	3.9725	10.846	23.270
454.5	3.1834	3.8379	10.598	24.390
456.9	2.3660	3.9986		25.065
459.7			10.109	
462.3			9.687	17.052
465.0			9.476	16.777
467.9			9.367	16.351
470.7	2.1406		8.814	15.946
473.4	2.1406	5.1869	8.657	14.920
476.2	2.1406	5.2522	8.462	14.557
479.0	2.3660	5.6415	7.784	13.451
481.7	2.3660	5.5949	7.785	14.187
484.2	3.1823	5.6101	8.073	13.359
486.9	2.3660	5.7260	7.866	12.743
489.6		5.6855	7.772	12.031
492.2		4.9436	6.867	12.119
494.8	4.4857	5.0446	7.288	11.459
497.4	4.7293	4.6922	7.288	11.948
500.0	4.4221	4.6922	7.180	11.874
502.6	4.4519	4.5670	7.339	11.919
505.1	5.0653	4.8356	7.718	10.603
507.8	5.5013	5.3354	7.552	12.415
510.4	5.8969	5.9671	7.036	12.582
512.9	6.3704	7.3637	7.219	12.807
515.5	6.5794	7.4204	6.905	12.679
517.6	6.3667	7.5958	7.542	12.407

TABLE (4.4). (CONTINUED)

Wavelength (nm)	Arti.sea water I	Arti.sea water II	Nat.Sea water I	Nat. sea water II
520.1	6.4353	8.0502	7.249	12.171
522.7	6.2195	8.1146	7.180	11.889
525.2	7.6421	7.8204	6.845	11.745
527.8	7.7761	8.0263	7.211	11.099
530.3	7.7728	8.0233	6.667	
532.8	7.9004	8.1142		
535.3	8.0250	8.1076		
537.9	7.6216	8.3473		
540.4	7.0158	9.0209		
542.8	8.0376			
545.2	8.0376			
572.5			11.604	14.838
574.4	12.5921	11.3321	11.957	15.601
576.8	13.3349	11.5179	12.506	16.296
579.2	14.0913	12.9242	12.712	16.296
581.5	13.9224	13.9224	13.379	17.430
584.0	16.9088	14.4391	14.645	18.441
586.1	17.2911	14.8608	15.517	18.663
588.2	18.2322	16.1852	15.004	
590.4	19.0472	17.1942	15.428	
592.8	19.6631	19.7962	16.164	
595.2	21.4880	21.1514	21.465	
597.5	24.7274	22.2628	24.885	29.336
599.8	26.2044	28.1626	28.432	32.096
602.3	29.0429	30.4350	30.290	34.551
604.6	30.8514	30.0490	31.406	35.486
606.9	32.8532	31.5984	31.150	35.121
609.3	32.4821	30.7532	30.746	35.121
611.5	32.5659	30.6277	30.968	34.919
613.9	32.6802	30.5726	31.573	35.440
616.2	32.6270	30.4785	30.991	34.814
618.5	32.9568	29.6756	30.977	35.427
620.8	32.7983	31.4490	31.155	36.357
623.2	32.2350	31.4289	31.823	36.138
625.5	31.6772	30.8733	31.759	35.640
627.8	32.6344	30.6267	31.990	35.245
630.1	32.4824			

4.5 ATTENUATION STUDIES IN NATURAL SEA WATER

4.5.1 Preparation

Two samples of natural sea water were also taken up for investigation. Samples were collected from the Arabian Sea. Sample I was collected 30 km to the west of Cochin (salinity = 35.46 ppt) and sample II from 3 km to the west of Cochin (salinity = 28.65 ppt) both from 10 metres depth. To remove large size suspended particles both samples were filtered using 5-10μm pore size filters.

Experimental procedures were same as described before. Measurements were taken spanning over a period of one month. No significant variation of the attenuation was observed. This indicates that the suspended particulate matter present in the sample were not of settling nature.

4.5.2 Results and Discussion

The attenuation coefficients for the two samples of natural sea water are shown in Table (4.4) and plotted in Fig.(4.3) along with that for artificial sea water sample II. There exists wide variation between the curves of artificial sea water and natural sea water. The attenuation coefficient for natural sea water are higher than those for artificial sea water especially below 520 nm. The dissolved constituents of both natural sea water and artificial sea water being almost

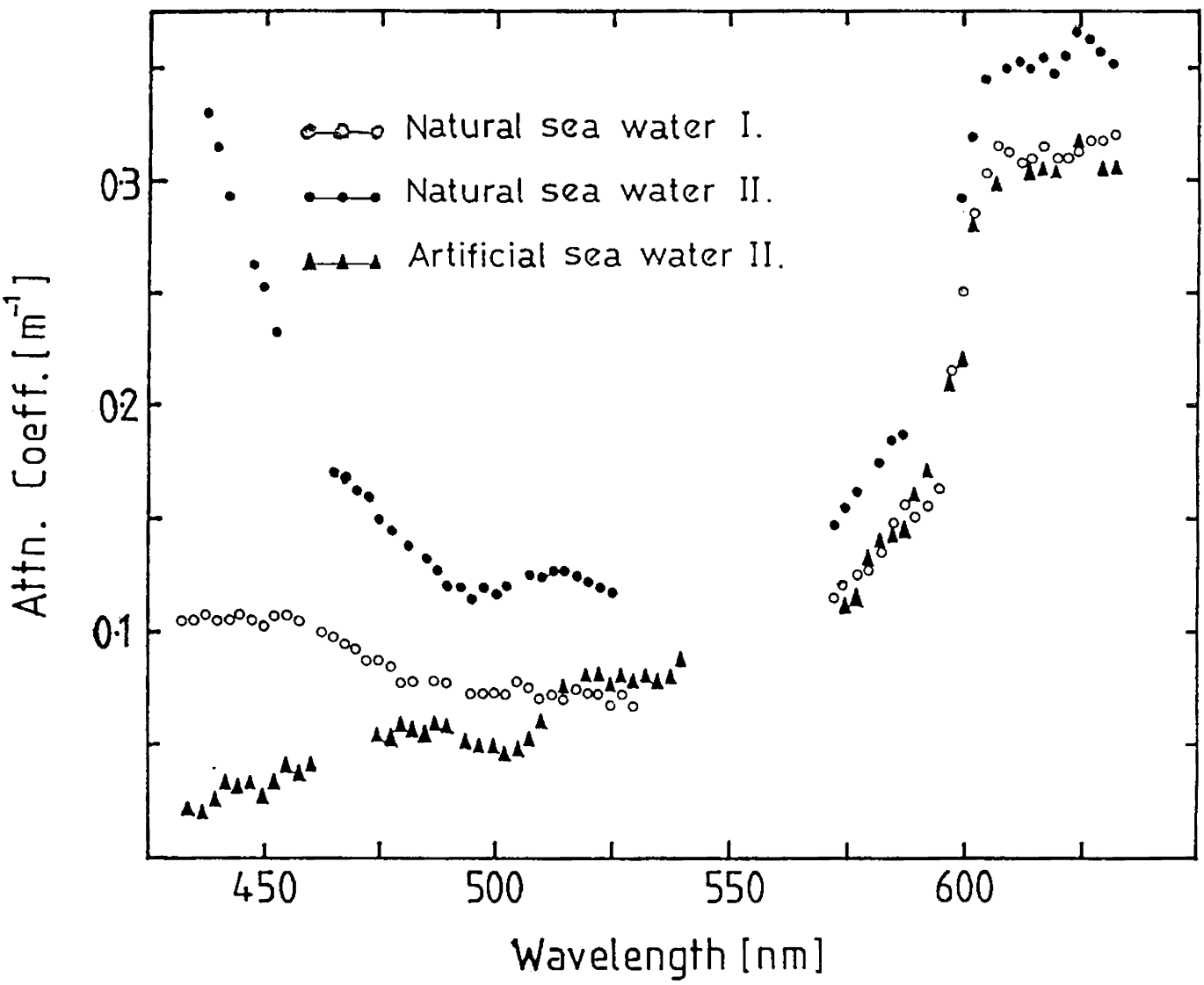

Fig.4.3 Attenuation coefficients of the two samples of natural sea water compared with those of artificial sea water.

the same, the difference in attenuation will be mainly due to the presence of suspended particles in the natural sea water.

Among the natural sea water samples, sample II collected 3 km off the coast showed very high attenuation in the blue region as compared to sample I collected 30 km off the coast. Based on the results of artificial sea water, it can be shown that this variation cannot be due to salinity and one can attribute it to the suspended particles. It is safe to conclude that the suspended particles would influence considerably at the coastal belt while this factor will be much lower as we proceed to the interior regions.

Due to the large attenuation in the blue end of the spectrum, the region of minimum attenuation shifted to 490-510 nm. The minimum value of attenuation for the distilled water was around $0.02\ m^{-1}$ in the region 450 nm. In the sea water far away from the coast the minimum value of the attenuation obtained was about $0.07\ m^{-1}$ in the region 490-515 nm.

4.6 CONCLUSIONS

A detailed study on the dependence of optical attenuation on the constituents of sea water shows that the attenuation in general does not depend on the dissolved constituents. However variations to this effect may be observed in certain localised

points where some of the coloured constituents dominates. The present studies have not taken into consideration the dissolved organic matter as its influence is reported to be less.

Attenuation being found to be independent of the dissolved constituents, within the concentration levels applicable to sea water, it is fair to assume that salinity does not affect the attenuation.

It has been shown that the suspended particles contribute much to the attenuation. This leads to the conclusion that in general, the higher value of attenuation if shown by the sea water, will mainly be due to the presence of suspended particles. The attenuation thus depends greatly upon the size and concentration of the particulate matter.

The minimum value of attenuation for the artificial sea water was in the region around 450 nm. The natural sea water collected from 30 km off the coast showed minimum attenuation in the region 490-510 nm. Farther into the sea, the region of minimum attenuation may lie in the region 480-500 nm. In the coastal waters, this region is likely to move towards higher wavelength side, due to the presence of large quantity of dust particles, as observed in measurements of sea water sample II (Fig.4.3).

The attenuation for the region above 600 nm, is fairly same for natural sea water and artificial sea water in spite of

the presence of suspended particulate matter. This substantiates that the transmissivity measurements using sources of wavelength greater than 600 nm, may not give sufficient information about the concentration of suspended particles, as pointed out by Spinrad et al.[8]

REFERENCES

1. N.G.Jerlov, Reports of Swedish Deep Sea Expedition of 1947-48 (1951), Vol.III.

2. N.G.Jerlov, Kgl.Vetenskap.Vitterh Handl.Foljdon Ser.B., S(11) (1961).

3. S.Q.Duntley, J.Opt.Soc.Am., 53, 214 (1963).

4. R.E.Morrison, J.Geophys.Res., 75, 612 (1970).

5. D.C.Heathershaw and J.H.Simpson, Estaur and Coast.Marine Sci., 2, 91 (1974).

6. S.Miura, Y.Ishikawa, K.Tohma, K.Kondo, T.Matsui and H.Nagatomo, J.Radio Res.Lab., 23, 149 (1976).

7. T.J.Petzold in 'Light in the Sea', Ed. J.E.Tyler (Dowden, Hurchinson & Ross Inc., Benchmark Papers on Optics, 1977), Vol.3, p.152.

8. R.W.Spinrad, J.R.V.Zaneveld and H.Pak, J.Geophys.Res., 84, 355 (1979).

9. H.Bradner and G.Blackinton, Appl.Opt., 23, 1009 (1984).

10. S.A.Sullivan, J.Opt.Soc.Am., 53, 962 (1963).

11. M.R.Querry, P.G.Cary and R.C.Waring, Appl.Opt., 17, 3587 (1978).

12. A.C.Tam and C.K.N.Patel, Appl.Opt., 18, 3348 (1979).

13. G.M.Hale and M.R.Querry, Appl.Opt., 12, 555 (1973).

Chapter 5

LASER PROPAGATION STUDIES IN TURBULENT MEDIUM

Abstract

The chapter describes the experiments on laser propagation through a turbulent medium. The variance, power spectrum and the probability distribution function of the irradiance fluctuations are studied. It is shown that the behaviour of laboratory simulated turbulence is very much like that of atmospheric turbulence. The studies on the probability distribution show that it is the Rice-Nakagami distribution which fits well in the strong turbulence. The studies are then extended to understand the dynamics of the turbulence. The dimension of the attractor, and the Kolmogorov entropy of the system is determined for various turbulence strengths. It is observed that beyond a critical turbulence strength, the system tends to more ordered states. A new method of observing transition to turbulence is also presented.

5.1 INTRODUCTION

The laser propagation through a turbulent medium is a subject of wide applications. Considerable efforts have been expended in recent years in understanding the relationship between the statistical properties of the irradiance fluctuations due to propagation through a random medium and characteristics of the random medium. The probability distribution of the irradiance fluctuations, its power spectrum etc. are examples of quantities which can be measured and which are important for designing optical systems operating under such conditions.

Almost all of the experimental work reported in this area were conducted in the atmospheric turbulence. The first experiments in line-of-sight optical propagation in the atmosphere were carried out by Tatarskii et al.[1] and Gurvich et al.[2] They found quite good agreement between the theoretical results for the variance and covariance of the fluctuations in the log-amplitude. They also found that the irradiance fluctuations were log-normally distributed. The Soviet scientists Gracheva et al.[3,4] were the first to observe the so called saturation phenomenon. They observed that the log-amplitude variance would increase as predicted by theory with increasing path length or C_n^2 (the refractive index structure

constant), only to stop increasing to saturate when $0.31\ K^{7/6}L^{11/6}C_n^2 > 1$. This phenomenon of saturation behaviour was later observed by several other workers.[5,6] Several reports[7-9] on experiments in laboratory simulated turbulence are also available in the literature.

Turbulence is described adequately by the Navier-Stokes equation (1-50) which is purely deterministic. The chaotic behaviour of this equation has been shown by Ruelle and Takens.[10] The reason for the chaotic behaviour of such deterministic systems is reported to be due to the presence of 'strange attractors' in the phase space. These strange attractors have fractal dimensions. Knowledge about the strange attractors will contribute much to understand the complexities of the system. A method of characterising the strange attractors of a chaotic system has been put forward by Grassberger and Procaccia[11] and Atmanspatcher and Scheingraber.[25] This method involves the evaluation of static and dynamic invariants of the chaotic system.

The description of the experimental setup used to study the optical propagation in turbulent medium and the studies on variance, power spectrum and probability distribution of irradiance fluctuations are given in this chapter. The second half of this chapter describes the calculation of the characteristic invariants involved in the dynamics of the

turbulent system, from the measurements of intensity fluctuations of the propagated laser beam. A new method of observing transition to turbulence is also described in this chapter.

5.2 EXPERIMENTAL SETUP

The experimental setup (Fig.5.1) consists of a turbulence chamber and a detection system. Turbulence is created in a glass tank of dimensions 50x20x15 cms. which is three-fourth filled with distilled water. This tank is placed on an aluminium plate which rests on electric heaters rated 3 kW. The water is heated uniformly from below. A set of parallel copper tubes are placed horizontally just below the water surface, through which cold water is circulated. This cools the upper layer of water which descends and mixes with the warm ascending water. The velocity of these vertically moving eddies will depend on the heater power. Large convection eddies are avoided by placing 25 mm size honey comb structures at the bottom of the tank. The temperature variations in the medium will result in refractive index variations. The physics governing the production of refractive index irregularities is basically the same as in real case, ie., the presence of warmer boundary at the bottom layer in a gravitational field.

A 5 mW helium-neon laser beam expanded to 25 mm diameter is passed through this tank. The propagation distance is varied in steps of 0.5 m by multipass arrangements. The

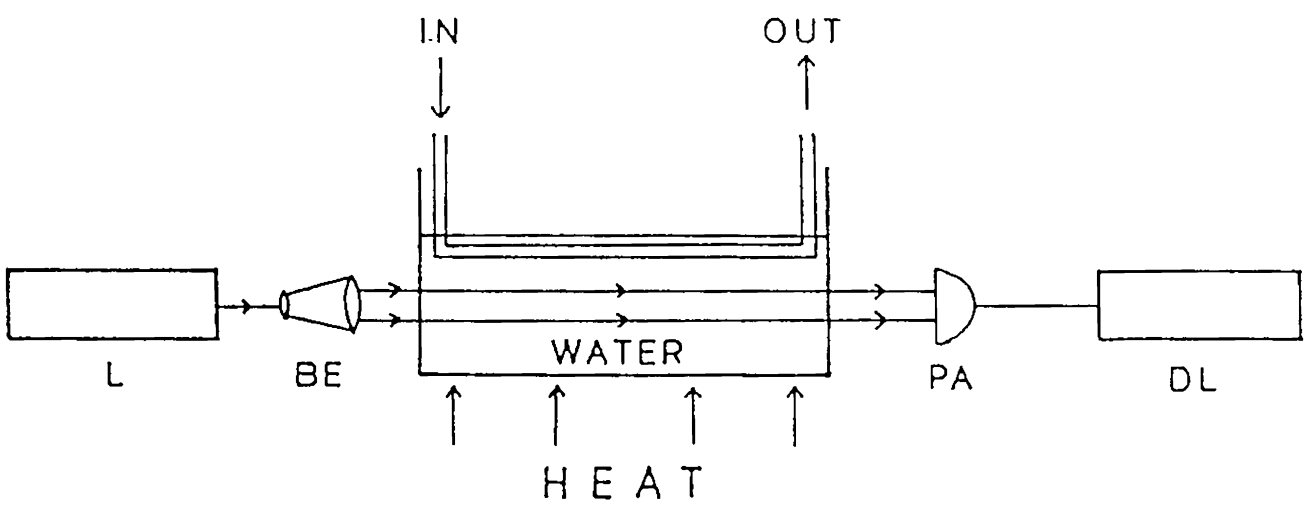

Fig.5.1 The experimental setup for laser propagation studies in a turbulent medium. L - laser, B - beam expander, PA - photodiode assembly, DL - data-logger.

transmitted beam intensity is detected by a photodiode. The photodiode signal is amplified and fed to a data logger which is capable of sampling and storing the signal at intervals of 1 ms.

The strength of turbulence is varied by changing the heater power. The heater power is varied from 210 W to 1325 W. The recording of the intensity fluctuations for the lowest and highest turbulence strengths for a path length of 2 meters are shown in Fig.(5.2). Similar experimental arrangements were used by some of the earlier workers[7-9] who simulated turbulence in the laboratory.

5.3 SCINTILLATION STUDIES

The variance, power spectrum and probability distribution of the irradiance fluctuations are determined for various turbulence strengths and propagation lengths and are discussed below.

5.3.1 Variance

The variance of the logarithm of intensity (log-intensity) of the transmitted beam is calculated from the intensity measurements. In the weak turbulence region, the variance of log-intensity according to Rytov theory is given by the equation

$$\sigma^2_{\ln I} = 1.23\, C_n^2 L^{11/6} k^{7/6}$$

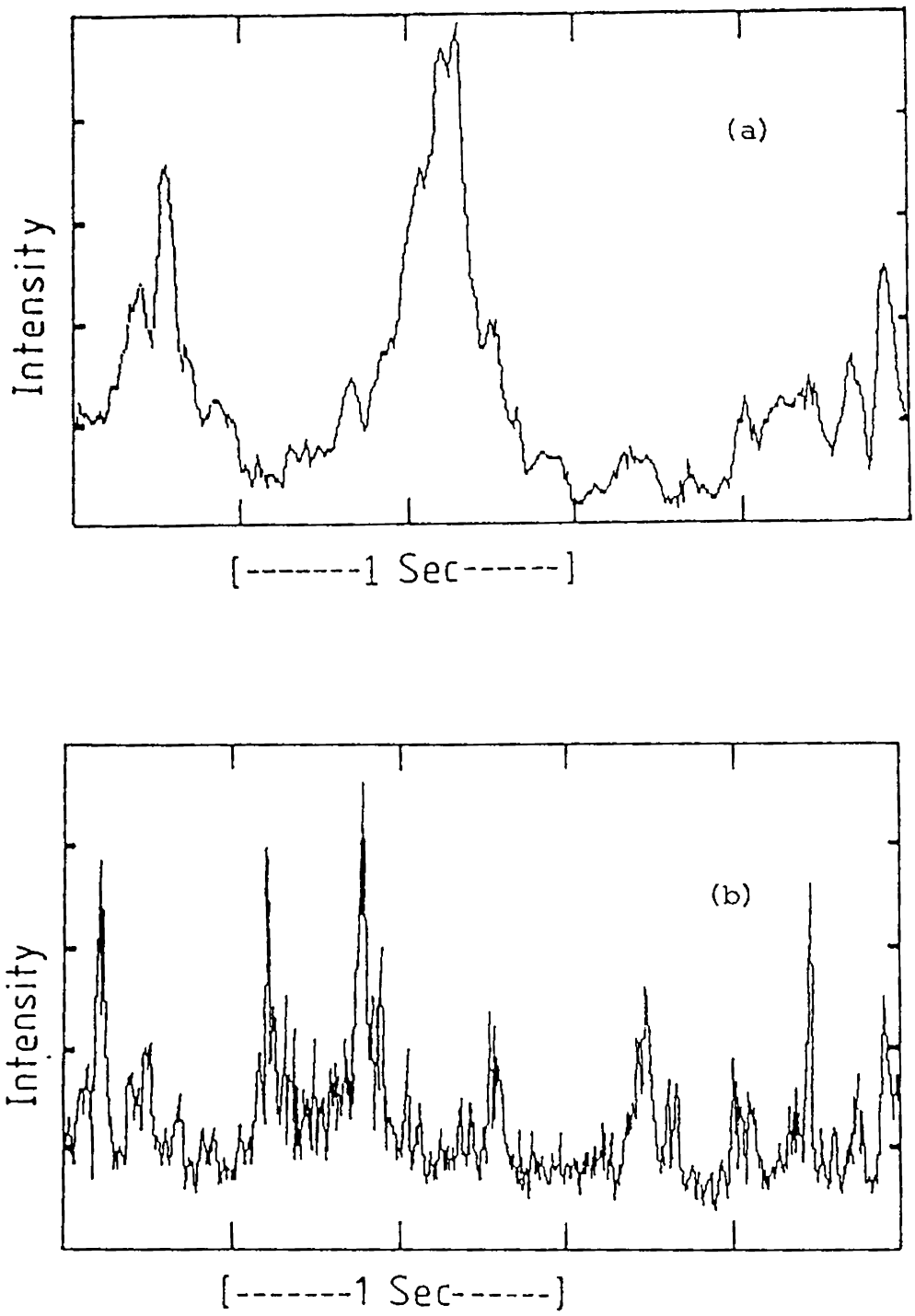

Fig.5.2 Record of the intensity fluctuations of the laser propagated through the turbulent medium for a path length of 2 m and for a) heater power of 210W and b) heater power of 1325W.

Thus in the weak turbulence region, the variance of log-intensity is proportional to $L^{11/6}$ where L is the path length.

The plot of σ_{lnI} against $L^{11/6}$ is shown in Fig.(5.3) for the lowest turbulence strength (heater power = 210 W). The values shown are the average of five independent measurements of intensity for a duration of 2.5 seconds sampled at 100 Hz. It can be seen that even for the lowest turbulence strength, the variance approaches saturation value for path lengths above one metre. This implies that the strong turbulence region prevails for all the cases in which the path length is greater than one metre.

This shows that the behaviour of the variance of log-intensity of the propagated beam through the laboratory simulated turbulence is very much like that for the atmospheric turbulence.[4]

5.3.2 Power Spectrum of the Intensity Fluctuations

The temporal frequency spectrum of the irradiance fluctuations are determined by Maximum Entropy Method (MEM). Compared to the Fast Fourier Transform (FFT) method, the MEM has the advantage of obtaining highly resolved spectrum from a time series.[12] The contribution from the low frequencies can be extracted to a sufficient degree of accuracy by MEM even when the signal is of small duration. This is an

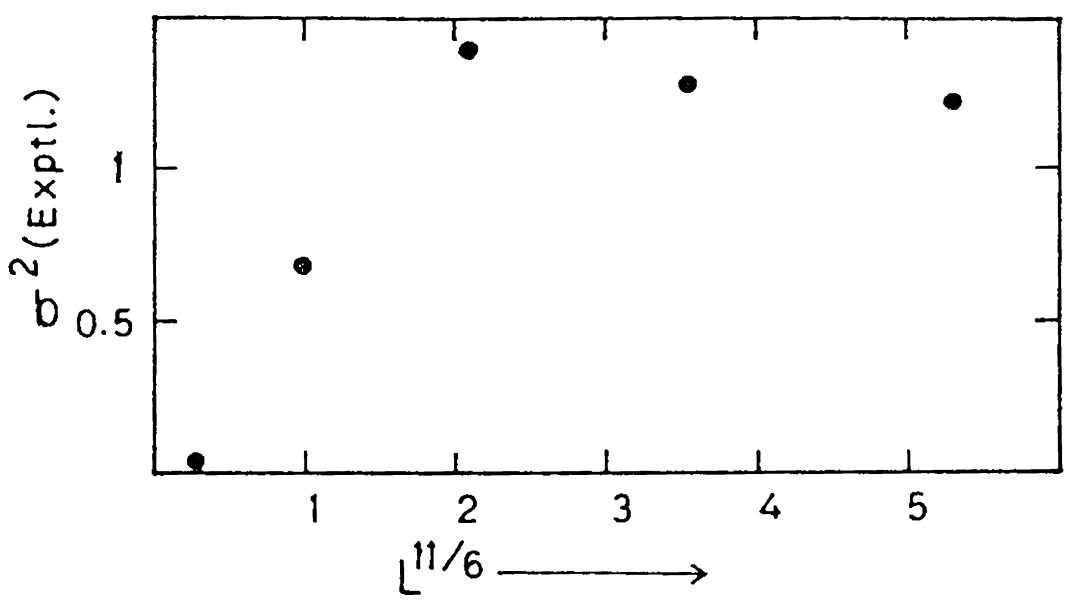

Fig.5.3 Plot of the measured values of variance of log-intensity versus $L^{11/6}$ (where L is the path-length) for the lowest heater power (210W).

additional advantage of MEM. Different methods of power spectral analysis by MEM are given by Murty.[13] A detailed treatment of the technique and the steps involved in the calculation are given in the Appendix I.

The results presented in this section are from the measurements of intensity, for a time duration of 2.5 sec, sampled at an interval of 10 ms. The normalised power spectrum described by Tatarskii is given by

$$U(f) = fW(f) / \int_0^\infty W(f)\,df \qquad (5.1)$$

where W(f) is the power spectrum. For Kolmogorov turbulence, W(f) is given by eqn.(1.77). Hence U(f) is proportional to $f^{-5/3}$.

The log-log plot of the power spectrum of the irradiance fluctuations for the lowest turbulence strength (heater power 210 W) and lowest path length of 0.5 m is shown in Fig.(5.4a). It shows the characteristic -5/3 power behaviour as predicted for Kolmogorov-Obukhov's turbulence in the inertial subrange. But this region is limited to a narrow frequency band. In the low frequency region the slope is +1, and in the high frequency region, the power falls off rapidly with a slope of nearly -4. Such a behaviour had been reported by Majumdar and Gamo.[9]

Fig.(5.4b) shows the power spectrum for a path length of 1.5 m for the same turbulence strength. The -5/3 slope

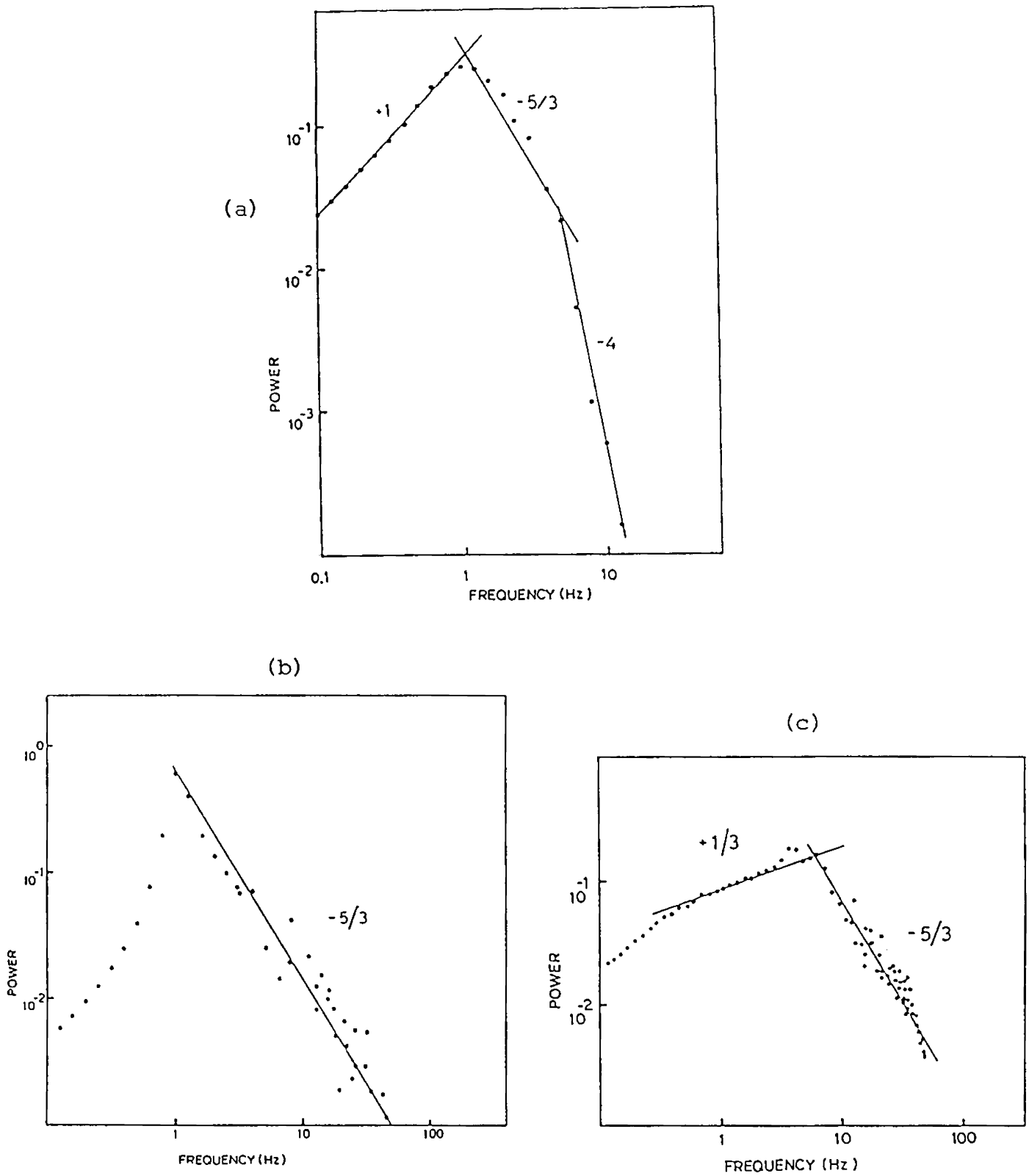

Fig.5.4 Power spectrum of the intensity fluctuation of the laser beam for a heater power of 210W and path length of a) 0.5 m, b) 1.5 m, and c) 2.5 m.

region is found to be extended to the high frequency limit (50 Hz). (The limit being due to the signal sampling frequency which is 100 Hz).

The power spectrum for a path length of 2.5 m for the same turbulence strength is shown in Fig.(5.4c). A notable development in this spectrum is the +1/3 power behaviour in the low frequency side. For the earlier two cases it was +1 in that region.

From the Fig.(5.3) it can be seen that the latter two cases (path lengths 1.5 m and 2.5 m) lie in the saturation region.

An analysis of the power spectrum shows that it has a gradual development which can be related to the propagation length. The Kolmogorov region of -5/3 slope extends to higher frequency side as the path length increases. No substantial shift in the peak frequency is observed. Further increase of path length broadens the spectrum with a 1/3 slope in the low frequency side.

The general behaviour is similar to that observed in the case of atmospheric turbulence except in the magnitude of time scales involved in the dynamics. The velocities of the eddies in the atmosphere will be of the order of several meters per second, while in the liquid it will be only centimetres per second.

An analogous result is recently reported for the inverse energy cascade in two dimensional turbulence.[14]

5.3.3 Probability Distribution Function

The probability distribution of the irradiance fluctuation of an optical wave propagating in a random medium is an unsolved problem especially in the strong turbulence region. It is generally accepted that the distribution is log-normal in weak turbulence.

Experiments conducted by Gracheva et al.[3,4] showed that the largest deviation from the log-normal distribution occur for intermediate values of turbulence strengths. For very low and very high strengths of turbulence they observed that the distribution is close to log-normal. Ochs and Lawrence[6] observed that even in the saturation region, the distribution is close to log-normal. Elliot et al.[8] observed deviation from log-normal for higher turbulence strengths. Majumdar and Gamo[9] found that for weak turbulence ($\sigma_R^2 < 1$) the distribution is close to log-normal, while for $\sigma_R^2 < 1$, it is close to k distribution. Thus the type of probability distribution function involved in the statistics is not yet understood well.

Mathematically there are several approaches that will lead to the knowledge about the probability distribution of a propagating wave. They include applying the central limit theorem, calculating moments, finding the characteristic functions and trial and error. Strohbehn et al.[15] suggested some methods of experimental analysis which includes the use of hypothesis testing

and goodness of fit tests for a better understanding of the probability distribution. For the present analysis the method suggested by Majumdar[16] is adopted. The method is to compare the higher order skewness and excess coefficients using central moments with those for some known distribution.

The central moment μ_n of order n = 2,3...8 is defined as

$$\mu_n = \langle (I - \langle I \rangle)^2 \rangle \tag{5.2}$$

Using this, the following nondimensional coefficients are defined as

$$\text{Skewness} = \Gamma_3 = \mu_3/\mu_2^{3/2} \tag{5.3}$$

$$\text{Excess} = \Gamma_4 = \mu_4/\mu_2^2 - 3 \tag{5.4}$$

$$\text{Superskewness} = \Gamma_5 = \mu_5/\mu_3\mu_2 - 10 \tag{5.5}$$

$$\text{Superexcess} = \Gamma_6 = \mu_6/\mu_2^3 - 15 \tag{5.6}$$

$$\text{Hyperskewness} = \Gamma_7 = \mu_7/\mu_3\mu_2^2 - 105 \tag{5.7}$$

$$\text{Hyperexcess} = \Gamma_8 = \mu_8/\mu_2^4 - 105 \tag{5.8}$$

The expressions for higher order skewness and excess coefficients for three distributions, log-normal, Rice-Nakagami and Gamma distribution are derived by Majumdar[9,16] and are given in Appendix II.

The experimentally obtained values of these higher order coefficients are compared with the theoretically calculated values to identify the best fit distribution. Among the cases discussed here, only the first one falls in the weak turbulence region. All others are for 2 metre path length for higher turbulence strengths and hence are in the strong turbulence region.

Table (5.1) gives the ratio of the values of higher order skewness and excess coefficients for the three distributions referred above to those of experimentally obtained values. Because of the finite sampling duration, the error involved in the values of higher order moments will be larger. Therefore while judging which distribution fits well, more weightage is given to lower order moments. The best fit distribution is shown in the table.

The present results substantiates that in the weak turbulence region the distribution is close to log-normal as reported by previous workers.[6,8,9] In the saturation region where the results in the literature are confusing, the present results support the Rice-Nakagami distribution. This distribution is found to fit for four out of five observations presented here. But, for an intermediate region and for the strongest turbulence the distribution is observed to be more close to Gamma distribution.

In addition, the results for the weak turbulence, projects out another similarity in the behaviour of laboratory simulated turbulence with that of atmospheric turbulence.

Table (5.1). Comparison of theoretical and experimental values of higher order skewness and excess coefficients. Column 1 shows heater power (W) and path length (m). Column 2 denotes distribution (LN - Log-Normal, RN - Rice-Nakagami, & G - Gamma)

Heater power & path	Distrib.	Γ_n (theoretical)/ Γ_n (experimental) n = 3	4	5	6	7	8	Best-Fit
210 W (0.5M)	LN.	0.670	2.141	0.783	3.728	1.649	11.306	Log-norm.
	RN.	0.332	0.391	0.090	0.631	0.196	1.498	
	G.	0.950	3.586	0.985	6.573	2.270	21.508	
210 W (2.0m)	LN.	1.361	1.327	1.229	2.153	2.921	6.447	
	RN.	0.662	0.225	0.122	0.208	0.175	0.205	
	G.	1.300	0.969	0.624	1.131	1.047	1.795	Gamma.
375 W (2.0m)	LN.	1.801	6.621	44.75	97.85	903.7	9937.2	
	RN.	0.853	0.949	2.876	1.501	3.939	2.881	Rice-Nak.
	G.	1.052	1.549	5.247	3.072	8.685	8.473	
588 W (2.0m)	LN.	1.942	7.051	27.95	75.26	466.1	5371.4	
	RN.	0.917	1.017	1.852	1.344	2.572	2.324	Rice-Nak.
	G.	1.172	1.790	3.677	3.015	6.236	7.736	
850 W (2.0m)	LN.	1.481	4.731	25.50	126.7	1565	40443	
	RN.	0.726	0.711	1.584	1.164	2.859	2.642	Rice-Nak.
	G.	0.758	0.793	1.836	1.398	3.559	3.575	
1070W (2.0m)	LN.	1.341	3.370	51.32	19.65	767.7	405.30	
	RN.	0.639	0.525	4.249	0.905	17.05	1.982	Rice-Nak.
	G.	1.008	1.442	13.60	3.264	67.13	11.748	
1325W (2.0m)	LN.	1.106	1.451	1.619	1.767	2.391	3.494	
	RN.	0.539	0.249	0.164	0.182	0.155	0.130	
	G.	1.086	1.126	0.881	1.035	0.972	1.186	Gamma.

5.4 STRANGE ATTRACTORS AND CHAOTIC MOTION

The topic of strange attractors is one that finds abundant applications in a wide variety of nonlinear phenomena. They include the onset of turbulence in fluids[17], nonlinear wave interaction in plasma,[18] lasers[19] etc. The pioneering work in this topic was done by Lorenz,[17] who suggested the relevance of strange attractors in the onset of turbulence in fluid flows. Lorenz was interested in explaining the presence of chaotic behaviour in numerical solutions of a model system of three coupled first order nonlinear ordinary differential equations to explain the instability which results when a fluid layer subjected to gravity is heated sufficiently strongly from below. By an analysis of the computer generated solutions and analytical reasoning, Lorenz deduced that the solutions of these coupled nonlinear equations were eventually trapped in a region of phase space of the system which had very intricate geometric structure. This is termed as the 'strange attractor', by Ruelle and Takens,[20] who went on to conjucture that these strange attractors are the cause of turbulent behaviour of fluid flow.

Recent progress in the theory of nonlinear dynamical systems has provided new methods for the study of complex systems in the fields of hydrodynamics[21], chemistry[22] and human brain activity.[23,24] Such systems may be studied by analysing the experimental data recorded as a series of measurements in time

of a pertinent and easily accessible variable of the system. In most cases, such variables describe a global or averaged property of the system. For example, consider the time series obtained by recording intensity fluctuations of a laser beam propagating in a turbulent medium. Although it may seem that such data offer only a one-dimensional view of the dynamics, it can be shown that a time series may provide information about a large number of pertinent variables which may subsequently be used to explore and characterise the dynamics of the system.

More specifically, by using such a time series one can characterise the attractor and thereby establish the deterministic character of the dynamics of the underlying system. This topological entity ie., the attractor, portrays the essential features of the dynamics and can be characterised by its dimension. In general, a non-integer dimension will prove the existence of chaotic attractor or strange attractor, the main feature of which is its sensitivity to the initial conditions. Another quantity which can be derived is the Kolmogorov entropy which is a dynamic invariant of the system.

In the following section, studies in this direction carried out in the context of hydrodynamic turbulence is given.

5.4.1 Dimension of Attractor and Kolmogorov Entropy

There are two invariants for a chaotic system which can be easily extracted from the experimental data. They are the

dimension of the attractor in phase space and the entropy connected with the evolution of the system is phase space. These characteristic invariants will change if some control parameter of the system is varied. The method of calculating the dimension and the entropy is given by Atmanspacher and Scheingraber.[25] According to them, these invariants can be estimated from a measure of time series of a single variable of the system. In the present case, the measured variable is the intensity of a laser beam propagated through a turbulent medium. The refractive index of the medium will have spatial and temporal fluctuations due to the turbulent motion of the liquid. This introduces temporal fluctuations in the intensity of the propagated beam. The nature of these fluctuations will contain certain information about the dynamics of the turbulence.

As indicated earlier, a chaotic system is characterised by the presence of a fractal dimensional attractor, in phase space. In other words, the system is trapped in certain volume in phase space whose dimension is fractal. Fractional dimension can be conceived by a generalized definition of dimension given by Housdorff. Consider a cube and double its linear size in each spatial directions. Then we get a cube whose volume is eight times larger than the original one as $2^3 = 8$. In general, taking an object of dimension H and if its linear size in each spatial direction is increased l times, then the new volume will be $K = l^H$ or

$$H = \frac{\log K}{\log l} \tag{5.9}$$

Thus H can have fractional values also.

Let $X_o(t)$ be the original time series. Then d additional data sets (d = 1,2,3,...) are obtained by introducing a time delay (d Δt). From the resulting data sets d dimensional phase space is constructed such that d is greater than actual dimension of the phase space.

If each data set contains N values spaced by a time increment τ then the following data sets can be obtained for various values of d.

$$X_o(t) \ldots . X_o(t\ )$$

$$X_o(t_1 + \Delta t) \ldots . X_o(t_N + \Delta t)$$

$$\vdots$$

$$X_o(t_1 + d\ \Delta t) \ldots . X_o(t_N + d\ \Delta t)$$

such that $t_i = t_1 + (i-1)\tau$

Within the vector representation,

$$\bar{X}_i = (X_o(t_i) \ldots . X_o(t_i + d\ \Delta t)) \qquad (5.10)$$

and the total set becomes

$\bar{X}_1 \ldots . \bar{X}_N$ where $\bar{X}_i$ is a point in the constructed d dimensional space. Inside the attractor, these points will be distributed uniformly.

We can determine the distance $|\bar{X}_i - \bar{X}_j|$ which is the usual Euclidean norm.

The correlation function can be calculated as

$$C(r) = \lim_{N\to\infty} \frac{1}{N^2} \sum_{i,j=1}^{N} H(r - |\bar{X}_i - \bar{X}_j|) \qquad (5.11)$$

where H(x) is the Heaviside function. $H(x) = 0$ for $x \leqslant 0$ and $H(x) = 1$ for $x > 0$. The function C(r) counts the number of pairs of those points with a distance $|\bar{X}_i - \bar{X}_j|$ smaller than r. When the distances between all pairs of points are less than r, then $C(r) = 1$. Since the points are distributed uniformly within an attractor, C(r) essentially represents a volume element in the phase space. The rate of increase of this volume element with r depends on the dimension of the attractor and is given by the relation (5.9). Thus the dimension of the attractor is given by

$$D = \lim_{r\to 0} \frac{\log C(r)}{\log r} \qquad (5.12)$$

which is otherwise called the correlation exponent.[26] Eventhough the dimension of the attractor and correlation exponent are not exactly equal, it has been shown[26] that for several of such systems, they are equal. When D is an integer, the system is regular, when it is fractal, the system is chaotic and when D = d, the dimension of the constructed space, the system behaviour in completely stochastic.

The dimension of an attractor is a static invariant, as it does not depend on any time scale. But the entropy of a system is always a quantity which is to be specified per unit time. Therefore it is a dynamic invariant describing the properties of the considered process.

Another quantity which can be evaluated from the time series is the Kolmogorov entropy of the system, the lower limit of which is defined as

$$K = \lim_{r \to 0} \lim_{d \to \infty} \frac{1}{\tau} \frac{\log C_d(r)}{\log C_{d+1}(r)} \qquad (5.13)$$

where logarithm is to the base 2.

$K > 0$ is a sufficient condition for the existence of deterministic chaos. Furthermore, K can be used to quantify the degree of chaos.

The curves of log C(r) versus log r for different d are shown in Fig.(5.5), for the case of the time series shown in Fig.(5.2). As the dimension d of the constructed phase space increases, the slope ν converges to a limiting value. This is illustrated in Fig.(5.6). The converging value of the slope is the dimension D of the attractor. The line $\nu = d$ denotes complete stochastic behaviour. The fractal or non-integer values of D is sufficient criterion for the contribution of deterministic chaos to the behaviour of the system and the existence of strange attractor.

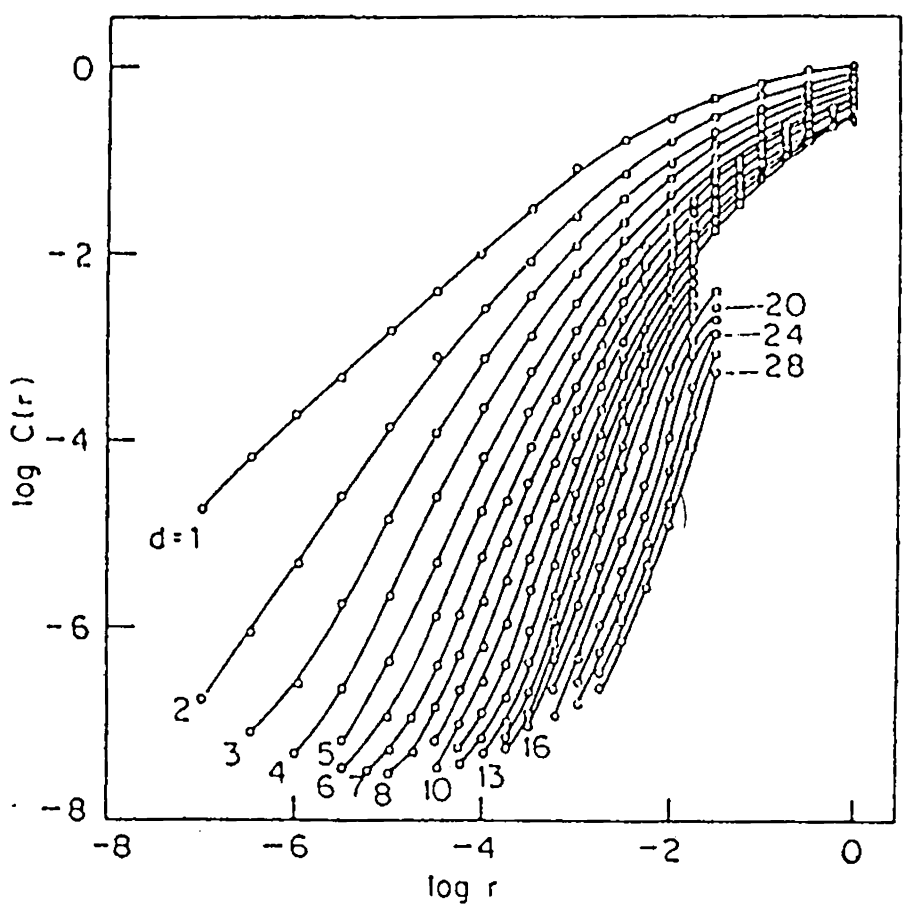

Fig.5.5 Log-log plot of correlation function C(r) versus distance r, for different dimensions d.

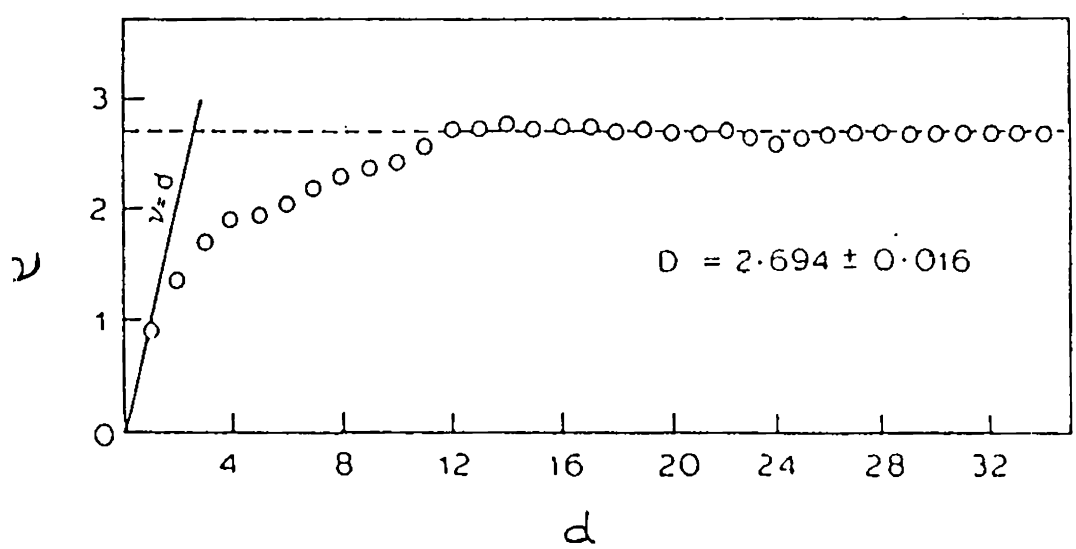

Fig.5.6 Slope ν in the linear range of the different curves in Fig.(5.5) as a function of d of the constructed phase space. The limiting value of slope gives the dimension D = 2.694.

From the values of D it is possible to extract the number of degrees of freedom of the system. The dimension of d of the constructed phase space is usually larger than the actual number of degrees of freedom of the system. The obtained value D = 2.69 indicates that the investigated process needs only next higher integer number of degrees of freedom (ie., three) to be successfully modelled.

In certain cases the statistical error prevents the discrimination between an integer and a fractal value of D. This was observed for the case where the heater power was 375 W. In such cases, the Kolmogorov entropy turns out to be useful since it provides an additional sufficient condition for chaotic behaviour namely $K > 0$.

K is estimated from the vertical distance (at identical r) between curves belonging to successive dimensions d. In the Fig.(5.7), it is shown how K approaches a limiting value of high dimension d. The indicated values for each particular d have been calculated for the mean value $C_d(r)/C_{d+1}(r)$ over the linear range of r. Compared with the value of D, a considerably higher value of d is needed for the convergence of K.

The obtained values of D and K for different turbulence strengths are calculated and are shown in Fig.(5.8). The D increased steadily with the strength of turbulence upto a heater power of 1075 W, after which it showed a decrease. A similar behaviour was observed for the entropy K.

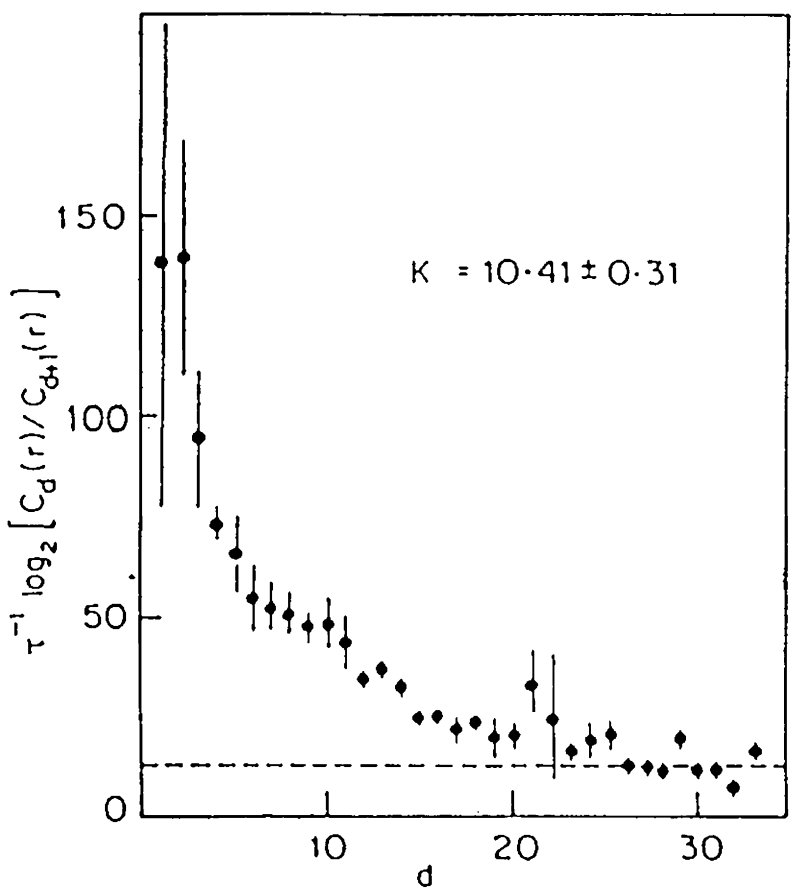

Fig.5.7 Mean value of $(1/\tau)$ log $C_d(r)/C_{d+1}(r)$ as a function of d obtained from the linear range of curves in Fig.(5.5). The limiting value for large d gives the value of K.

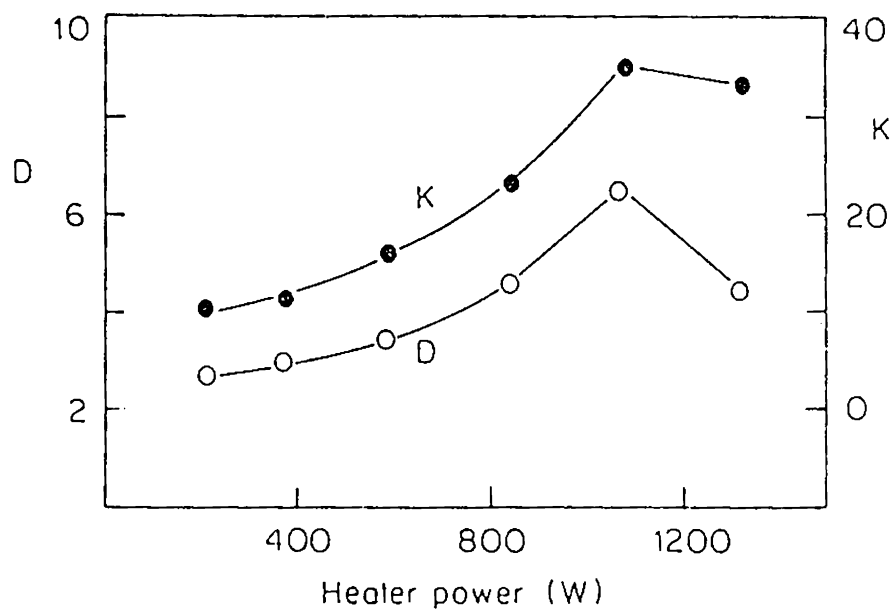

Fig.5.8 The behaviour of the dimension D and entropy K for different heater powers (turbulence strengths).

The steady increase of D with turbulence strength shows that the minimum number of variables which are needed to successfully model the system is increasing. Evidently the number of degrees of freedom of the system is increased. This is substantiated by a corresponding increase in the value of K.

The decrease of D after a particular heater power (turbulence strength) implies a simplification of turbulence by reducing the degrees of freedom. Similar results were obtained by Atmanspacher and Schiengraber[25] for the studies of dynamical instabilities in a multimode CW dye laser. The reduction in the complexities of the system is further confirmed to by the decrease in K. It shows that beyond a critical turbulence strength, a hydrodynamical turbulent system tends to more ordered states.

5.4.2 Phase Space Pictures and Fourier Space Representations

Several methods are adopted to get the knowledge of the nature of strange attractor and the transition to turbulence. One of the methods to obtain an indication of transition to turbulence is to find the Fourier transform of the time series. The transition to turbulence is indicated by a broad band in the frequency spectrum. But to know how turbulent a system is, this method cannot be used, because of the irregular shape of the spectrum. Raux et al.[27] have suggested a new method for constructing phase space for the case of chemical turbulence.

Turbulence is described by surveying the trajectories in phase space. A system is turbulent when these trajectories describe a strange attractor. A three dimensional representation of the attractor would be obtained by the recording of three selected signals. This being quite difficult, two other procedures have been proposed. Starting with the recording of the time variations of a signal (X(t)), one can construct a finite dimensional phase space picture. The idea behind these conjectures is that any set of independent quantities calculated at a given time, from the time variation record will define an attractor, diffeomorphically equivalent to the true one. The three quantities typically used are the values of each state-space coordinate x(t), y(t) and z(t). Packard et al.[28] found that beginning with a time series obtained by sampling a single co-ordinate, one can obtain a variety of three independent quantities which appears to yield a faithful phase-space representation of the dynamics in the original x, y, z space. One possible set of three such quantities is the value of the co-ordinate with its values at two previous times eg., $x(t)$, $x(t-\tau)$, and $x(t-2\tau)$. Another set obtained by making time delays small and taking differences $x(t)$, $\dot{x}(t)$ and $\ddot{x}(t)$.

In the present experiment, the time series measured is the intensity of a laser beam propagated through the turbulent medium. The two dimensional phase space diagram of the system constructed by plotting $x(t)$ versus $x(t+\tau)$ for three different turbulence strengths are shown in the Fig.(5.9). These curves

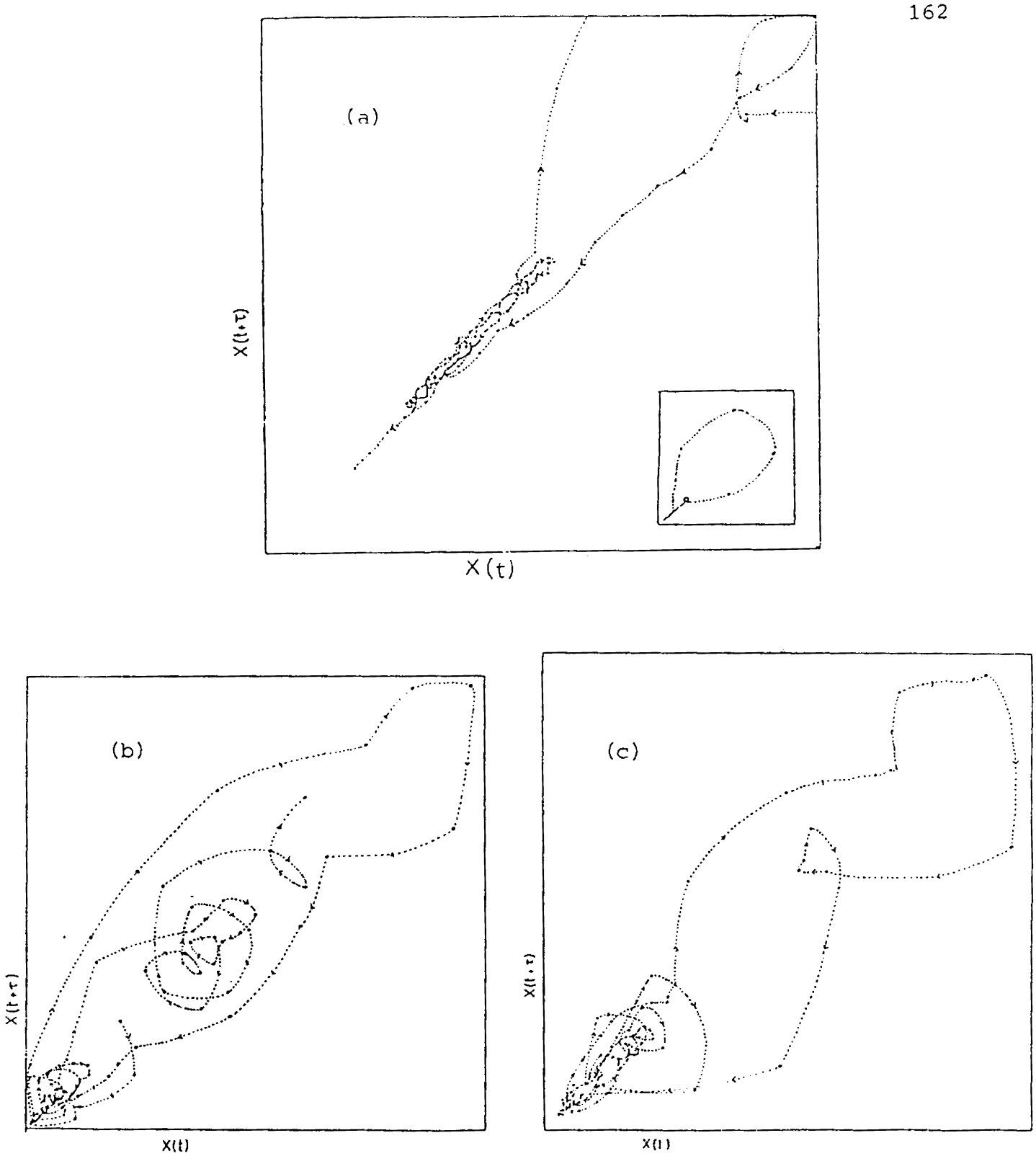

Fig.5.9 Two dimensional phase space picture of the turbulent system obtained from the time series X(t) of the intensity fluctuation for three heater powers a) 475W (a reduced scale picture is given in insite), b) 740W and c) 1060W.

are made out of the time series obtained from a record of intensity fluctuations for a duration of 1.5 seconds, with τ = 10 ms.

A more clear picture of the transition to turbulence is obtained by plotting the Fourier components in Fourier space. This method was used by Pratap[29] to study the spatial density distribution of the asteroidal belt. The measured time series $\underset{\sim}{x}(t)$ is Fourier analysed to evaluate the a_n and b_n coefficient.

$$X(t) = \sum_{n=0}^{N} (a_n \cos n\omega t + b_n \sin n\omega t)$$

$$= \sum_{n=0}^{N} R_n \cos(n\omega t + \phi_n) \qquad (5.14)$$

Each frequency has an amplitude $R_n = (a_n^2 + b_n^2)^{\frac{1}{2}}$ and phase $\phi_n = \tan^{-1}(-b_n/a_n)$. $a_n = R_n \cos \phi_n$ and $b_n = -R_n \sin \phi_n$. Fig.(5.10) gives the plot of points R_n defined by the above equations in (a_n, b_n) space for same experimental observations described in Fig.(5.9). For low strengths of turbulence, the curve obtained by joining the points R_n shows an inward clockwise spiralling behaviour. As the strength of turbulence increases, the spiral structure smears out gradually. This smearing out of the spiral starts from the high frequency side (ie., the inner part of the spiral) and extends to lower frequencies as the turbulence increases.

Plotting of R_n in Fourier space, thus appears to be an attractive method to observe the transitions to turbulence.

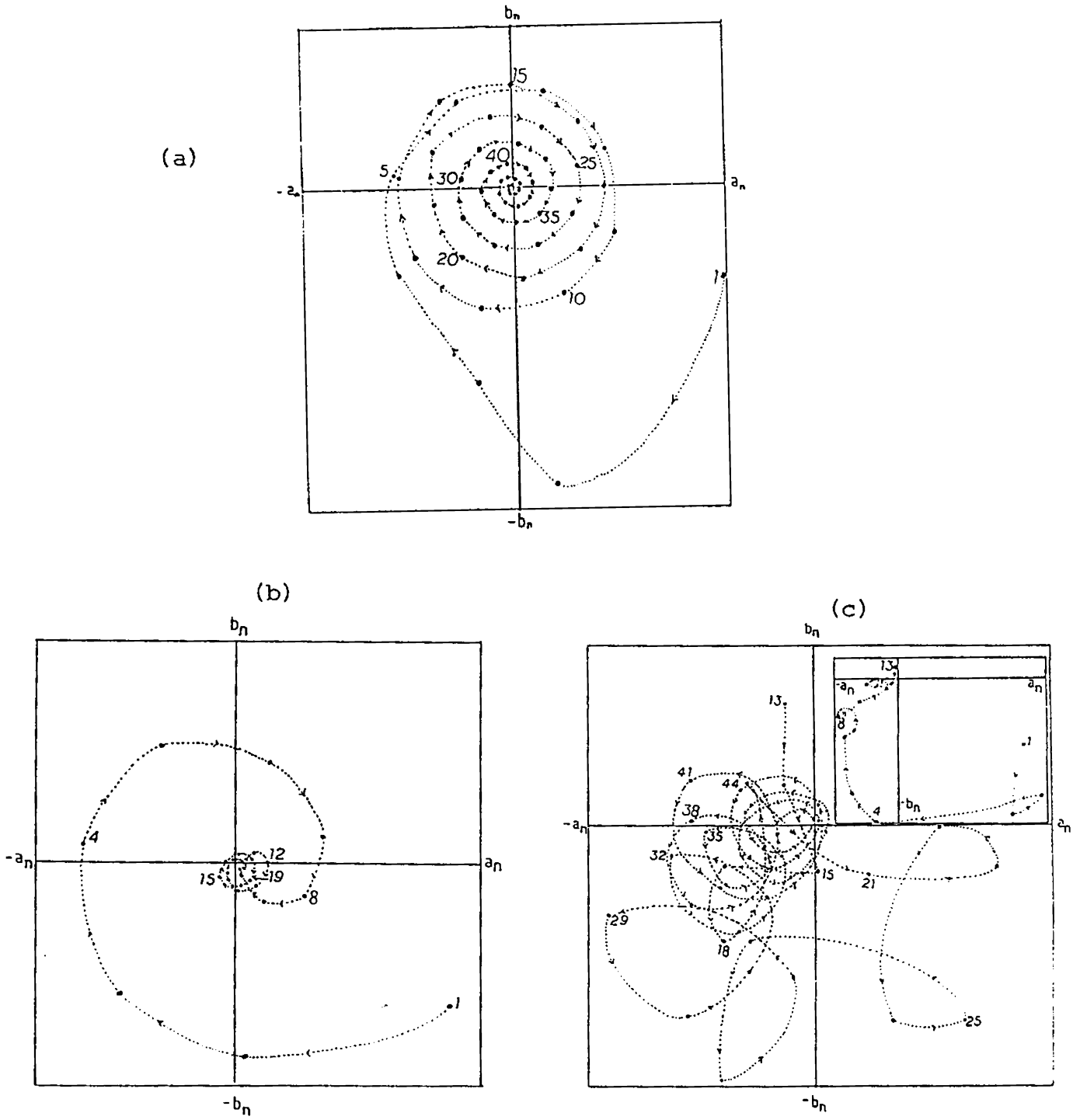

Fig.5.10 Plot of R_n in (a_n, b_n) space for the respective cases in Fig.(5.9).(In (c) the points 1 to 13 are plotted in a reduced scale and are given in the insite).

REFERENCES

1. V.I.Tatarskii, A.S.Gurvich, M.A.Kallistratova and L.V.Terenteva, Astronom.Zh., 35, 623 (1958).

2. A.S.Gurvich, V.I.Tatarskii and L.R.Tsvang, Dokl.Akad.Nauk.SSR., 123, 655 (1958).

3. M.E.Gracheva and A.S.Gurvich, Izv.VUZ.Radiofiz., 10, 775 (1965), (English transl. Radio Phys.Quant.Electron., 8, 511 (1965).

4. M.E.Gracheva, A.S.Gurvich, S.S.Kashkarov and VI.V.Pokasov in 'Laser Beam Propagation in the Atmosphere', Ed. J.W.Strohbehn (Springer-Verlag, Berlin, 1978), p.107.

5. G.E.Mevers, D.L.Fried and M.P.Keister Jr., J.Opt.Soc.Am., 55, 1575 (1965).

6. G.R.Ochs and R.S.Lawrence, J.Opt.Soc.Am., 59, 226 (1969).

7. L.R.Bissonnette, Appl.Opt., 16, 2242 (1977).

8. R.A.Elliot, J.R.Kerr and P.A.Pincus, Appl.Opt., 18, 3315 (1979).

9. A.K.Majumdar and H.Gamo, Appl.Opt., 21, 2229 (1982).

10. D.Ruelle and F.Takens, Commun.Math.Phys., 20, 167 (1971).

11. P.Grassberger and I.Procaccia, Phys.Rev.Lett., 51, 346 (1983).

12. H.R.Rodoski, P.F.Fougere and E.J.Zawalick, J.Geophys.Res., 80, 619 (1975).

13. C.S.R.Murty, Physical Research Lab. (Ahmedabad), Technical Note TN - 81-01 (1981).

14. B.K.Shivamoggi, Phys.Lett.A., 122, 145 (1987).

15. J.W.Strohbehn, T.I.Wang and J.P.Speck, Radio Science, 10, 59 (1975).

16. A.K.Majumdar, J.Opt.Soc.Am., 69, 199 (1979).

17. E.N.Lorenz, J.Atmos.Sci., 20, 130 (1963).

18. J.C.Adam, M.N.Bussac, and G.Laval in 'Intrinsic Stochasticity in Plasmas', Ed.G.Laval and D.Gresillon (Les Editions de Physique Courtaboef, Orsay, France, 1980), p.415.

19. H.Haken, Phys.Lett.A., 53, 77 (1975).

20. D.Ruelle and E.Takens, Commun.Math.Phys., 50, 69 (1976).

21. A.Brandstater, J.Swift, H.L.Swinney and A.Wolf, Phys.Rev.Lett., 51, 1442 (1983).

22. J.C.Roux, R.M.Simoyi and H.L.Swinney, Physica D., 8, 257 (1983).

23. P.E.Rapp, I.D.Zimmerman, A.M.Albano and N.N.Greenbaun, Phys.Lett.A., 110, 335 , (1985).

24. Lalaja Varghese, V.P.N.Nampoori and R.Pratap, Int.J.Neuroscience, (in press).

25. H.Atmanspacher and H.Scheingraber, Phys.Rev.A., 34, 253 (1986).

27. J.C.Roux, A.Rossi, S.Bachelart and C.Vidal, Phys.Lett., 77A, 391 (1980).

28. N.H.Packard, J.P.Crutchfield, J.D.Farmer and R.S.Shaw, Phys.Rev.Lett., 45, 712 (1980).

29. R.Pratap, Pramana, 8, 438 (1977).

Chapter 6

CONCLUSIONS

Abstract

The general conclusions drawn from the results are given. The wavelength region of minimum attenuation in sea water is found to be around 500 nm. The value of attenuation coefficient in this region permits propagation of a laser beam through more than 300 metres in sea water, using less sophisticated laser systems and detection techniques. The behaviour of the fluctuations in the intensity of the propagated laser beam due to the turbulence in the water medium is similar to that in the case of atmosphere. The major difference between the two cases is in the time scales in which the fluctuations occur.

The work presented in this thesis is mainly concentrated on some preliminary studies to explore the feasibility of using lasers for underwater applications like communication, photography etc. The wavelength region of minimum attenuation in sea water, its dependence on various constituents of sea water and the propagation of laser beam through a turbulent medium, constitutes the major topics of the present investigation. These are some of the relevant subjects to be studied carefully before designing any underwater optical system.

A simple and versatile pulsed dye laser is fabricated to use as a source for the attenuation studies in sea water. This laser is capable of giving out narrow bandwidth pulses, the wavelength of which is tunable over the entire visible region. A motor controlled drive facilitates smooth scanning in the wavelength scale. A counter attached to the scanning system directly reads wavelength in angstrom units. The pulse energy of $\sim 2\,\mu J$, the divergence of 0.31 mrad, and the line width of 0.04 nm are comparable to and in certain cases even better than most of the commercially available systems.

Using this laser as the source, an experimental arrangement is set up to measure the attenuation coefficient of transparent liquids. The split-pulse laser method, which is the one adopted for the present studies has the capability of measuring very weak attenuation of the order of $10^{-4} cm^{-1}$,

as it uses a 10 metre path length through the liquid. In addition, this method has the design advantage of eliminating most of the errors usually found in conventional techniques, such as fluctuations in the source intensity and reflection losses at the cell windows etc. Moreover, this is capable of giving the absolute values of attenuation coefficient (which includes both absorption and scattering).

Using this setup, the attenuation coefficient of distilled water is determined for the entire visible region (430-630 nm). The region of minimum attenuation is found to be around 450 nm, where its value is nearly 2×10^{-4} cm^{-1}. The present values are compared with some of the earlier reported values by other experimental techniques. To study the effect of dissolved constituents of sea water on optical attenuation, artificial sea water samples were prepared and investigated. These results show that the dependence of attenuation on the dissolved constituents is negligible. The attenuation coefficients of artificial sea water were found to be very close to that of distilled water.

The results obtained for artificial sea water are then compared with those obtained for natural sea water samples. Two samples of natural sea water were studied. It is observed that the attenuation spectrum of natural sea water is different from the artificial sea water, especially in the lower wavelength region, eventhough the concentration of the dissolved

constituents of both the samples were almost the same. The reason for this behaviour is attributed to the scattering due to the suspended particles present in the natural sea water. This argument is strengthened by the observation that coastal waters (which contain large number of suspended particles) showed higher attenuation than that collected far away from the coast, ie., the attenuation decreases as we go interior to the sea. Further into the sea, where the suspended particles are substantially less, the attenuation may reach close to the values of water. The presence of suspended particles, shifts the minimum of the attenuation region from 450 nm for distilled water to 490-510 for sea water, ie., as the concentration of suspended particles increases, the region of minimum attenuation shifts to higher wavelength side.

The minimum value of the attenuation for the artificial sea water is found to be $\sim 3 \times 10^{-4} cm^{-1}$. This implies that after passing 300 metres through the sea water the intensity of the beam will be 0.01% of the original intensity. If a 5 W beam is passed through 300 metres of the sea water, the output intensity will be 0.5 mW, well within the detectable range. These calculations have not taken into consideration losses due to large size suspended particles and living organisms. Moreover, due to the turbulent motion of the sea water, there will be beam wandering and small angle scattering, which also reduces the intensity of the transmitted beam.

The studies on optical propagation in sea water will be complete only when the effect of turbulence on propagation is also studied. The optical propagation in atmospheric turbulence is a subject which is very widely studied both theoretically and experimentally. No experimental studies are reported in the subject of optical propagation in ocean turbulence. Thus the present studies on optical propagation in water turbulence assumes additional importance.

A turbulence chamber is constructed in which water is used as the medium. The intensity of a laser beam propagated through this medium is studied. It is shown that the variance power spectrum and probability distribution of the intensity fluctuations behave similar to the atmospheric turbulence. This is a very useful result in the sense that the theory applicable to atmospheric propagation is atleast partially valid for propagation in the ocean turbulence. The major difference between the two cases is in the magnitude of the spatial and temporal time scales involved in the phenomenon. In the atmosphere, for example, the eddy velocity is of the order of several metres per second, while in the sea it is only of the order of centimetres per second.

The studies on the probability distribution of irradiance fluctuations show that the distribution is more close to log-normal for weak turbulence. In the strong turbulence region,

for which there exists diverse experimental results in the literature, the results of the present investigations supports the Rice-Nakagami distribution. It has also been shown that in this region, the distribution deviates from log-normal.

The latter part of the work is directed to study the chaotic behaviour of the hydrodynamic turbulent system. The chaotic behaviour of such systems are due to the presence of strange attractors in phase space. The dimension of the attractor is one of the important invariants of a chaotic system. Another such invariant is the entropy connected with the evolution of the system in phase space. The values of these invariants gives a quantitative measure of the chaotic behaviour. These invariants are calculated for different turbulence strengths. The analysis shows that as the strength of turbulence increases, the attractor dimension and entropy increases. Beyond a particular strength, both these quantities decrease indicating that the complexity of the system decreases. In other words the number of degrees of freedom involved in the dynamics of the system is reduced. At higher strengths of turbulence, the system can be represented in a lesser dimensional space.

The present investigations has also brought out a new method of observing transition to turbulence. The observed time series is Fourier analysed and the points R_n, described by the Fourier coefficients a_n and b_n are plotted in (a_n, b_n) space.

The trajectories joining the R_n is found to have the shape of a regular spiral. As the strength of turbulence increases, the regular shape of this spiral gets smeared. This smearing is observed to start from the inner side of the spiral ie., the high frequency side. Thus a new qualitative method of observing transition to turbulence is identified.

APPENDIX I

MAXIMUM ENTROPY METHOD TO EVALUATE POWER SPECTRUM OF A TIME SERIES

The procedure for calculating the power spectrum of a time series by maximum entropy method (MEM) is described here. In this technique the entropy of a distribution is maximised subject to constraints, that the Fourier transform of the spectral density is equal to the autocorrelation function of the observed time series.

The entropy function to be maximised is the logarithm of the spectral density integrated over the frequency range.

$$E = \int_{-f_o}^{f_o} \ln P(f)\,df \qquad \text{(A1.1)}$$

where $f_o = \frac{1}{2\Delta t}$ is the Nyquist frequency and Δt is the sampling time increment. The mathematical formulation of the maximum entropy spectrum is that we must determine the spectral density P(f) that maximises the quantity E subject to N+1 constraints that the autocorrelation $C(\tau)$ is given by

$$C(\tau) = \int_{-f_o}^{f_o} P(f)e^{i2\pi f}\,df \qquad \text{(A1.2)}$$

where $\tau = m\Delta t$ for m = 0,1,2,...M. M measures the maximum

lag time of the autocorrelation and the order of the spectrum. Solving the above equations one obtains for P(f) the following expression,

$$P(f) = \frac{P_{M+1}}{2f_o \left| 1 + \sum_{k=1}^{M} {}_M A_k \exp(-i2\pi fk \Delta t) \right|^2} \qquad (A1.3)$$

where ${}_M A_k$ for k=1 to M are the prediction error filter (PEF) coefficients. P_{M+1} is the mean output power of the PEF containing M+1 coefficients.

The coefficients ${}_M A_k$ and P_{M+1} satisfy the following matrix equation.

$$\begin{bmatrix} r_o & r_1 & \cdots & r_M \\ r_1 & r_o & \cdots & r_M \\ \vdots & \vdots & & \vdots \\ r_M & r_M & \cdots & r_o \end{bmatrix} \begin{bmatrix} 1 \\ {}_M A_1 \\ \vdots \\ {}_M A_M \end{bmatrix} = \begin{bmatrix} P_{M+1} \\ 0 \\ \vdots \\ 0 \end{bmatrix} \qquad (A1.4)$$

The above matrix R of elements (r_{ij}) is constructed from the autocorrelation function $C(\tau) = C(n \Delta t)$ by setting $n = i-j$ and $r_{ij} = C(|i-j| \Delta t)$. (A1.5)

The matrix equation (A1.4) can be solved to obtain the values ${}_M A_k$ for k = 1 to M and P_{M+1}, which in turn can be

used to determine the power spectrum from equation (A1.3) at any value of the frequency f.

Estimate R_k, the autocorrelation corresponding to lag k for k = 0 to M from the given data. Substitute the autocorrelations in the matrix equation. As the equation is a set of M+1 equations in M+1 unknowns, the unknown parameters ${}_MA_k$ for k = 1 to M and P_{M+1} can be obtained by inverting the autocorrelation matrix and premultiplying the RHS vector with the inverse matrix.

However, orders of magnitude in time are saved by using Levinson's recursion relations between the coefficients for the matrices of order N and N+1. Thus the coefficients ${}_MA_k$ and P_{M+1} contained in the matrix equation of order M+1 can be obtained from the coefficients ${}_{M-1}A_k$ and P_M in the matrix equation of order M.

The recursive relations connecting the coefficients ${}_MA_k$ and P_{M+1} with ${}_{M-1}A_k$ and P_M are given by

$$ {}_MA_k = {}_{M-1}A_k + {}_MA_M \; {}_{M-1}A_{M-k} \quad \text{for } k=1 \text{ to } M-1 \qquad \text{(A1.6)} $$

$$ P_{M+1} = P_M \left(1 - {}_MA_M^2\right) \qquad \text{(A1.7)} $$

$$ P_1 = \sum_{t=1}^{N} X_t^2 \; {}_N $$

From these equations the coefficients ${}_{M}A_{k}$ for k = 1 to M-1 and P_{M+1} can be obtained provided ${}_{M}A_{M}$ is known, as the other coefficients ${}_{M-1}A_{k}$ and P_{M} are available from matrix equations of order M. ${}_{M}A_{M}$ can be determined by the following relations.

Initially we put for M = 0.

$$ {}_{O}F_{t} = X_{t} \quad \text{for } t = 1 \text{ to } N \tag{A1.8} $$

$$ {}_{O}B_{t} = X_{t} \quad \text{for } t = 1 \text{ to } N \tag{A1.9} $$

where X_t is the time series. Then

$$ {}_{M}F_{t} = {}_{M-1}F_{t} + \left({}_{M-1}A_{M-1}\right)\left({}_{M-1}B_{t}\right) \quad \text{for } t=1 \text{ to } N-M \tag{A1.10} $$

and

$$ {}_{M}B_{t} = {}_{M-1}B_{t+1} + \left({}_{M-1}A_{M-1}\right)\left({}_{M-1}F_{t+1}\right) \quad \text{for } t=1 \text{ to } N-M \tag{A1.11} $$

$$ {}_{M}A_{M} = -2 \sum_{t=1}^{N-M} \left({}_{M}F_{t}\right)\left({}_{M}B_{t}\right) \Big/ \sum_{t=1}^{N-M} \left({}_{M}F_{t}^{2} + {}_{M}B_{t}^{2}\right) \tag{A1.12} $$

${}_{1}F_{t}$ and ${}_{1}B_{t}$ can be obtained from (A1.10) and (A1.11) with ${}_{o}A_{o} = 0$. ${}_{1}A_{1}$ and P_2 can be obtained by (A1.12) and (A1.7). For M = 2 to M, ${}_{M}A_{M}$ and P(M+1) can be obtained by using the relations (A1.10), (A1.11), (A1.12), (A1.7) and (A1.6) in that order.

APPENDIX II

SKEWNESS AND EXCESS COEFFICIENTS FOR CERTAIN DISTRIBUTION FUNCTIONS

The expressions for higher order skewness and excess coefficients for the lognormal, Rice-Nakagami and Gamma distributions are given below, as reported by Majumdar (Refs.9 and 16 of chapter 5).

1. Lognormal Distribution

$$p(I) = \frac{1}{2\pi\sigma I} \exp[-(\ln I - \lambda)^2/2\sigma^2] \qquad \text{(A2.1)}$$

where λ and σ^2 are the mean and variance of lnI respectively. Let $\omega = \exp(\sigma^2)$, then,

$$\text{Skewness} = \Gamma_3 = 3(\omega-1)^{\frac{1}{2}} + (\omega-1)^{3/2} \qquad \text{(A2.2)}$$

$$\text{Excess} = \Gamma_4 = 16(\omega-1)+15(\omega-1)^2+6(\omega-1)^3+(\omega-1)^4 \qquad \text{(A2.3)}$$

$$\text{Superskewness} = \Gamma_5 = \frac{\omega^{10}-5\omega^6+10\omega^3-10\omega+4}{[(\omega-1)^3(\omega+2)]} - 10 \qquad \text{(A2.4)}$$

$$\text{Superexcess} = \Gamma_6 = \frac{\omega^{15}-6\omega^{10}+15\omega^6-20\omega^3+15\omega-5}{(\omega-1)^3} - 15 \qquad \text{(A2.5)}$$

$$\text{Hyperskewness} = \Gamma_7 = \frac{\omega^{21}-7\omega^{15}+21\omega^{10}-35\omega^6+35\omega^3-21\omega+6}{[(\omega-1)^4(\omega+2)]} - 105 \qquad \text{(A2.6)}$$

$$\text{Hyperexcess} = \Gamma_8 = \frac{\omega^{28}-8\omega^{21}+28\omega^{15}+56\omega^{10}+70\omega^{6}-56\omega^{3}+28\omega-7}{(\omega-1)^4} - 105 \quad \text{(A2.7)}$$

2. Rice-Nakagami Distribution

$$p \qquad p(I) = \frac{1}{\sigma^2}\exp(-(I+I_c)/\sigma^2) I_o[2(II_c)^{\frac{1}{2}}/\sigma^2] \quad \text{(A2.8)}$$

$\langle I \rangle$ is the mean of I; $I_c = \langle I \rangle - \sigma^2$ and I_o is the modified Bessel function.

Let $\beta = I_c/\sigma^2$ then

$$\text{Skewness} = \Gamma_3 = \frac{3}{\sqrt{2}} (\beta+\tfrac{1}{2})^{-3/2} (\beta+1/3) \quad \text{(A2.9)}$$

$$\text{Excess} = \Gamma_4 = 6(\beta+\tfrac{1}{4})(\beta+\tfrac{1}{2})^{-2} \quad \text{(A2.10)}$$

$$\text{Superskewness} = \Gamma_5 = \frac{10(\beta+1/5)}{(\beta+1/3)(\beta+\frac{1}{2})} \quad \text{(A2.11)}$$

$$\text{Superexcess} = \Gamma_6 = \frac{90(\beta+1/6)}{(\beta+\frac{1}{2})^3} + \frac{90(\beta+\frac{1}{4})}{(\beta+\frac{1}{2})^2} + \frac{45(\beta+1/3)^2}{(\beta+\frac{1}{2})^3} \quad \text{(A2.12)}$$

$$\text{Hyperskewness} = \Gamma_7 = \frac{210(\beta+1/7)}{(\beta+1/3)(\beta+\frac{1}{2})^2} + \frac{210(\beta+1/5)}{(\beta+1/3)(\beta+\frac{1}{2})} + \frac{210(\beta+\frac{1}{4})}{(\beta+\frac{1}{2})^2} \quad \text{(A2.13)}$$

$$\text{Hyperexcess} = \Gamma_8 = \frac{2520(\beta+1/8)}{(\beta+\frac{1}{2})^4} + \frac{2520(\beta+1/6)}{(\beta+\frac{1}{2})^3} + \frac{2520(\beta+1/5)(\beta+1/3)}{(\beta+\frac{1}{2})^2} + \frac{1260(\beta+\frac{1}{4})}{(\beta+\frac{1}{2})^4} + \frac{1260(\beta+\frac{1}{4})}{(\beta+\frac{1}{2})^2} + \frac{1260(\beta+1/3)}{(\beta+\frac{1}{2})^3} \quad \text{(A2.14)}$$

3. Gamma Distribution

$$p(I) = \frac{1}{\beta^{\alpha}\,(\alpha)}\; I^{\alpha-1} \exp(-I/\beta) \qquad \text{(A2.15)}$$

Skewness $= \Gamma_3 = 2\alpha^{-\frac{1}{2}}$ (A2.16)

Excess $= \Gamma_4 = 6\alpha^{-1}$ (A2.17)

Superskewness $= \Gamma_5 = 12/\alpha$ (A2.18)

Hyperexcess $= \Gamma_6 = \frac{120}{\alpha^2} + \frac{130}{\alpha}$ (A2.19)

Hyperskewness $= \Gamma_7 = 360/\alpha^2 + 462/\alpha$ (A2.20)

Hyperexcess $= \Gamma_8 = 5040/\alpha^3 + 7308/\alpha^2 + 2380/\alpha$ (A2.21)